ETH
Eidgenössische Technische Hochschule Zürich
Swiss Federal Institute of Technology Zurich

Multiple market regimes in an equilibrium model of fundamentalist and noise traders

Master Thesis

Madis Ollikainen

Monday 26ᵗʰ September, 2016

Supervisors: Prof. Dr. Didier Sornette and Ralf Kohrt

Department of Physics, ETH Zürich

Abstract

Recently, Kaizoji et al. (2015) proposed an equilibrium model of fundamentalist and noise traders, which exhibits transient super-exponential bubble growth. This emergent bubble growth phenomena makes the model interesting as a potential testing environment for financial bubble detection mechanism. In order to enhance future endeavour in this direction, the current thesis is studying the different market regimes present in the model of Kaizoji et al. (2015) in more detail.

We focus on analysing the market dynamics from the perspective of the noise trader imitation and trend following. For elaborating on the effects of the self-referential nature of noise traders, we introduce a mean-field Ising based toy model of noise trader behaviour. We observe that besides the standard paramagnetic disordered and ferromagnetic ordered phases, the toy model has two additional ordered phases, indicating that the self-referential tendencies of noise traders enhance order.

Motivated by the observations from the toy model, we analyse the full artificial market model in the limiting cases of noise trader strategy, where all traders invest in the same asset type (either risky or risk-free), *i.e* they are *ordered*. Using these limits, we derive fixed points for the price growth rate, which present rough bounds for the long-term average price growth. Combining these fixed points with the necessary criteria for the emergence of ordered noise traders, we propose an analytic phase diagram of the market model.

Both, the fixed points and the phase diagram, are compared with numeric simulations. The numeric results verify the analytic fixed points. We find that the numeric phase diagram exhibits all of the features proposed analytically. However, there is one extra regime, which our limiting case analysis did not predict. The final phase diagram has five different regimes: (1) noise traders only invest in the risky asset; (2) noise traders invest either only in the risky or only in the risk-free asset, depending on the initial perturbations; (3) noise traders only invest in the risk-free asset; (4) noise traders are invested in both assets; (5) noise trader allocations undergo regular oscillations. The first four regimes are present in both the analytical and numerical phase diagram, while the fifth is only observed on the numerically.

Acknowledgements

Contents

Chapter 1

Introduction

It has been argued by Arthur (1999) that in order to fully appreciate the features of the financial markets, it is crucial to embrace the fact that the world economy is an organically evolving complex system. A natural framework for exploring such an adaptive system is presented by the so-called *agent based models* (ABMs), which focus on the properties and actions of the individual market participants. Farmer and Foley (2009) have urged the necessity and potential of employing ABMs as testing environments for policy-making. In this spirit, the thesis at hand studies the behaviour of a promising ABM proposed by Kaizoji et al. (2015), which shows transient super-exponential bubble growth and has recently been used by Kohrt (2016) as a testing environment for the Johansen-Ledoit-Sornette (JLS) bubble detection technique (Sornette and Johansen, 1997; Johansen and Sornette, 1999; Johansen et al., 2000). We analyse limiting cases of the Kaizoji et al. (2015) and Kohrt (2016) model and elaborate on different market regimes and their dependence on the herding and trend following nature of the traders.

The literature on ABMs is vast and an overarching introduction is beyond this thesis. For a general introduction to ABMs in social context, we suggest reviews by Bonabeau (2002) and Castellano et al. (2009), while the reviews by Sornette (2014), Chakraborti et al. (2011) and Samanidou et al. (2007) have a stronger focus on financial markets. Like Bonabeau put it, agent based modelling is not just a technique, but rather an ideology of bottom-up description of the world. He emphasises that one of the primary benefits of a bottom-up approach, is the capability to model the emergence of non-trivial collective behaviour. In other words, ABMs enable the modelling of systems which are more than the sum of their parts. In statistical physics, such systems are said to exhibit *emergent phenomena*. An enlightening example of emergent phenomena in the socio-economic context is the work of Schelling (1971) on racial segregation. He showed that large scale segregation, *e.g* existence of urban ghettos, does not require strong preferential differences between the

1

segregated groups. Schelling (1971) conducted manual Monte Carlo simulations of two groups of people on a square lattice. People from both groups were modelled to slightly prefer neighbours belonging to the same group. He observed that, even with very small preferential differences, large scale spatial segregation emerged.

From the viewpoint of physics, the Schelling (1971) model of segregation reminds us of a square lattice Ising model with Kawasaki dynamics, *i.e* constant magnetisation. The Ising model was originally introduced as a mathematical model of ferromagnetism (Brush, 1967). It is one of the simplest statistical physics models encompassing the struggle between order and disorder. The Ising model considers a large number of magnetic spins, pointing either up or down, positioned on some specific graph structure. The interactions between neighbouring spins tend to align the spins in the same direction, *i.e* interactions create order. Thermal noise, on the other hand, pushes the system towards random configurations. Due to this competition between imitation and random noise, in system with at least two dimensions, the model exhibits a non-trivial phase transition between para- and ferromagnetic states.

There is a long history of applying Ising based models in socio-economic context. For example, the similarity between polarised opinion and magnetisation was pointed out already by Weidlich (1971) and Galam et al. (1982). For a wider review of using Ising-like models in finance and sociology see Sornette (2014), Phan et al. (2004) or Stauffer (2013). Here, we will only provide a short motivation for usage of the Ising model in finance by its connection with discrete choice models. The latter consider systems consisting of agents, who have to choose between a finite set of alternatives. For example, such a model could be used for describing voter dynamics. One of the most common discrete choice models is the Logit model, which is very similar to Boltzmann statistics that describes the Ising model. Due to this, the Ising model can be mapped onto a binary choice model of interacting agents. For a more detailed argumentation, refer to section 20.2.1 of Phan et al. (2004).

Let us now return our focus to stock markets. Consider forming a portfolio of N different assets. This can be formulated as some specific N-choice model. The aforementioned connection has been used by Kaizoji et al. (2015), who introduced a two asset, risky and risk-free, artificial market model with two different competing trading strategies. The first group of traders, called *fundamentalists*, base their decisions on maximising their constant relative risk aversion expected utility, which results in a value investor mentality: buy-low-and-sell-high. The second group, called *noise traders*, are driven by social imitation and trend following, both of which are modelled with an Ising like dynamics. As a results of these two strategies, the artificial market has highly non-trivial dynamics. Most interestingly, the model exhibits transient faster-than-exponential bubble growth with approximate log-periodic oscillations,

which has been shown to correspond well with the characteristics observed during the 1995–2000 *dot-com* bubble.

Owing to its emergent bubble growth phenomena, the artificial market model of Kaizoji et al. (2015) can be employed as a testing environment for financial bubbles detection techniques. Recently, Kohrt (2016) has done just that. He used a modified version of their model for evaluating the potential impact of exploiting bubbles detected with the Johansen-Ledoit-Sornette (JLS) model (Sornette and Johansen, 1997; Johansen and Sornette, 1999; Johansen et al., 2000). In the JLS framework, bubbles are modelled as super-exponential price growth fuelled by imitation induced positive-feedbacks. Based on the theory of critical phenomena, during such a bubble, prices are expected to follow log-periodically oscillating power-laws, which have a finite time singularity. This singularity is explained as a reflection of the bubble bursting. Real world stock crashes have been shown to agree with JLS model (Johansen and Sornette, 1999; Johansen et al., 2000; Sornette, 2009). Kohrt (2016) showed that if bubbles are *ad-hoc* postulated to have a log-periodic power-law shape, then it is possible to compose successful JLS model based trading strategies. Moreover, he concluded that the profits of the bubble exploiters are mainly due to losses by the noise traders and successful bubble exploitation results in milder bubbles, while unsuccessful trials of exploitation lead to more sever bubbles. These are very promising results and call for further investigation.

In order to empower future work on financial bubble detection techniques, the current thesis is focused on a more in-depth analysis of the underlying market model used by Kohrt (2016). Specifically, we explore the effects of noise trader imitation and trend following in greater detail. In Kaizoji et al. (2015) and Kohrt (2016) the noise trader decision process relied equally on social factors and the market trend. We have extended the model such that we can control the relative importance of these indicators. This allows us to further investigate the impact of the noise trader strategy. More specifically, we focus on the different market regimes and conclude with profiling a phase diagram of the model. In the following we highlight the structure of this thesis.

A detailed introduction of the market model is given in chapter 2. In chapter 3 we call attention to the most relevant characteristics of the market model. Section 3.1 presents the model parameters used in this thesis and highlights the typical features of the model dynamics. In order to elaborate on the self-referential nature of the noise traders, in section 3.2 we introduce a simplified toy model of the noise trader behaviour, which is based on a coupled iterative mean-field Ising model. We show that besides the standard disordered paramagnetic and ordered ferromagnetic phases, the toy model has two additional ordered regimes which we visualise in a phase diagram. In chapter 4 we consider the limiting cases of the noise trader strategy, where all traders invest in the same asset type (either risky or risk-free), *i.e* they are ordered. Using

these special ordered states of the market, we derive two fixed points for the risky asset price growth. These fixed points effectively act as upper and lower bounds on the long-term average price growth. In chapter 5 we employ the results from chapter 4 to propose an analytical phase diagram, with four different regimes, for the market model. The analytic results are compared with numeric simulations in chapter 6, where we map a numeric phase diagram of the market model. We find that this numeric phase diagram exhibits all of the features proposed analytically, however, it has one extra regime. The final phase diagram, with five regimes, is sketched in section 6.2.3. Finally, in chapter 7 we conclude the theses.

Chapter 2

The artificial market formulation

The following chapter presents the artificial market model used in this thesis. It is an agent based model adapted from the model used in Kohrt (2016), which in itself is a modification of the model proposed in Kaizoji et al. (2015). In its core, it is a simple two asset, risky and risk-free, market model with two ideologically different trader types. The first of these are value investors named *fundamentalists*, whose investment decisions are based on maximising their constant risk averse utility. The second group, called *noise traders*, base their decision on their perception of market trend and sentiments of other traders. Both of the trader groups can be equivalently reformulated into the framework of a single representative trader. The risk-free asset has a perfectly elastic supply and constant return on investment. The risky asset, on the other hand, pays a dividend and its price is determined by a market clearing condition. We model the noise traders as giving market orders, *i.e* their investment decisions do not depend on the current price. The fundamentalists, on the other hand, are modelled following the mentality of Walrasian auctions (Walras, 1874): they simultaneously calculate their demand for each possible current price. The equilibrium risky asset price is then determined so that the total demand would equal the total supply. Before the equilibrium price formation can be discussed, the different trader strategies must be introduced. Therefore, we start by introducing the assets and the dividend process in section 2.1. We define the fundamentalist strategy in section 2.2 and the noise trader strategy in section 2.3. Finally, in section 2.4 we derive the equilibrium price equation.

2.1 The assets and the dividend process

For the sake of simplicity and clarity, the market model has only two assets: a risk-free asset and a risky asset. The risk-free asset can be thought of as cash or a government bond. It has perfect elastic supply, *i.e* it is guaranteed to pay a fixed interest r_f on an arbitrary amount of investments. It is convenient to

define the risk-free growth factor $R_f \equiv 1 + r_f$. Holding a risk-free investment of W_0 for t market time steps provides an output $W_t^{risk-free}$

$$W_t^{risk-free} = W_0 \left(1 + r_f\right)^t = W_0 R_f^t. \tag{2.1}$$

On the other hand, the risky asset can be considered to represent an index fund. At every market time step t, it will pay a dividend d_t and its price P_t is set by supply and demand. As in Kohrt (2016), the dividends undergo a multiplicative stochastic growth process with respect to time

$$d_t \equiv d_{t-1} \left(1 + r_t^d\right) = d_0 \prod_{k=1}^{t} \left(1 + r_k^d\right). \tag{2.2}$$

At time step t, the growth rate r_t^d is Gaussian distributed around a positive mean value $r_d > 0.0$ with variance σ_d^2

$$r_t^d \equiv r_d + \sigma_d u_t, \tag{2.3}$$

where the random variables u_t are identical and independently distributed according to the standard normal distribution (zero mean and unit variance)

$$u_t \overset{i.i.d}{\sim} \mathcal{N}\left(0, 1\right). $$

It is convenient to define the average dividend growth factor R_d

$$R_d \equiv 1 + r_d. \tag{2.4}$$

The total risky asset return consists of two terms. First is due to the speculative nature of the market, namely the *price return* R_t, which describes the profitability of buying with P_{t-1} and selling with P_t

$$R_t \equiv \frac{P_t}{P_{t-1}} \equiv 1 + r_t. \tag{2.5}$$

In the above, r_t is the *price return rate*. Both R_t and r_t are used throughout this thesis. The second term in the risky asset return is, of course, the *dividend yield* $\frac{d_t}{P_{t-1}}$. Thus, holding W_0 in the risky asset for t market time steps provides an output W^{risky}

$$W^{risky} = W_0 \prod_{k=1}^{t} \left(\frac{P_k}{P_{k-1}} + \frac{d_k}{P_{k-1}}\right) = W_0 \prod_{k=1}^{t} \left(R_k + \frac{d_k}{P_{k-1}}\right). \tag{2.6}$$

Naturally, the risk-free rate can be viewed as a lower base line for capital returns. Any investment strategy should at least earn as much as the risk-free asset, otherwise it should be discarded. Therefore, it is convenient to define the *excess return* of the risky asset over the risk-free rate

$$R_{\text{excess},t} \equiv R_t - R_f + \frac{d_t}{P_{t-1}} = r_t - r_f + \frac{d_t}{P_{t-1}}. \tag{2.7}$$

The excess return $R_{\text{excess},t}$ provides a measure for the profitability of the risk of buying the risky, instead of the risk-free, asset.

2.2 Fundamentalist traders

The fundamentalist traders are risk averse value investors. They allocate a fraction x^f of their wealth to the risky asset and all else into the risk-free asset. Decisions on their portfolio diversification are done via myopic mean-variance maximisation of their constant relative risk aversion expected utility. This means that, at every time step, they reconsider their wealth allocations based on the current expected portfolio value and its variance. For simplicity, all of the fundamentalists are assumed to be identical. Consequently, their behaviour can be reformulated as that of a single representative trader.

The investment strategy of the fundamentalists can be described by their choice of *risky fraction* x^f. Its derivation, presented in the following, is based on Kaizoji et al. (2015). Consider the capital gains of fundamentalists, who have at time $t-1$ allocated x_{t-1}^f of their wealth W_{t-1}^f into the risky asset and the rest into the risk-free asset. The change of their market value from W_{t-1}^f to W_t^f is given by

$$\begin{aligned} W_t^f - W_{t-1}^f &\equiv W_{t-1}^f \left[\left(1 - x_{t-1}^f\right) r_f + x_{t-1}^f \left(r_t + \frac{d_t}{P_{t-1}}\right)\right] \\ &= W_{t-1}^f \left[r_f + x_{t-1}^f \left(r_t - r_f + \frac{d_t}{P_{t-1}}\right)\right] \\ &= W_{t-1}^f \left(r_f + x_{t-1}^f R_{\text{excess},t}\right), \end{aligned} \tag{2.8}$$

where r_t and $R_{\text{excess},t}$ are the risky asset price return rate and excess return over the risk-free rate r_f, respectively, as defined in equations (2.5) and (2.7). Recall that fundamentalists are maximising their constant relative risk aversion expected utility. Their utility function $U(W)$ is chosen so that it would be compliant with their relative risk aversion γ being constant (Kaizoji et al., 2015). Consider the Arrow-Pratt measure of relative risk aversion (Pratt, 1964; Arrow, 1965, 1970)

$$\gamma\left(W\right) \equiv -W\frac{U''(W)}{U'(W)}, \tag{2.9}$$

where $U''(W)$ and $U'(W)$ are the first and second derivatives of the utility function $U(W)$ with respect to the wealth W. The risk aversion γ is constant for the isoelastic utility function

$$U\left(W\right) \equiv \begin{cases} \log W & \text{for } \gamma = 1, \\ \dfrac{W^{1-\gamma}}{1-\gamma} & \text{for } \gamma \neq 1. \end{cases} \tag{2.10}$$

As stated before, the fundamentalists are myopic mean-variance maximisers of their expected utility. This means that, at every time step t, they choose allocations x_t^f which would maximise their expected utility in the mean-variance approximation. It is shown in Kaizoji et al. (2015), that the mean-variance optimal risky fraction is independent of the trader wealth and it is given by

$$x_t^{f,\text{opt}} = \frac{1}{\gamma}\frac{\mathbb{E}_t\left[R_{\text{excess},t}\right]}{\text{Var}_t\left[R_{\text{excess},t}\right]}. \tag{2.11}$$

Here $\mathbb{E}_t\left[\cdot\right]$ and $\text{Var}_t\left[\cdot\right]$ denote the expectation and variance as estimated at time t, *i.e* all information available up-to and at time t is being taken into account. The expected value of the excess returns is given by

$$\mathbb{E}_t\left[R_{\text{excess},t}\right] = \mathbb{E}_t\left[r_{t+1}\right] - r_f + \frac{d_t}{P_t}\left(1 + r_d\right) = \mathbb{E}_t\left[R_{t+1}\right] - R_f + \frac{d_t}{P_t}R_d. \tag{2.12}$$

The fundamentalists consider the expected value of the price return $\mathbb{E}_t\left[R_{t+1}\right] \equiv \mathbb{E}_{R_t}$ and the variance of the excess returns $\text{Var}_t\left[R_{\text{excess},t}\right] \equiv \sigma_{R_{ex}}^2$ to be constants. Therefore, the risky fraction of fundamentalist traders at time t is given by

$$x_t^f \equiv \frac{\mathbb{E}_{R_t} - R_f + \frac{d_t}{P_t}R_d}{\gamma\sigma_{R_{ex}}^2} = x_{min}^f + \frac{d_t}{P_t}\frac{R_d}{\gamma\sigma_{R_{ex}}^2}, \tag{2.13}$$

where x_{min}^f is the minimum risky fraction of the fundamentalists

$$x_{min}^f \equiv \frac{\mathbb{E}_{R_t} - R_f}{\gamma\sigma_{R_{ex}}^2}. \tag{2.14}$$

Considering equation (2.13) explains why these traders are called fundamentalists. They regard the underlying "fundamental" value of the risky asset to be the dividend payments. Accordingly, they expect the long-term price growth to be due to the growth of dividends, thus $\mathbb{E}_{R_t} \approx R_d$. This does not mean that they are blind to speculative behaviour of the markets. Rather, they benchmark the risky asset against the *fundamental state*, where price and dividend growth are of similar order $R_{avg} \sim R_d$. Thus, any deviations from the *fundamental state* are perceived as investment opportunities. As is evident from equation (2.13), the current dividend-price ratio $\frac{d_t}{P_t}$ is used for probing whether the asset is over or under valued. The corresponding signal is used for a clear cut strategy: buy at low price (high $\frac{d_t}{P_t}$) and sell at high price (low $\frac{d_t}{P_t}$).

2.3 Noise traders

The noise traders are significantly different from the fundamentalists. They embody the lack-of-diversification puzzle (Kelly, 1995; Baxter and Jermann, 1997), over-reactions (De Bondt and Thaler, 1985, 1987), imitation and herding (Welch, 2000) as well as chartist trend following.

None of the N_n noise traders ever diversify their portfolio. They are always either fully invested in the risky or the risk-free asset. At every time step t, all of the noise traders have a probability to change their position: switch from risky to risk-free asset, or *vice versa*. In a few paragraphs we explain how the evolution of these *switching probabilities* incorporates imitation and trend following into the noise trader strategy. However, as a reflection of idiosyncratic properties, at any given time step t, the decisions of different noise traders are independent from each other, *i.e* their specific choices correspond to *i.i.d* random numbers. At time t, there are N_t^+ and N_t^- noise traders invested in the risky and the risk-free asset, respectively. Therefore, even as individual noise traders are proponents of the "all or nothing" mentality, on the group level they can still be characterised by their *risky fraction x_t^n*

$$x_t^n \equiv \frac{N_t^+}{N_t^+ + N_t^-} = \frac{N_t^+}{N_n} \in [0, 1]. \tag{2.15}$$

Clearly, the larger the risky fraction x^n the more noise traders are currently viewing the risky asset as a good investment, and *vice versa* for smaller x^n values. Following Lux and Marchesi (1999), the risky fraction can be mapped onto the noise trader *opinion index s*

$$s_t \equiv \frac{N_t^+ - N_t^-}{N_n} = 2x_t^n - 1 \in [-1, 1]. \tag{2.16}$$

Evidently, the sign of the opinion index indicates whether the prevailing sentiments on the risky asset are optimistic ($s_t > 0.0$) or pessimistic ($s_t < 0.0$). Zero valued opinion index corresponds to the special case when the noise traders are neutral regarding the risky asset.

As mentioned earlier, each noise trader makes the decision, whether to change their position or not, in a probabilistic manner. Those invested in the risky asset at time t, will sell their stocks and buy the risk-free asset with probability p_t^+. Similarly, traders owning the risk-free asset at time t, will decide to sell it and buy the risky asset with probability p_t^-. Accordingly, the risky fraction x^n evolves as

$$x_t^n = \frac{1}{N_n} \sum_{k=1}^{N_{t-1}^+} \left(1 - \xi_k\left(p_{t-1}^+\right)\right) + \frac{1}{N_n} \sum_{l=1}^{N_{t-1}^-} \xi_l\left(p_{t-1}^-\right), \qquad (2.17)$$

with $\xi(p)$ being Bernoulli random numbers: $\xi(p) = 1$ with probability p and $\xi(p) = 0$ with probability $1 - p$. The *switching probabilities* $p_t^\pm$ define the noise trader behaviour. Correspondingly, they should reflect their trend following and imitative nature. Thus, the dynamics of $p_t^\pm$ must depend on the sentiments of other traders and the market trend. Equation (2.16) has already defined the opinion index, which noise traders use as a proxy for other traders sentiments. Similarly, a measure of the market trend must be defined. The notion of *price momentum* H_t is used for this. Following Kaizoji et al. (2015), it is defined as an exponential moving average of the historical price returns

$$H_t \equiv \theta H_{t-1} + (1 - \theta) r_t = \theta H_{t-1} + (1 - \theta)\left(\frac{P_t}{P_{t-1}} - 1\right), \qquad (2.18)$$

where $0 \leq \theta < 1$ is a measure of the noise trader memory length. The smaller it is, the longer their memory $\tau_{\text{noise}} \sim \frac{1-\theta}{\theta}$. Now, the dynamic equation for the switching probabilities $p_t^\pm$ can be defined. It has a Ising model like structure

$$p_t^\pm = \frac{p_\pm}{2}\left(1 \mp \kappa_t\left(c_s s_t + c_h H_t\right)\right)^{[1]}. \qquad (2.19)$$

Here κ_t describes the time-dependent part of the noise trader social interaction strength. In the following, we use the naming convention introduced in Kaizoji et al. (2015), *i.e* κ_t is called the *herding propensity*. The constants p_+ and

---

[1]It should be noted that compared to the switching probabilities used in Kohrt (2016) there have been two changes. One of them is the addition of the weight coefficients c_s and c_h. This is highly relevant for the current thesis, as it enables the comparison between the effects of trend following and imitation. The second modification is a cosmetic one. Namely, the herding propensity used in Kohrt (2016) has been slightly redefined: $\kappa = \frac{\kappa^{\text{Kohrt (2016)}}}{p_+}$. This allows a more elegant formulation for equation (2.19).

p_- control the average holding time of the corresponding assets when there is no imitation nor trend following. As already mentioned in the introduction (chapter 1), this thesis focuses on the effects of the noise trader imitation and trend following. Thus we have introduced the weight coefficients c_s and c_h, which determine the relative importance of herding and trend-following to the noise traders behaviour. In order to make these effect clearer, in most of this theses a constant valued herding propensity $\kappa_t = \kappa$ is considered. Therefore, the coefficients c_s and c_h determine the feedback mechanisms that noise traders induce.

Thus far, no mention of the noise trader wealth has been made. As with fundamentalist, the noise trader strategy is also independent of their current wealth. A critical difference between the two trader types, besides the obvious, is that while all of the fundamentalists are always making identical investment choices, this is not true for noise traders. This thesis will continue in the same spirit as Kaizoji et al. (2015) by only considering the aggregate impact of the noise traders rather than describing their heterogeneity. Therefore, it is appropriate to re-frame the group of non-diversifying noise traders into a representative noise trader, who is diversifying by micro managing N_n equal sized endowments.

2.4 Equilibrium price equation

The price of the risky asset is set by the market clearing condition: the asset price P_t always has a value at which the excess demands of all market participants sum to zero. In short, an equilibrium of supply and demand is postulated. In the following, expressions for the excess demands will be derived and used for finding the equilibrium price.

First, it should be emphasised that the risky fraction does not equal the number of stocks owned. Throughout this thesis, the focus is usually on the risky fraction, or the noise trader opinion index, as they are more convenient than the number of stocks owned. Nevertheless, one should always bear in mind that constant risky fraction does not imply constant number of stocks. It only states how much of the trader's wealth has been invested into the risky asset. Taking this into account, it is helpful to define the number of stocks a trader holds at time step t

$$n_t^i \equiv \frac{x_t^i W_t^i}{P_t}, \tag{2.20}$$

where $i \in \{f, n\}$ can indicate either the fundamentalists or noise traders. Using the number of stocks the trader holds at a certain time step, it is possible to define their excess demand of the risky asset during the transition $t - 1 \to t$

$$\Delta D^i_{t-1\to t} \equiv n^i_t P_t - n^i_{t-1} P_t$$
$$= x^i_t W^i_t - x^i_{t-1} W^i_{t-1} \frac{P_t}{P_{t-1}}. \tag{2.21}$$

Now, consider the wealth W^i_t of traders, who at time $t-1$ invested x^i_{t-1} of their wealth W^i_{t-1} into the risky asset and all else into the risk-free asset

$$W^i_t = W^i_{t-1} + W^i_{t-1}\left(r_f + x^i_{t-1} R_{\text{excess},t}\right)$$
$$= W^i_{t-1}\left[R_f + x^i_{t-1}\left(R_t - R_f + \frac{d_t}{P_{t-1}}\right)\right]. \tag{2.22}$$

Inserting the wealth equation (2.22) into the excess demand equation (2.21) gives

$$\Delta D^i_{t-1\to t} = W^i_{t-1}\left\{x^i_t\left[R_f + x^i_{t-1}\left(R_t - R_f + \frac{d_t}{P_{t-1}}\right)\right] - x^i_{t-1}\frac{P_t}{P_{t-1}}\right\},$$

which can be rewritten into a more convenient format

$$\Delta D^i_{t-1\to t} = W^i_{t-1} x^i_{t-1}\left(x^i_t - 1\right)\frac{P_t}{P_{t-1}}$$
$$+ W^i_{t-1} x^i_t\left\{x^i_{t-1}\left[\frac{d_t}{P_{t-1}} - R_f\right] + R_f\right\}. \tag{2.23}$$

Substituting i with either f or n in equation (2.23) gives the excess demands for fundamentalists $D^f_{t-1\to t}$ and noise traders $D^n_{t-1\to t}$. Now, the equilibrium price P_t can be found from the market clearing condition

$$\Delta D^f_{t-1\to t} + \Delta D^n_{t-1\to t} = 0, \tag{2.24}$$

Let us note, that we are modelling the market clearing as a Walrasian auction (Walras, 1874). In a Walrasian auction, each agent simultaneously calculates their demand for each possible price value and the price is then set so that demand and supply would be in an equilibrium. Now, as it is clear from equations (2.17) and (2.19) that noise traders do not take the current price into consideration, we can conclude that fundamentalists follow the Walrasian auction mentality and noise traders just give market orders. That is,

they state the amount of assets they wish to buy or sell, independent of the price. Recall the fundamentalist risky fraction x^f given in equation (2.13). It depends linearly on the current dividend-price ratio

$$x_t^f = x_{min}^f + \frac{d_t}{P_t} \frac{R_d}{\gamma \sigma_{R_{ex}}^2}.$$

Inserting the definition of fundamentalist risky fraction in equation (2.13) together with the excess demands given by equation (2.23) for both traders into the market clearing condition in equation (2.24) gives a quadratic equation for the equilibrium price

$$a_t P_t^2 + b_t P_t + c = 0, \tag{2.25}$$

where the terms a_t, b_t and c_t are given as follows

$$a_t = \frac{1}{P_{t-1}} \left[\nu_{t-1}^{nf} x_{t-1}^n (x_t^n - 1) + x_{t-1}^f \left(x_{min}^f - 1 \right) \right], \tag{2.26}$$

$$b_t = x_{t-1}^f \frac{1}{\gamma \sigma_{R_{ex}}^2} \frac{d_t (1 + r_d)}{P_{t-1}}$$

$$+ x_{min}^f \left[x_{t-1}^f \left(\frac{d_t}{P_{t-1}} - R_f \right) + R_f \right] \tag{2.27}$$

$$+ \nu_{t-1}^{nf} x_t^n \left[x_{t-1}^n \left(\frac{d_t}{P_{t-1}} - R_f \right) + R_f \right],$$

$$c_t = \frac{d_t (1 + r_d)}{\gamma \sigma_{R_{ex}}^2} \left[x_{t-1}^f \left(\frac{d_t}{P_{t-1}} - R_f \right) + R_f \right]. \tag{2.28}$$

In the above, ν_t^{nf} is the wealth ratio

$$\nu_t^{nf} \equiv \frac{W_t^n}{W_t^f}. \tag{2.29}$$

The quadratic equation is solved by

$$P_t = \frac{-b_t \pm \sqrt{b_t^2 - 4a_t c_t}}{2a_t}. \tag{2.30}$$

Consider the signs of the terms a_t, b_t and c_t. We can take it as given that the model parameter are always such that $x_t^n - 1 \leq 0$, $x_{min}^f - 1 < 0$ and for any $x_{t-1}^i \in \{x_{t-1}^f, x_{t-1}^n\}$

13

$$x_{t-1}^i \left(\frac{d_t}{P_{t-1}} - R_f \right) + R_f > 0.0. \tag{2.31}$$

Consequently, the following inequalities are true

$$a_t < 0.0, \quad b_t \geq 0.0, \quad c_t \geq 0.0. \tag{2.32}$$

It is reasonable to expect that only positive prices are economically valid. Considering equation (2.32) it can be seen that only one of the solution in equation (2.30) gives positive prices

$$P_t = \frac{-b_t - \sqrt{b_t^2 - 4a_t c_t}}{2a_t} = \frac{b_t + \sqrt{b_t^2 + 4|a_t|c_t}}{2|a_t|}.$$

Chapter 3

Market model characteristics

In chapter 2 we have introduced the artificial market model studied in this thesis. Based on the previous work of Kohrt (2016) and Kaizoji et al. (2015), it consists of two trader types, the *fundamentalists* and the *noise traders*, investing in a two asset market. The first asset is a fixed interest rate risk-free asset, while the other is a dividend paying risky asset, whose price is determined by supply and demand. The fundamentalists maximise their constant risk aversion expected utility, which leads them to the buy-low-and-sell-high strategy: their risky fraction x_t^f is a linear function of the risky asset dividend-price ratio $\frac{d_t}{P_t}$. Consequently, they induce negative feedback to deviation from the *fundamental state* $R_{avg} \sim R_d$. The noise traders, however, invest according to social factors and market trend, which they measure with the noise trader opinion index s_t and the price momentum H_t. Their decision process is self-referential in nature. Depending on the signs of the imitation and trend following weight coefficients, c_s and c_h, they have either *conformist* or *contrarian* attitudes towards opinion s_t and momentum H_t. Correspondingly, their behaviour imposes a non-trivial combination of feedback loops upon the market.

This chapter aims to give a qualitative overview of characteristic features of the above mentioned market model. Section 3.1 considers the artificial market model in general, while section 3.2 turns a tighter focus on the Ising-like noise trader behaviour by introducing an iterative coupled mean-field Ising based toy model.

3.1 Typical model dynamics

In this section, we elaborate on the typical set-up and features of the artificial market model (see chapter 2). First, in section 3.1.1, we present the general parameter set-up used throughout this thesis. Following that, in section 3.1.2, we qualitatively highlight several important features of market dynamics in

two sets of time series plots in figures 3.1 and 3.2. Both of these correspond to a market where $c_s = c_h = 1$, *i.e* noise traders have a *full-conformist* attitude. The difference, between the two considered markets, is in the functional form of the noise trader herding propensity κ_t: figure 3.1 corresponds to a constant herding propensity, while figure 3.2 corresponds to an Ornstein-Uhlenbeck herding propensity, which is adapted from Kaizoji et al. (2015).

3.1.1 Model parameters and set-up

In chapter 2 we introduced the mathematical formulation of the artificial market model studied in this thesis. The model is adapted from the works of Kohrt (2016) and Kaizoji et al. (2015). In this section, we present the general parameter set used throughout the thesis. As we only ever make slight changes to the model parameters, we find it convenient to define the most often used *basic parameter set*. The full basic parameter set is listed in table 3.1.

Table 3.1: The basic parameter set used for the market simulations throughout the thesis. In cases where different parameter set is used, the difference is always specifically highlighted.

$x_0^n = 0.5$	$\nu_0^{nf} = 1$	$p_+ = 0.199375$	$p_- = 0.200625$
$x_0^f = 0.5$	$d_0 = 0.00016$	$R_d = 1.00016$	$H_0 = 0.00016$
$\theta = 0.99$	$\mathbb{E}_{R_t} = 1.00016$	$P_0 = 1.0$	$R_f = 1.00008$
$N_n = 1000$	$\sigma_d = 0.000016$	$\sigma_{R_{ex}}^2 = 0.02$	$\kappa = 0.98$

Note, that table 3.1 does not give an explicit value to the fundamentalist constant risk aversion γ. However, using the definition of the fundamentalist risky fraction, given in equation (2.13), we can express the constant risk aversion γ as a function of $\mathbb{E}_{R_t}$, R_f, d_0, P_0 and x_0^f

$$\gamma = \frac{\mathbb{E}_{R_t} - R_f + \frac{d_0}{P_0} R_d}{x_0^f \sigma_{R_{ex}}^2}. \tag{3.1}$$

Let us consider the basic parameter set given in table 3.1. We can see that both trader types start out with the same wealth, *i.e* their wealth ratio is $\nu_0^{nf} = 1$, and their initial allocations follow an equal weights portfolio $x_0^f = x_0^n = 0.5$. There are $N_n = 1000$ noise traders with a memory parameter $\theta = 0.99$, which corresponds to a memory length ~ 100 simulation time steps. The constants p_+ and p_- are defined as in Kohrt (2016). Notice, that $p_- > p_+$, which means that on average noise trader hold the risky asset longer than the risk-free asset.

Similarly, the mean value of the herding propensity $\kappa = 0.98$ is the same as in Kohrt (2016)[1].

As in Kohrt (2016), we start with a unit price $P_0 = 1$ and let the initial dividends be $d_0 = \frac{0.04}{250} = 0.00016$. Thus, if one simulation time step represents one day, then the initial yearly dividend yield is 4%. The average dividend growth rate is also set to $r_d = 0.00016$, thus $R_d = 1.00016$. Notice, that the initial price momentum equals the dividend growth rate $H_0 = r_d = 0.00016$ and the fundamentalists expectation for the price growth equals the average dividend growth $\mathbb{E}_{R_t} = R_d = 1.00016$. The risk-free rate is set to be half of the dividend rate $r_f = 0.5 r_d$ and thus the risk-free growth $R_f = 1.00008$. Similarly to Kohrt (2016), the standard deviation of the dividend process $\sigma_d = 0.1 r_d$ and the constant fundamentalists perception of the standard deviation of the excess returns $\sigma_{R_{ex}}^2 = 0.02$.

It might be argued that the standard deviation of the dividend process σ_d, given in table 3.1, is too small. Indeed, with the basic parameters set, the dividend process is nearly deterministic. However, in chapter 6 we show that the numeric phase diagram is rather robust to changes in σ_d: even for $\sigma_d \approx 6 r_d$ the phase diagram is the same as for $\sigma_d = 0.1 r_d$. Thus, for the purposes of this thesis, taking $\sigma_d = 0.1 r_d$ is still reasonable. We stress the fact that calibration of the model to the real world market is beyond the scope of this thesis. Rather we aim to compile a phase diagram of the market model on the c_s-c_h plane. Nevertheless, in the following we find it worthwhile to discuss one of the key ideas for connecting the model parameters to the real world.

Thus far, we have only used the notion of a simulation time step, or equivalently an iteration step $t \rightarrow t + 1$. However, in order to make a connection between the model and the real-world, we need to know what is the time scale of the market simulations. We now argue, that this time scale is actually a good starting point for calibrating the model to the real world. It is important to recall that the typical real world daily volatility is around 1% (Sornette, 2009). Now, if we wish to calibrate our model to the real world, of course, we wish to have the same typical daily volatility. The key idea is to reverse engineer the correct time scale of the simulations. We start by roughly approximating the price returns with a Wiener process. Then, we know that the relation between period T_a volatility σ_{T_a} and period T_b volatility σ_{T_b} is given by

$$\sigma_{T_a} = \sigma_{T_b} \sqrt{\frac{T_a}{T_b}}. \tag{3.2}$$

---

[1] Recall that compared to Kohrt (2016) the noise trader switching probability equation (2.19) is modified and the herding propensity is re-defined as: $\kappa = \frac{\kappa^{\text{Kohrt (2016)}}}{p_+}$. Thus the exact numeric value of κ is not the same as in Kohrt (2016), rather the product κp_+ is numerically equal the herding propensity used in Kohrt (2016).

This allows us to evaluate the number of time steps T_N, so that the T_N time step volatility would match the daily volatility $\sigma_{T_N} \equiv \sigma_{daily}$

$$T_N = \left(\frac{\sigma_{daily}}{\sigma_{sim}}\right)^2 = \left(\frac{0.01}{\sigma_{sim}}\right)^2, \tag{3.3}$$

σ_{sim} is the one time step volatility of market model, *i.e* the one time step standard deviation of the price returns. Therefore a single time step in our simulation corresponds to τ days, where τ is given by

$$\tau = \frac{1}{T_N}. \tag{3.4}$$

As pointed out earlier, calibration of the model is beyond the scope of this thesis. Therefore, throughout the thesis, we find it more convenient to measure "time" in simulation time steps not in days. Nevertheless, we provided the estimated simulation time scale τ for each of the market model time series plots found in this thesis. Additionally, in chapter 6 we provide a colour-coded heat-map of the time scale τ values over the c_s-c_h plane for the basic parameter set in table 3.1.

Finally, let us consider the noise trader herding propensity κ_t. As stated before, in this thesis we study the effects of noise trader imitation and trend following by introducing weight coefficients c_s and c_h for the opinion index s_t and the price momentum H_t respectively (see equation (2.19)). In the works of Kohrt (2016) and Kaizoji et al. (2015), these coefficients were equal to one. Also, both of them used a time-dependent herding propensity κ_t. In Kaizoji et al. (2015) the herding propensity followed an Ornstein–Uhlenbeck process. Kohrt (2016), on the other hand, used a constant κ_t for most of the time, but had transient log-periodic signals imprinted into κ_t, such that *ad-hoc* log-periodic power-law bubbles could be generated in a controlled manner. In this thesis we are using a constant valued herding propensity $\kappa = 0.98$. This is because a time-dependent herding propensity can be interpreted as moving along a line in the c_s-c_h plane. The slope of this line is set by the ratio of the coefficients c_s and c_h used in equation (2.19). Thus, in order to analyse the different effects of opinion and momentum, it is helpful to set the herding propensity to a constant value.

Nevertheless, the time series we present in section 3.1.2 are generated using both the constant herding propensity $\kappa = 0.98$ (figure 3.1) and a Ornstein–Uhlenbeck herding propensity (figure 3.2). This is done exactly because a time-dependent herding propensity can be seen as moving on the c_s-c_h plane. Thus, using the Ornstein–Uhlenbeck κ_t, we can compactly see the characteristic features of different market regimes. In chapter 6, we present the time

series for all of the different market regimes separately. Before turning to the time series in section 3.1.2, let us define the Ornstein–Uhlenbeck κ_t

$$\kappa_{t+1} = \kappa_t + \eta \left(\kappa_\mu - \kappa_t \right) + \sigma_\kappa u_t,$$
$$\eta = \frac{1}{\Delta T} \log \left(\frac{0.2 \frac{p_-}{p_+}}{\frac{p_-}{p_+} - \kappa_\mu} \right), \quad \sigma_\kappa = 0.2 p_- \sqrt{2\eta}. \tag{3.5}$$

In the above, the mean value of the Ornstein-Uhlenbeck herding propensity is equal to the constant herding propensity $\kappa_\mu = \kappa = 0.98$. The mean-reversion rate η and the steps size σ_κ are calculated using the formulas from Kaizoji et al. (2015)[2]. Here $\Delta T = 20$ and thus the mean-reversion rate $\eta \approx 0.044$ and the step size $\sigma_\kappa \approx 0.006$.

3.1.2 Qualitative time series description

In section 3.1.1, we presented the common set-up of the market model throughout the thesis. Here, we give a qualitative overview of the characteristic market dynamics. We base this description on the time series shown in figures 3.1 and 3.2. In the following, we point out key features of the typical model behaviour, several of which are essential for the analysis in chapters 4 and 5.

The general structure of figures 3.1 and 3.2 is the following: the plots show eight panels, which contain time series for the risky asset price P_t, return rate r_t, momentum H_t, dividend-price ratio $\frac{d_t}{P_t}$, noise trader switching probabilities $p_t^\pm$, both of the risky fractions x_t^f and x_t^n, the traders wealth ratio $\nu_t^{nf} = W_t^n / W_t^f$ and the noise trader herding propensity κ_t. In order to emphasise that the price momentum H_t is the exponential moving average of the price return rate r_t, the momentum has also been plotted onto the price return rate panel. Similarly, to hold an comparison with the risky asset dividends and price, the average dividend growth rate r_d has been plotted onto the momentum panel.

The asset price P_t is depicted on a log-linear scale and all other time series are on a linear scale. Note, that the notation $1e - x$ indicates that the values on the y-axis are to be multiplied with 10^{-x}. Time series in both figures 3.1 and 3.2 are shown for the first $T = 5000$ time steps. Based on equating the daily model- and real-volatility, we estimate that each time step in figures 3.1 and 3.2 correspond to $\tau \approx 1.3$–1.4 days. In both figures 3.1 and 3.2, a market with unit weight coefficients $c_s = c_h = 1$ and the basic parameter set (table 3.1) is illustrated. The difference between figures 3.1 and 3.2 is in the herding

---

[2]The formulas have been modified to correspond to our different definition of equation (2.19).

propensity used: figure 3.1 corresponds to the constant herding propensity $\kappa = 0.98$ and figure 3.2 to the Ornstein-Uhlenbeck herding propensity defined in the end of section 3.1.1.

In the following we emphasise on qualitative features of the time series in figure 3.1. First, the switching probabilities look like mirror images of each other, which reflects the structure of the switching probability dynamic equation (2.19). A similar feature can be seen for the momentum and the dividend-price ratio: they are roughly moving in the opposite directions of each other. This becomes more pronounced during periods of high volatility. For example, examine the behaviour for the interval $t = 2000$–3000. Let us now consider the risky fractions. Recall, that the fundamentalist risky fraction x^f is a linear function of the dividend-price ratio (see equation (2.13)). With careful observations it is possible to detect that indeed fundamentalists follow the same movements as the dividend-price ratio. Due to the relatively small variance of the fundamentalists allocations, this is rather hard to notice in figure 3.1. Now, consider that the dividend-price ratio encodes fluctuations from both the price and the dividends. Nevertheless, we see that the noise traders, who follow the momentum and the opinion index, have much larger variations than fundamentalists. From this, we can conclude that noise traders self-referential decision making process is more prone to signal amplifications than the fundamentalist strategy.

We have seen that even with a constant herding propensity, the market can show relatively volatile periods. For the following, it is more convenient to turn to figure 3.2, because its more volatile nature makes noticing the market features easier. For example, we can now detect a mirroring effect for the risky fractions. The fundamentalists are always moving in the opposite direction to the noise traders. A rather more interesting feature of figure 3.2 is the existence of transient periods of extreme behaviour. Recall that the asset price P_t is plotted with a log-linear scale: a linear line on the price panel indicates an exponential relation. Thus, during these transient extreme periods the price is growing or declining super-exponentially; $i.e$ there are bubbles. We will now discuss how these bubbles shed light onto some of the main ideas used in chapters 4 and 5 for forming the analytical phase diagram.

First, we can observe that all bubbles end abruptly with a plateau like shape. Looking at the noise trader risky fraction x_t^n, we can find the reason for these abrupt stops. These plateaus correspond to noise traders reaching their maximum or minimum risky fraction, $i.e$ they become polarised into $x^n = 1$ or $x^n = 0$. Interestingly, the noise traders tend to have a transient lock-in effect to these polarised investment decisions. Consequently, there is a period during which no radical changes happen on the market. From the noise trader switching probabilities, we can observe a natural cause for these lock-in effects. Namely, during a lock-in, the corresponding switching probability, either p_t^+

(risk-free $\rightarrow$ risky) or p_t^- (risky $\rightarrow$ risk-free), is non-positive. As the simulation code treats all non-positive probabilities as zero valued, we can conclude that there is an actual lock in: the probability for noise traders to change their position is zero.

It is helpful to analyse these lock-in periods in more detail. For convenience, in the following the noise trader lock-in effect is referred to as just *lock-in*. Let us start with considering the price return rate r_t. We can see that during lock-ins, r_t is effectively constant. This results in an exponential decay or growth of the price momentum H_t, as is expected from the definition of H_t (see equation (2.18)). Now, let us take the dividend-price ratio. Evidently, during lock-ins the dividend-price ratio is nearly constant, which indicates that the average price and dividend growths are similar $R_{avg} \sim R_d$. In section 4.3 we analytically show that indeed, for both limiting cases $x^n = 1$ and $x^n = 0$, the price growth has fixed points, which are functions of the dividend and risk-free rates. For now, however, it is sufficient to recognize that during noise trader lock-ins, *i.e* when only fundamentalists are actively shaping the market, the price growth is similar to the dividend growth. From this we can claim that bubbles are driven by noise traders.

Finally, we call attention to the wealth ratio ν^{nf}. In both figures 3.1 and 3.2, there are two features to note. Firstly, the wealth ratio has an underlying downward trend: it appears that with these parameters on average the fundamentalists strategy earns more. Secondly, the wealth ν^{nf} ratio peaks together with the noise trader risky fraction x^n. There are two reasons for this. One is that the risk-free rate is smaller than the dividend rate $r_f < r_d$, *i.e* on average the risky asset pays more than the risk-free asset. A more subtle reason is, that during transient super-exponential price growth, the wealth invested into the risky asset temporarily grows super-exponentially. In other words, bubbles create fictitious riches.

We finish by highlighting features most relevant for chapters 4 and 5:

1. For certain $\kappa_t c_s$ and $\kappa_t c_h$ values, noise traders drive the price to grow or decay super-exponentially.

2. Extreme price growth can lead to non-positive noise trader switching probabilities and create a lock-in effect.

3. As the fundamentalists strategy depends linearly on the dividend-price ratio, they enforce a connection between the price and the dividends.

4. The self-referential nature of noise traders induces strong amplification even for a constant herding propensity.

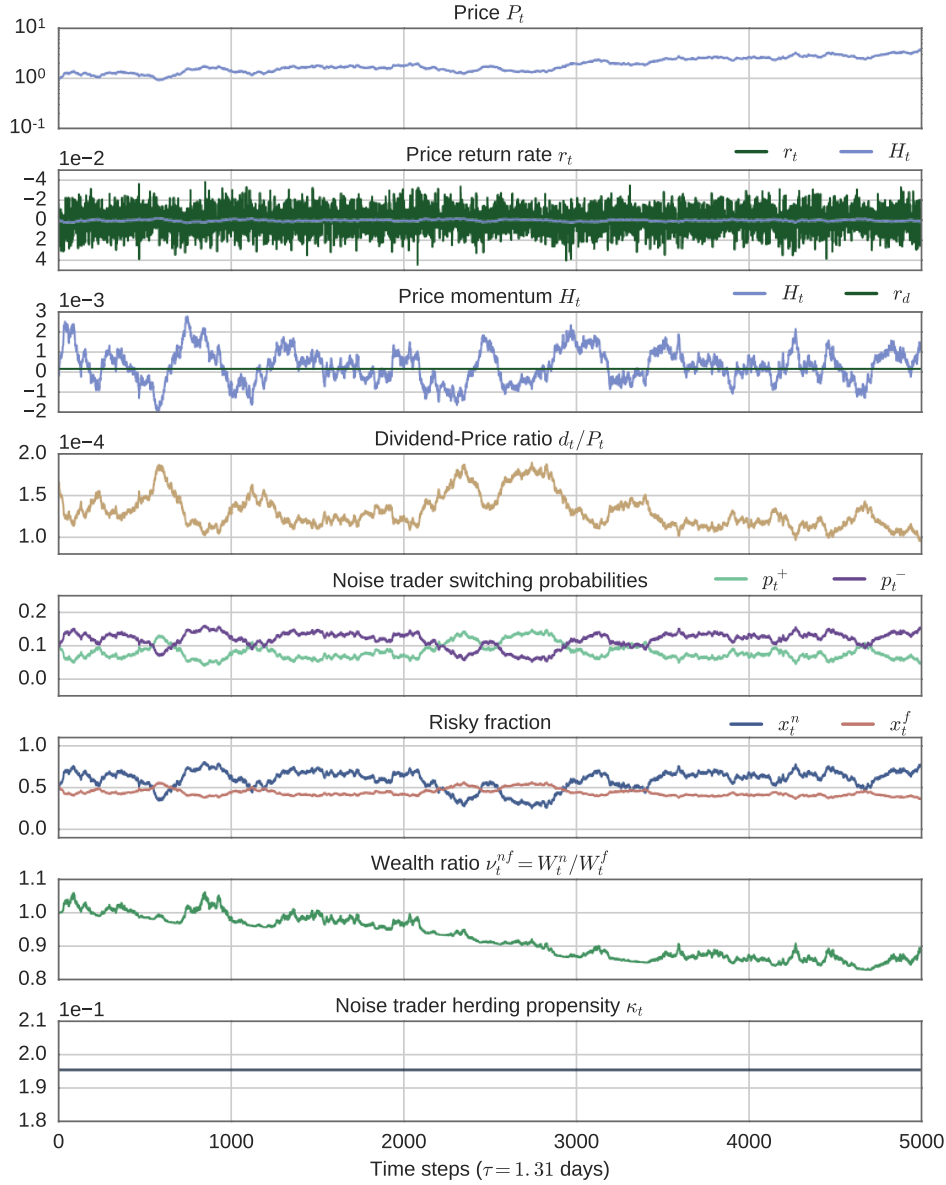5. On average, the risky asset pays more than the risk-free asset.

Figure 3.1: Typical time series of the market model (see chapter 2) with unit noise trader imitation and trend following weight coefficients, $c_s = 1.0$ and $c_h = 1.0$, and the constant herding propensity $\kappa_t = \kappa = 0.98$. The rest of the market parameters correspond to the *basic parameter set* given in table 3.1. Based on equating the daily model- and real-volatility, we estimate that each time step correspond to $\tau \approx 1.31$ days. Notice that the switching probabilities $p_t^{\pm}$ are each others mirror images. Similar mirroring feature can roughly be observed for momentum H_t and dividend-price ratio d_t/P_t as well. Recall, that the fundamentalists risky fraction x_t^f is a linear function of the dividend-price ratio. Noise traders, however, follow the opinion index $s_t = 2x_t^n - 1$ and the momentum H_t. We can see, that the noise traders self-referential investment decisions are much more volatile than the fundamentalists strategy. Finally, notice that the wealth ratio ν_t^{nf} peaks together with the noise trader risky fraction x_t^n, which indicates that the risky asset pays more than the risk-free asset.
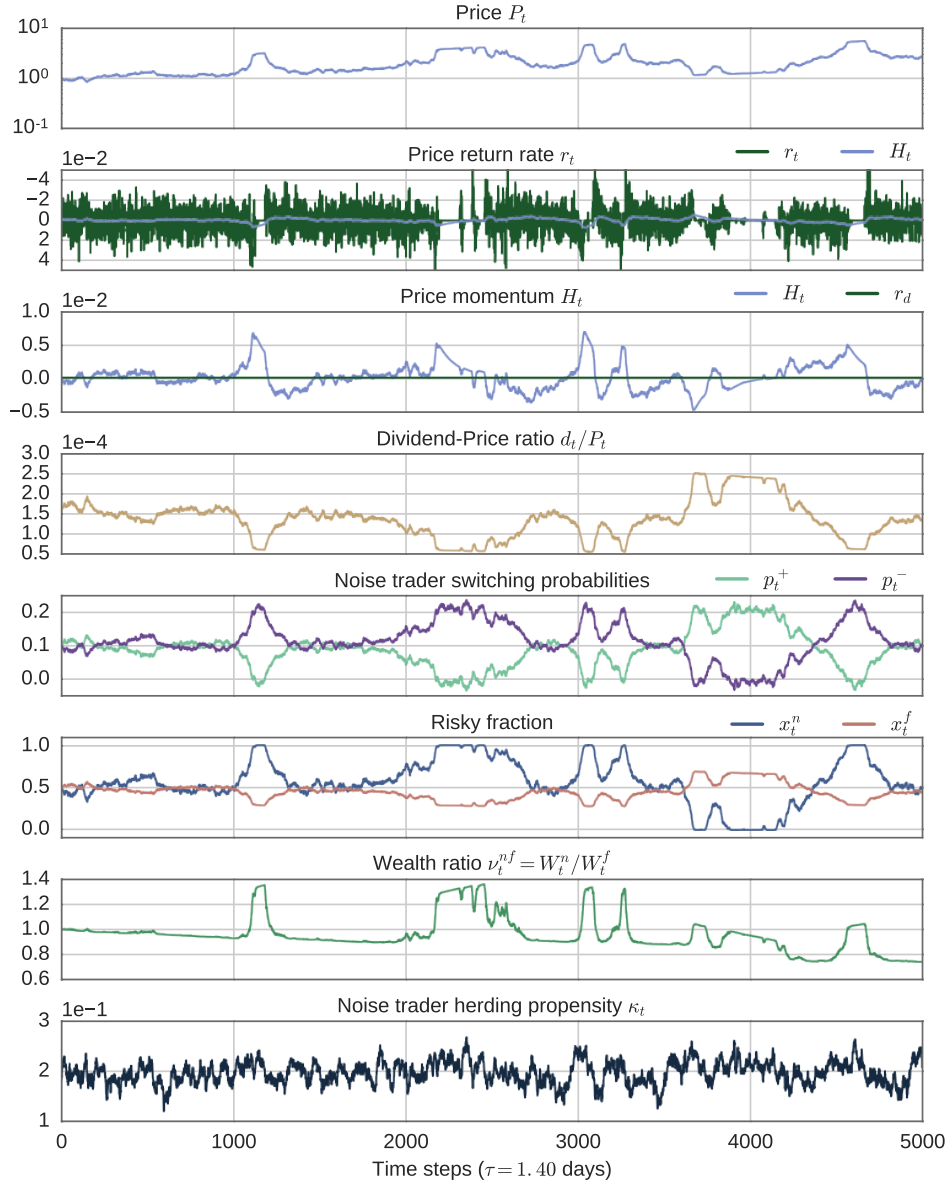
22

Figure 3.2: Typical time series of the market model (see chapter 2) with unit noise trader imitation and trend following weight coefficients, $c_s = 1.0$ and $c_h = 1.0$, and the Ornstein–Uhlenbeck herding propensity κ_t defined by equation (3.5). The rest of the market parameters correspond to the *basic parameter set* given in table 3.1. Based on equating the daily model- and real-volatility, we estimate that each time step correspond to $\tau \approx 1.40$ days. Notice that all transient periods with super-exponential price movements end with a plateau like shape. This can be explained by considering the noise traders. During these super-exponential price movements, one of the noise trader switching probabilities becomes non-positive, thus creating a transient lock-in effect for the corresponding asset type, which leads to polarised noise traders ($x^n \in \{0, 1\}$). While noise traders are locked-in, the market is calm: average price and dividend growth is of similar order $R_{avg} \sim R_d$. As during noise trader lock-in only fundamentalists actively effect the market, the above supports the claim that fundamentalists enforce a connection between the price and dividends. Finally, notice that the wealth ratio ν_t^{nf} peaks together with the noise trader risky fraction x_t^n, which is mainly due to temporary wealth growth during the bubble.

23

3.2   Toy model

In this section we introduce a simplified toy model, which qualitatively reproduces some of the characteristics of the more complicated artificial market model presented in chapter 2. We have already argued that the fundamentalists strategy enforces a connection between the risky asset price and dividends. Their behaviour is stabilising the system so that the average price and dividend growth is of similar magnitude $R_{avg} \sim R_d$. The noise traders strategy, however, introduces self-referential feedback loops. It is the effect of this self-enforcing behaviour that we aim to study with the toy model present in this section.

As already mentioned in chapter 1, using Ising based models of opinion dynamics dates back to the works of Weidlich (1971) and Galam et al. (1982). As stated before, that the Ising model is a mathematical model of ferromagnetism (Brush, 1967). It considers a large number of magnetic spins on a lattice structure, so that the interaction between neighbouring spins tends to order the spins in the same direction. At the same time, thermal noise is causing random fluctuations and thus introducing disorder. The Ising model is one of the simplest statistical physics models for describing the competition between imitation induced order and noise induced disorder. In chapter 1 we discussed how the Ising model can be linked with a binary choice model of interacting agents. This connection is used in our artificial market model: the noise trader switching probabilities have an Ising-like dynamic equation (2.19). Due to this, we base our toy model on the mean-field Ising model, which in itself is a common toy model for the full Ising model.

In sections 3.2.1 and 3.2.2 we briefly introduce the mean-field Ising model and define the used toy model, respectively. Finally, in section 3.2.3, we construct a numeric phase diagram of the toy model on the c_s-c_h plane.

3.2.1   The mean-field Ising model

In this section, we give a short overview of the mean-field Ising model. As stated before, the Ising model is a model for explaining the transition between paramagnetic (disordered spins) and ferromagnetic (ordered spins) phases. In statistical physics, when considering phase transitions, it is common to define a so-called *order parameter*, which distinguishes between the different phases. For magnetic phase transitions, a suitable order parameter is the average magnetisation m, as this is zero for the paramagnetic regime and non-zero in the ferromagnetic regime. Let us now write the Hamiltonian, *i.e* the energy of the system, for the Ising model

$$\mathcal{H} = -J \sum_{<i,j>} \sigma_i \sigma_j - H_{ex} \sum_i \sigma_i, \qquad (3.6)$$

where $< i, j >$ indicates that spins σ_i and σ_j are nearest neighbours, J is the interaction strength between spins and H_{ex} is the external magnetic field.

In the mean-field paradigm, instead of separately considering the effects of all spins on their neighbours, we approximate these effects with that of the mean magnetisation $\langle \sigma \rangle \equiv m$. Thus the mean-field Hamiltonian reads

$$\mathcal{H}_{mf} = -Jm \sum_i \sum_{j=1}^{z_i} \sigma_j - H_{ex} \sum_i \sigma_i = -(Jmz + H_{ex}) \sum_i \sigma_i, \qquad (3.7)$$

where z_i is the number of nearest neighbours of spin σ_i and z is the average number of nearest neighbours for each spin. Observe that the Hamiltonian $\mathcal{H}_{mf}$ in equation (3.7) is equivalent to the Hamiltonian of non-interacting spins in an effective field $H_{eff} \equiv Jmz + H_{ex}$. Using equation (3.7) we can express the single spin Boltzmann distribution

$$p(\sigma_i) = \frac{e^{\beta H_{eff} \sigma_i}}{\sum_{\sigma_j \in \{+1, -1\}} e^{\beta H_{eff} \sigma_j}}. \qquad (3.8)$$

In the above, $\beta = \frac{1}{Tk_B}$ is the inverse temperature, where T is the temperature and k_B is the Boltzmann factor. This leaves us with the final step in the mean-field approximation. Namely the self-consistency condition, which demands that the mean magnetisation, calculated using the single spin distribution function in equation (3.8), has to equal the mean magnetisation used to define the distribution function $\langle \sigma \rangle = m$. Therefore, we get

$$m = \sum_{\sigma_j \in \{+1, -1\}} p(\sigma_j) \sigma_j = \frac{e^{\beta H_{eff}} - e^{-\beta H_{eff}}}{e^{\beta H_{eff}} + e^{-\beta H_{eff}}} = \tanh \beta (Jmz + H_{ex}). \qquad (3.9)$$

It is convenient to analyse the self-consistency condition in equation (3.9) graphically. This is done in figure 3.3. It shows two panels, one with a zero external field $H_{ex} = 0$ for illustrating the effects of temperature (figure 3.3a) and the other for illustrating the effects of the external field (figure 3.3b). Both panels show a plane where both axes correspond to the mean magnetisation m. Thus, the self-consistency condition $m = m$ defines a line with a unit slope on these planes. The self-consistency condition is satisfied only at the points where the self-consistency line $m = m$ and the the hyperbolic tangent magnetisation $m = \tanh \beta (Jmz + H_{ex})$ cross.

Let us first discuss the effects of temperature. In figure 3.3a three hyperbolic tangent lines are drawn using equation (3.9) with different inverse temperature β values. Notice, that there is a special inverse temperature value, for

(a) Temperature dependence ($H_{ex} = 0$) (b) Field dependence ($\beta < \beta_c$)
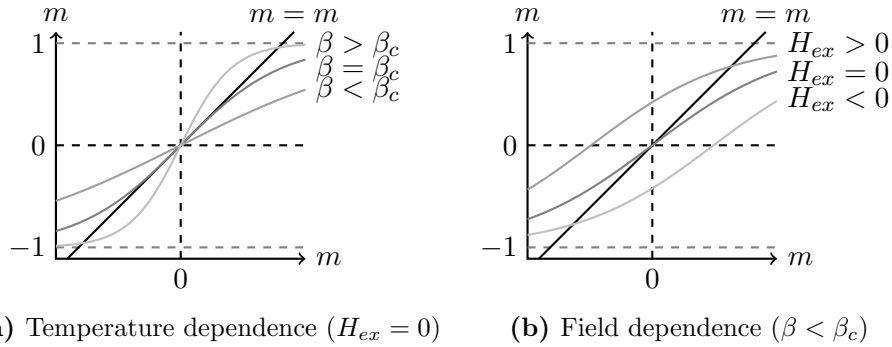
Figure 3.3: Graphical analysis of the self-consistency equation (3.9) of the mean-field Ising model. Panel (a) demonstrates the temperature dependence of the system and panel (b) demonstrates the field dependence. In (a) there is no external field $H_{ex} = 0$ and in (b) the inverse temperature is below the critical inverse temperature $\beta < \beta_c$ (above the critical temperature $T > T_c$). Both panels show a plane where both axes correspond to the mean magnetisation m and thus the diagonal straight black line corresponds to the self-consistency condition $m = m$. Panel (a) demonstrates that for inverse temperatures below the critical temperature $\beta < \beta_c$, the self-consistency condition is only satisfied at $m = 0$, while above the critical inverse temperature $\beta > \beta_c$ the self-consistency condition is also satisfied at two non-zero magnetisation values. It can be shown (not done here) that the for $\beta > beta_c$ these non-zero magnetisations are stable, while $m = 0$ is not. Thus the system is in the ordered ferromagnetic phase. The critical inverse temperature is given by the condition that at $m = 0$ the slopes of the straight line and the hyperbolic tangent are equal, which gives equation (3.10) and leads to equation (3.11). From panel (b) we see, that even at inverse temperatures below the critical value $\beta < \beta_c$, if there is a non-zero external field $H_{ex} \neq 0$, then the self-consistency condition is satisfied at a non-zero magnetisation value. It can be shown (not done here) that in case of inverse temperature values above the critical value $\beta > \beta_c$, a non-zero external field breaks the symmetry between the positive and negative ordering.

which the slope of the hyperbolic tangent is exactly one at the origin, *i.e* it overlaps with the self-consistency line $m = m$. This is the *critical inverse temperature* β_c, which corresponds to the *critical temperature* T_c. If the inverse temperature is lower than the critical value $\beta < \beta_c$ ($T > T_c$), the hyperbolic tangent crosses the self-consistency line only at the origin, meaning that the self-consistency condition is satisfied only for zero mean magnetisation $m = 0$. On the other hand, if the inverse temperature is higher than the critical value $\beta > \beta_c$ ($T < T_c$), then the lines cross at three points and the self-consistency condition is satisfied also for non-zero magnetisation values $m = \pm m_0$. It can be shown, that for $\beta > \beta_c$ the non-zero magnetisation values correspond to stable minima, while the zero magnetisation is unstable. Therefore, the critical temperature marks the boundary between para- and ferromagnetic phases. We can find the value of the critical inverse temperature β_c, by demanding that the slope of figure 3.3 at the origin is equal to one

$$1 = \frac{d}{dm} \tanh \beta \left(Jmz + H_{ex} \right) \bigg|_{m=0, H_{ex}=0} = \beta Jz. \tag{3.10}$$

Therefore, the critical inverse temperature β_c is given by

$$\beta_c = \frac{1}{Jz}. \tag{3.11}$$

Let us shortly discuss the effects of the external field as well. In figure 3.3b three hyperbolic tangent lines are drawn using equation (3.9) with an inverse temperature below the critical value $\beta < \beta_c$ and with zero, positive and negative external field values. We can see that turning on the external field shifts the hyperbolic tangent, so that the self-consistency condition is satisfied for a single non-zero magnetisation already below the critical inverse temperature. Thus, the external field forces the system to order. It can also be shown that in case of inverse temperature values above the critical value $\beta > \beta_c$, a non-zero external field breaks the symmetry between the positive and negative ordering.

3.2.2 Toy model definition

Let us now turn to our toy model. As stated above, this model is designed to highlight the effects of the self-referential feedback loops in the noise trader strategy. We have already pointed out that the Ising model can be linked with a binary choice model of interacting agents. Of course, interacting binary decision makers is exactly what our noise traders are: they constantly have to decide whether to buy the risky or risk-free asset. The interaction between the noise traders is represented by their imitating and trend following tendencies. We can see two mediators for these interactions. First is the market: the noise traders are following the price momentum, which reflects the composition of the decisions of all the market participants. Second is the overall social communications between the noise traders, *i.e* they are aware of the noise trader opinion index. The respective interaction strengths are given by the products of the herding propensity κ_t and the corresponding weight coefficients c_h and c_s.

We can incorporate this into the mean-field Ising framework, by modelling the opinion index s as corresponding to the magnetisation and the momentum H as corresponding to the external field. The interaction strengths are represented by $\kappa_t c_s$ and $\kappa_t c_h$. For the sake of parsimony, in the following we only consider cases with constant herding propensity $\kappa_t = \kappa$. Thus, for the toy model, the mean-field magnetisation equation (3.9) turns into

$$s = \tanh \left[\kappa \left(c_s s + c_h H \right) \right]. \tag{3.12}$$

Consider, for a moment, the critical herding propensity κ_c^0 for which equation (3.12) satisfies the self-consistency condition for a non-zero opinion $|s| > 0$ at a zero valued momentum. Similarly to the derivation of the critical inverse temperature in section 3.2.1 (see equations (3.10) and (3.11)) we get

$$1 = \frac{d}{ds} \tanh \kappa \left(c_s s + c_h H \right) \Big|_{s=0, H=0} \quad \Rightarrow \quad \kappa_c^0 = \frac{1}{c_s}. \qquad (3.13)$$

Recall that, in the market model, the noise traders are dynamically updating their investment positions. Therefore, it is reasonable to change equation (3.12) into a dynamical formulation, so that s_t depends on the previous opinion and momentum values $s_t = s_t \left(s_{t-1}, H_{t-1} \right)$. Besides the opinion, we need to define the evolution of the momentum H_t. In the market model, the price momentum is the exponential moving average of the price return rate; it is defined by equation (2.18). We wish to use a similar structure in our toy model. The main question is how to model the non-trivial relation between the opinion and the price returns. For the sake of simplicity, we approximate this with a one-to-one correspondence between price return rate r_t and the noise trader opinion index s_t. Thus, the toy model is given by the following set of iterative equations

$$\begin{cases} s_{t+1} & = \tanh \left[\kappa \left(c_s s_t + c_h H_t \right) \right], \\ H_{t+1} & = \theta H_t + (1 - \theta) \, s_t. \end{cases} \qquad (3.14)$$

The toy model has some features, which resemble the full artificial market (see chapter 2). For, example the term inside the hyperbolic tangent $\kappa \left(c_s s_t + c_h H_t \right)$ is exactly the non-constant term in the noise trader switching probability equation (2.19). On the other hand, there also are several differences between the two models. Let us highlight these differences:

1. The toy model does not explicitly consider the fundamentalists. This can be interpreted in two ways: (a) the toy model considers a market which only consists of noise traders; (b) in the toy model, the effect of the fundamentalists is decimated into the coefficients c_s and c_h.

2. The toy model approximates the non-trivial functional relation between the opinion index s and the price return rate r_t with a simple one-to-one correspondence.

3. In the toy model the stochastic dynamics of the noise traders risky fraction, given by equation (2.17), is approximated by a deterministic threshold-like behaviour of the hyperbolic tangent function.

It is enlightening to consider the fixed point of the iterative system given in equation (3.14). Let us assume that a fixed point exists

$$H_{t+1} = H_t = H \ \text{ and } \ s_{t+1} = s_t = s. \tag{3.15}$$

From equation (3.14), it is straightforward to see that momentum fixed point must equal the opinion fixed point

$$H = \theta H + (1 - \theta)\, s \ \ \Rightarrow \ \ H = s. \tag{3.16}$$

Inserting the above into the fixed point equation for the opinion, we get

$$s = \tanh\Big[s\kappa\,(c_s + c_h) \Big]. \tag{3.17}$$

We can find the critical herding propensity κ_c, of the fixed point in equation (3.17), by again using the self-consistency condition

$$1 = \frac{d}{ds}\tanh \kappa\,(c_s + c_h)\Big|_{s=0} \ \ \Rightarrow \ \ \kappa_c = \frac{1}{c_s + c_h}. \tag{3.18}$$

Finally, let us consider the difference between the two critical herding propensities κ_c and κ_c^0. The first, corresponds to the fixed point of the dynamical toy model in equation (3.14). The second, however, is the critical herding propensity of a static version of the toy model, where there is no self-referential effect of the momentum. This gives us the first glimpse of the effect of the self-referential momentum. Namely, for positive coefficient c_h value the critical herding propensity κ_c is lower than κ_c^0, *i.e* self-referential momentum enhances order. In the next section we use numerical analysis for composing a phase diagram of the toy model on the c_s-c_h plane. The resulting phase diagram shows that the self-referential nature of the toy model not only enhances order, but also induces new ordered regimes.

3.2.3 Toy model numerical phase diagram

In this section we use numerical simulations for profiling a phase diagram of the toy model on the c_s-c_h plane. This phase diagram enlightens us on the effects of the noise traders self-referential nature. Namely, we see that the interplay of positive and negative feedback mechanisms leads to the emergence of two new ordered regimes besides the regular "ferromagnetic" phase.

The phase diagram is constructed by a parametric scan over the coefficients c_s and c_h. For each pair of the coefficient values, we calculate a set of scalar indicators from the opinion and momentum time series. These indicators characterise the system behaviour for the corresponding coefficient values. To guide our choice of indicators, we conducted exploratory scans of the parameter

space, which revealed four regimes with distinct characteristics: (1T) "paramagnetic" disordered phase with $s \approx H \approx 0$; (2T) "jumping" regime, where the opinion systematically jumps between the polarised values $s = \pm 1$; (3T) "ferromagnetic" ordered phase with $s \approx H \approx 1$; (4T) "oscillating" regime, where opinion and momentum undergo smooth oscillations. The characteristic features of these regimes are demonstrated in figure 3.4, which shows eight panels with time series of s_t and H_t for the first 200 time steps. The two upper panels show the disordered regime (1T), the following two illustrate the usual ordered phase (3T), then there is one panel demonstrating the dynamics of the jumping regime (2T) and the final three panels characterise the oscillating phase (4T).

We have chosen three indicators, which are effective in distinguishing between the distinct characteristics illustrated in figure 3.4. For a time series of variable x, the indicators are: (1) mean value of x; (2) mean relative change $\Delta x / x$, where $\Delta x = x_t - x_{t-1}$; (3) the number of frequencies in the time series. The number of frequencies is found by counting peaks in the positive half of the Fourier spectrum. For each (c_s, c_h) pair, we equilibrate the system for 2000 time steps and calculate the three indicators for both s_t and H_t over the interval $t = 2000\text{--}10000$. We visualise the results with colour coded heat-maps on the c_s-c_h plane. For simplicity, we refer to these as just heat-maps. In the heat-maps, the value of an indicator at a certain point on c_s-c_h plane is represented by the colour of that point. We ensure the readability of the heat-maps, even when printed in greyscale, by employing a colour scheme from the cubehelix family introduced by Green (2011) for astrophysical intensity plots.

Figure 3.5a shows all six heat-maps corresponding to a toy model with unit herding propensity $\kappa = 1$ and the memory coefficient $\theta = 0.99$. On the left hand side, we find the the mean opinion and momentum heat-maps, which outline three regions $s_{avg} \approx H_{avg} \in \{0, 1, -1\}$. Areas with $s_{avg} = \pm 1$ correspond to the "ferromagnetic" ordered phase (3T). In figure 3.4 we can see the time series of the ordered phase for weight coefficients $c_s = 1.0$ and $c_h = 2.0$ with both positive and negative initial momentum. As we can see, the initial conditions determine which of the ordered states, $s = 1$ or $s = -1$, is realised. From figure 3.5a we see that the sign of c_h has similar effect. Let us now turn to the heat-maps for the relative change and the frequency counts. In these, we can see a triangular region in the lower right part of the plane, where there is a large number of frequencies and a distinctly uneven relative change. This corresponds to the oscillating phase (4T). On the left side of the plane, we can find an area with large negative valued relative change and a single opinion index frequency. This corresponds to the jumping regime (2T). In the middle of the heat-map for the opinion index frequency count, we can see a narrow region where the frequency count is strictly zero. This corresponds to the "paramagnetic" disordered phase (1T). These results are combined into the toy model phase diagram sketch in figure 3.5b.

Let us give an qualitative explanation to the four different phases. Consider the feedback mechanisms of the toy model. From equation (3.14) we can conclude that the signs of c_s and c_h define whether the system has positive or negative feedback from s and H respectively. Furthermore, the absolute value of c_s and c_h sets the strength of the corresponding feedback. In the following, we consider which feedback, positive or negative, is dominant in each of the four phases. First, take the ordered phase (3T). It is in the upper right corner of the plane, where we expect the system to be dominated by positive feedbacks. Usually such uncontrolled positive feedback would lead to infinite growth, but as the hyperbolic tangent is bound by ± 1, the toy model just saturates at one of the polarised states $|s| = 1$. Next, consider what happens if negative feedback dominates. This would mean that the system is always pulled back towards the neutral state $s = 0$. Both disordered (1T) and jumping (2T) regimes are located in areas where we would expect either both the negative and the positive feedback to be relatively weak or the negative feedback to dominate. In the case of (2T), the negative feedback is too strong and it always overshoots the neutral state $s = 0$. Finally, we come to the case where both feedbacks are of similar strength. This corresponds to the region around the diagonal on the lower right quarter of the plain, *i.e* it corresponds to the oscillating phase (4T).

Before concluding with the toy model, let us point out that we have tested several different memory parameter θ values. The memory parameter effectively controls the lag between the opinion and momentum. The larger the memory parameter is, the larger the lag. We can report that varying the memory parameter changes the layout and relation between the jumping and oscillating regimes. For example, for very small θ values, smooth oscillations vanish, while for medium valued memory parameter, we can find regimes which are a mixture of jumping and smooth oscillations. While the dependence on θ is interesting, its detailed investigation is beyond the scope of this thesis. For the purposes of this thesis, it is sufficient to note that the phase diagram has a significant dependence on the memory parameter.

We conclude by highlighting the most important findings from the toy model:

1. The toy model's self-referential nature induces new ordered regimes.

2. Balanced positive and negative feedback leads to smoothly oscillating dynamics, while overwhelmingly dominating (over shooting) negative feedback leads to "jumping" dynamics.
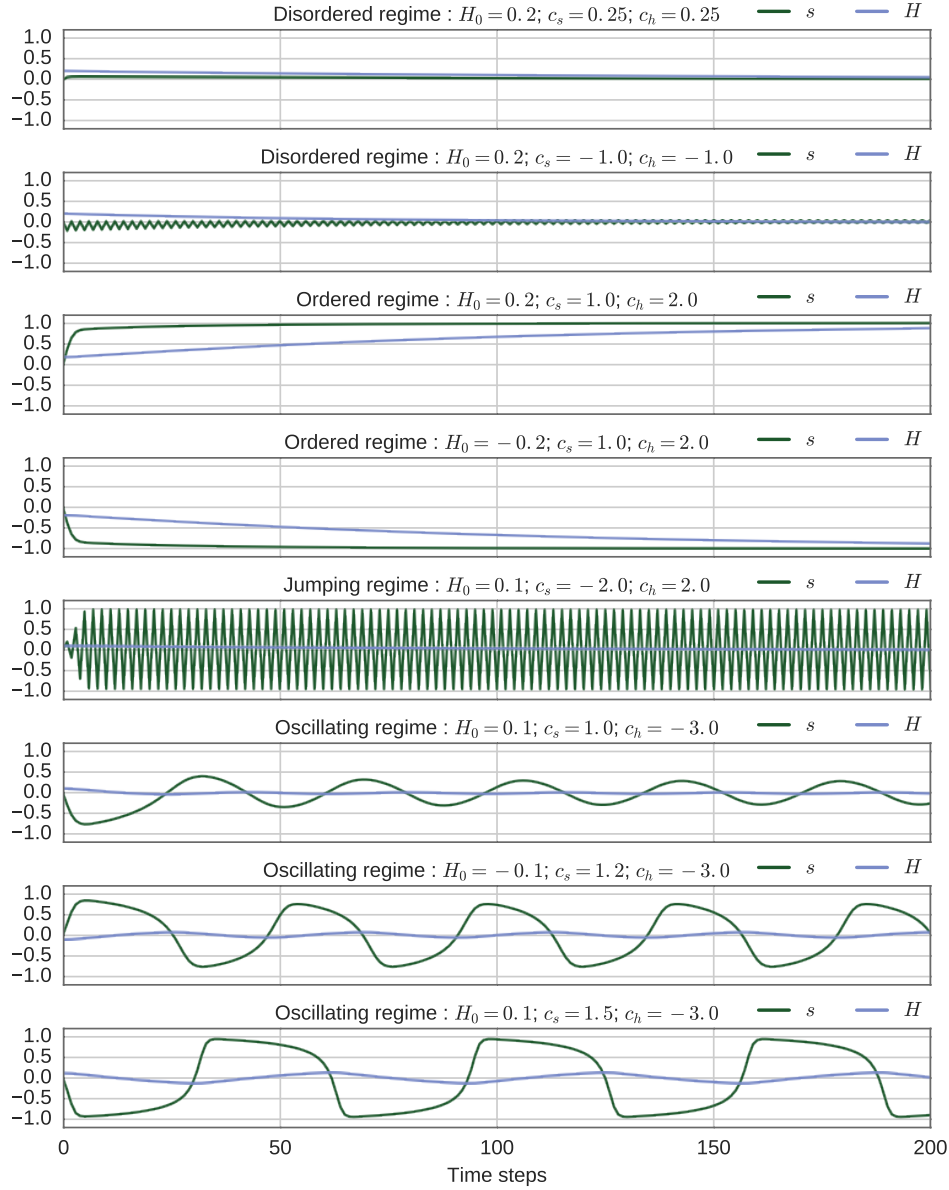
Figure 3.4: Characteristic toy model time series in different regimes. The toy model is a dynamic mean-field Ising-like model defined by equation (3.14). It features two coupled variables: the opinion index s and the momentum H. These time series are generated for a toy model with unit herding propensity $\kappa = 1$, memory parameter $\theta = 0.99$ and initial opinion $s_0 = 0$. The initial momentum and the noise trader imitation and trend following weight coefficients c_s and c_h are specified for each time series panel separately. Trials with different parameters have shown that the initial opinion and momentum values define two features: (a) in case of ordered phase, they define the sign of the opinion; (b) in case of jumping or oscillating regimes they define the cycle-phase. Considering the regimes on the sketch in figure 3.5b, the first two panels show time series correspond to disordered (paramagnetic) regime (1T). The following two panel show characteristics of the ordered (ferromagnetic) regime (3T). The fifth panel corresponds to the jumping phase (2T) and the final three all describe different smooth oscillations in regime (4T).
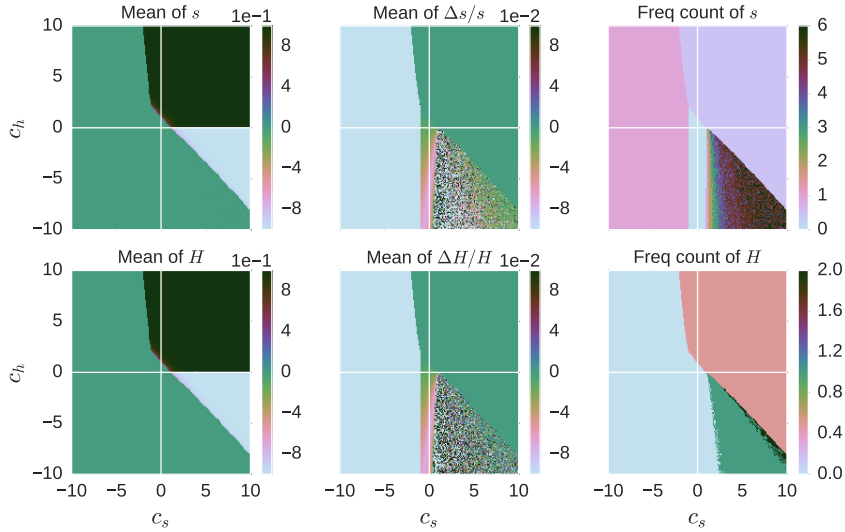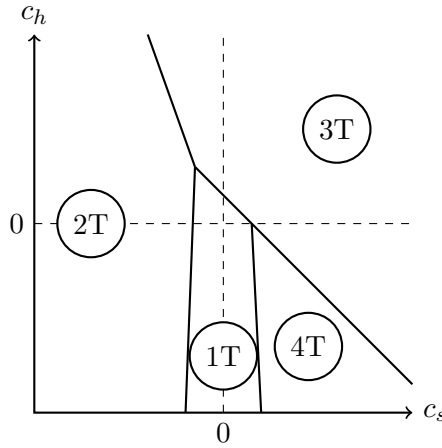
(a) The scalar indicator heat-maps on the c_s-c_h plane.

(b) Sketch of the toy model phase diagram c_s-c_h plane.

Figure 3.5: The toy model numeric phase diagram on the noise trader imitation and trend following weight coefficients c_s-c_h plane. The toy model is a dynamic mean-field Ising-like model defined by equation (3.14). It features two coupled variables: the opinion index s and the momentum H. Here we use unit herding propensity $\kappa = 1$ and memory parameter $\theta = 0.99$. In panel (a) we see three heat-maps for both opinion s and momentum H: (1) mean value of the time series; (2) mean value of the relative changes in the time series; (3) the number of frequencies in the time series. The number of frequencies is found by counting peaks in the positive half of the Fourier spectrum. The heat-maps indicate five separable regimes, which are highlighted with the sketch in panel (b): (1T) "paramagnetic" disordered phase with $s \approx H \approx 0$; (2T) "jumping" regime, where the opinion systematically jumps between the polarised values $s = \pm 1$; (3T) "ferromagnetic" ordered phase with $s \approx H \approx 1$; (4T) "oscillating" regime, where opinion and momentum undergo smooth oscillations. The characteristic time series of these regimes are shown in figure 3.4.

Chapter 4

Limiting noise trader behaviour

In chapter 3 we described the main characteristics of the artificial market. We argued that the fundamentalist traders enforce a connection between the risky asset price and dividends. Their buy-low-and-sell-high strategy pushes the market towards the *fundamental-state*, where the price and dividend growth is of the same order $R_{avg} \sim R_d$. The noise trader, on the other hand, have a more complex self-referential nature. In section 3.2 we elaborated on the noise trader behaviour by introducing a simplified toy model based on an iterative coupled Ising model. Besides the standard disordered paramagnetic and ordered ferromagnetic phases, we witnessed the emergence of two additional ordered regimes. From this, we concluded that the self-referential nature of the noise trader enhances order.

In this chapter, we focus on the limiting noise trader behaviour, where all trader are invested in the same asset type, *i.e* the noise trader opinion has a polarised value, either $s = 1$ or $s = -1$. Both of these are analogues to the ferromagnetic phase in the toy model and thus we refer to them as *positive* and *negative ordered* states. In Section 4.1 we consider the necessary conditions for these polarised regimes and observed that it is convenient to consider threshold momentum values below or above which the noise traders start ordering. These *critical momenta* are discussed in more detail in section 4.2, where we show that they naturally divide the noise trader imitation and trend following weight coefficients c_s-c_h plane into four quarters. In section 4.3 we use the limits of ordered noise traders to find two fixed points R_{min} and R_{max} for the price growth R_t, or equivalently r_{min} and r_{max} for the growth rate r_t. The naming convention of *min* and *max* is because these fixed points effectively act like bounds on the long-term average price growth R_{avg} and growth rate r_{avg}. All of these results are later used in chapter 5 to consider the feasibility and stability of the ordered states on different regions of the c_s-c_h plane and thus propose a theoretical phase diagram for the artificial market.

4.1 Ordered noise traders

Let us consider the limits, where all noise traders are invested in the same asset type. We refer to such regimes as ordered or polarised phases. These correspond to cases where after some relaxation time T_0 the risky fraction x_t^n of the representative noise trader is zero or one, or equivalently the opinion index is ± 1

$$\forall t > T_0 > 0, \ \ x_t^n \in \{0, 1\} \ \ \Leftrightarrow \ \ \forall t > T_0 > 0, \ \ s_t \in \{-1, 1\}. \tag{4.1}$$

The dynamics of the noise trader risky fraction x_t^n is given by equation (2.17), which reads

$$x_t^n = \frac{1}{N_n} \sum_{k=1}^{N_{t-1}^+} \left(1 - \xi_k\left(p_{t-1}^+\right)\right) + \frac{1}{N_n} \sum_{l=1}^{N_{t-1}^-} \xi_l\left(p_{t-1}^-\right).$$

Here $\xi_i(p)$ are one with probability p and zero otherwise, *i.e* they are Bernoulli random variables. The number of traders owning risky and risk-free asset at time t are given by N_t^+ and N_t^- respectively. For any time t, their sum is the total number of noise traders $\forall t, \ N_n = N_t^+ + N_t^-$.

By definition (equation (2.17)) the risky fraction x^n is stochastic. As long as the switching probabilities p_t^+ and p_t^- are non-zero, there is a finite probability for the risky fraction to change. For the condition in equation (4.1) to be satisfied for all time steps, one (and only one) of the switching probabilities must equal zero. This creates a lock-in effect for the corresponding asset, where none of the noise traders, who are invested in that asset, change their position. The aforementioned observation shifts the focus from finding conditions for polarised noise traders to finding conditions for zero valued switching probabilities. Recall that the switching probabilities $p_t^{\pm}$ have an Ising-like dynamics, given by equation (2.19)

$$p_t^{\pm} = \frac{p_{\pm}}{2} \left(1 \mp \kappa_t \left(c_s s_t + c_h H_t\right)\right).$$

The probability of selling the risky and buying the risk-free asset is given by p_t^+. Conversely, p_t^- is the probability of switching from risk-free to risky investment. The opinion index $s_t = 2x_t^n - 1 \in [-1, 1]$ measures the market sentiments and the the price momentum H_t the trend. Coefficients c_s and c_h indicate the relative weights of s_t and H_t, and whether the traders have a conformist or contrarian attitude. The noise trader herding propensity is given by κ_t and $p_{\pm}$ are constants. For simplicity, in this and the following chapter, we only consider a constant valued herding propensity $\kappa_t = \kappa$. The results can be extended to time-dependent herding propensities.

Evidently, switching probabilities in equation (2.19) are even allowed to become negative. However, such values are treated as zero. Necessary conditions for non-positive switching probabilities can be expressed from equation (2.19)

$$
\begin{aligned}
p_t^+ \leq 0.0: & \quad 1 - \kappa \left(c_s s_t + c_h H_t \right) \leq 0, \\
p_t^- \leq 0.0: & \quad 1 + \kappa \left(c_s s_t + c_h H_t \right) \leq 0.
\end{aligned}
\tag{4.2}
$$

In this thesis we focus on the interplay between the noise trader trend following and imitative behaviour. Thus, as with the toy model in section 3.2, different market regimes are considered on the c_s-c_h plane. Consequently, for constant herding propensity κ, the only free variables in equation (4.2) are opinion s_t and price momentum H_t. By definition (equation (2.16)), the opinion index is bound by ± 1. As the momentum is less restricted, it is convenient to reformulate the inequalities in equation (4.2) as

$$
\begin{aligned}
p_t^+ \leq 0.0: & \quad c_h H \geq \tfrac{1}{\kappa} - c_s s_t, \\
p_t^- \leq 0.0: & \quad c_h H \leq - \left(\tfrac{1}{\kappa} + c_s s_t \right).
\end{aligned}
\tag{4.3}
$$

The inequalities in equation (4.3) are valid only if the social herding propensity κ is positive. If κ is negative, the inequalities have opposite directions. For simplicity, we are going to consider only positive herding propensities. The results can be trivially extended for negative herding propensities. Equation (4.3) indicates the existence of threshold momentum values, beyond which the switching probabilities vanish. We refer to these as *critical momenta* $H_c^{\pm}$. They can be expressed from equation (4.3)

$$
H_c^{\pm} \equiv \pm \frac{1}{c_h} \left(\frac{1}{\kappa_t} \mp c_s s_t \right).
\tag{4.4}
$$

Let us consider the requirements for vanishing switching probabilities given in equation (4.3). Depending on the sign of the coefficient c_h, these are satisfied if the momentum value H_t is either higher or lower than the corresponding critical threshold (H_c^+ or H_c^-). Figure 4.1 gives a graphical illustration of the directions of these inequalities. It features the c_s-c_h plane cut in two by the line $c_h = 0.0$. The direction of the inequalities changes when crossing the line $c_h = 0$. On this line, the critical momenta diverge to $\pm\infty$. We discuss this divergence and other peculiar features of the critical momenta in more detail in section 4.2.
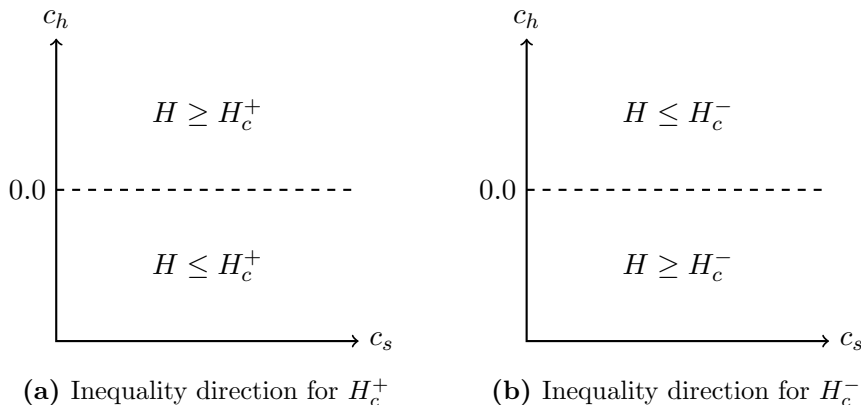
(a) Inequality direction for H_c^+ **(b)** Inequality direction for H_c^-

Figure 4.1: A graphical representation of the directions of inequalities in equation (4.3) on the noise trader imitation and herding weight coefficients c_s-c_h plane for both of the critical momenta: (a) H_c^+ and (b) H_c^-. $H_c^\pm$ are threshold momentum values, below or above which the corresponding switching probability $p_t^\pm$ vanishes, creating a lock-in effect for the respective asset, which leads to polarised noise trader opinion $s = \pm 1$. The critical momenta are defined in equation (4.4). For positive c_h, H_c^+ is the lower threshold for p_t^+ being zero, while H_c^- is the upper threshold for p_t^- being zero. The opposite holds for negative c_h.

4.2 The critical momenta

In section 4.1 we established that regimes with ordered, *i.e* polarised, noise traders are possible only if one of the switching probabilities $p_t^\pm$ is zero valued. The necessary conditions for vanishing $p_t^\pm = 0$ are defined by the inequalities in equation (4.3). We found it convenient to formulate the criteria in equation (4.3) with respect to threshold momentum values $H_c^\pm$. Such a formulation is illustrated in figure 4.1. In the following section, we elaborate on the specifics of the threshold *critical momenta* and demonstrate how they impose a natural frame of reference upon the c_s-c_h plane. Let us start by restating the definition of the critical momenta, as given in equation (4.4)

$$H_c^\pm = \pm \frac{1}{c_h} \left(\frac{1}{\kappa} \mp c_s s_t \right). \tag{4.5}$$

On a closer examination of equation (4.5) we can find two characteristic features of $H_c^\pm$ on the c_s-c_h plane. First, as $c_h \to 0$ the critical momenta tend towards infinity $H_c^\pm \to \pm\infty$. Notice, that when $c_h = 0$ the switching probabilities do not depend on the momentum and thus the concept of critical momenta is irrelevant when $c_h = 0$. Nevertheless, the line $c_h = 0$ arises as a natural reference when considering the critical momenta. In figure 4.1 we already demonstrated that on either side of $c_h = 0$ the direction of the inequalities in equation (4.3) are different. Let us now consider the signs of the
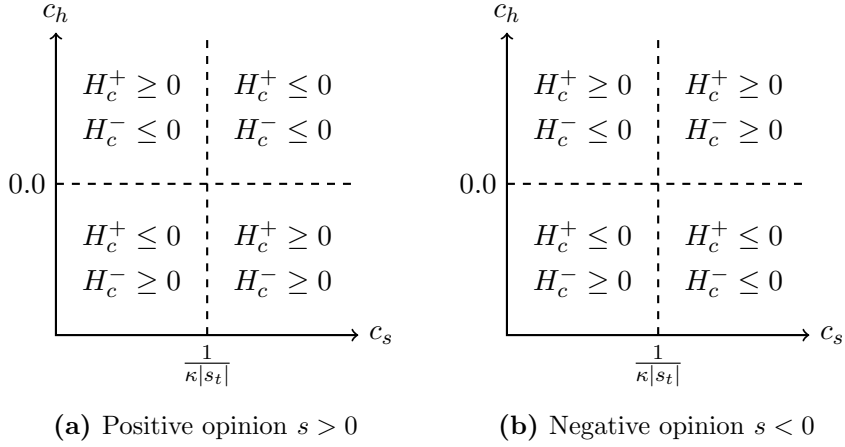
(a) Positive opinion $s > 0$ **(b)** Negative opinion $s < 0$

Figure 4.2: A graphic overview of the signs of the critical momenta $H_c^{\pm}$ on the noise trader imitation and herding weight coefficients c_s-c_h plane. $H_c^{\pm}$ are threshold momentum values, below or above which the corresponding switching probability $p_t^{\pm}$ vanishes, creating a lock-in effect for the respective asset, which leads to polarised noise trader opinion $s = \pm 1$. The critical momenta are defined in equation (4.5). The plane has been divided into four quarters by the lines $c_h = 0.0$ and $c_s = \frac{1}{\kappa|s_t|}$. Panel (a) shows signs for positive opinion $s > 0$ and panel (b) for negative $s < 0$. If the opinion is positive, H_c^{+} changes sign on crossing either of the division lines. As a result, its signs form a chequered pattern. On the other hand, H_c^{-} only changes sign when crossing the line $c_h = 0.0$. The case of negative opinion index is antisymmetric to the positive case. H_c^{-} signs have a chequered pattern on the plane, while the sign of H_c^{+} only changes when crossing the line $c_h = 0.0$. As the lines $c_h = 0.0$ and $c_s = \frac{1}{\kappa|s_t|}$ separate regions, where $H_c^{\pm}$ have different signs, they form a natural reference frame on the c_s-c_h plane. When considering $H_c^{\pm}$ as the threshold values for ordered noise traders $|s| = 1$, the relevant position of the critical point is $(\frac{1}{\kappa}, 0)$.

critical momenta. From equation (4.5) we see that the signs of $H_c^{\pm}$ depend on the signs of c_h and $\frac{1}{\kappa} \mp s_t c_s$. Which leads us to the second characteristic feature of $H_c^{\pm}$: if $\frac{1}{\kappa} \mp s_t c_s = 0$, then the corresponding critical momentum is zero. This defines an other natural reference line $c_s^{\pm} = \pm \frac{1}{\kappa s_t}$, where the plus and minus refer to H_c^{+} and H_c^{-} respectively.

In regard to the signs of $H_c^{\pm}$ the lines $c_h = 0$ and $c_s^{\pm} = \pm \frac{1}{\kappa s_t}$ define a natural frame of reference on the c_s-c_h plane. In figure 4.2 we illustrate this notion by using these lines to divide the c_s-c_h plane into four quarters and indicate the signs of $H_c^{\pm}$ in each of them for (a) positive opinion $s > 0$ and (b) negative opinion $s < 0$. Recall the definition of the critical momenta given in equation (4.5). We can see that for a finite c_h, the critical momenta H_c^{+} can only become zero valued when the opinion is positive and H_c^{-} can only become zero when the opinion is negative. In either case, the critical momenta become zero valued at $c_s = \frac{1}{\kappa|s_t|}$. This is reflected in figure 4.2 by the fact that for positive opinion, the signs of H_c^{+} have a chequered pattern on the c_s-c_h and H_c^{-} is

negative for $c_h > 0$ and positive for $c_h < 0$, while for negative opinion signs of H_c^- have a chequered pattern and H_c^+ is positive for $c_h > 0$ and negative for $c_h < 0$. Thus, the lines $c_h = 0$ and $c_s = \frac{1}{\kappa|s_t|}$ define a natural frame of reference on the c_s-c_h plane.

We have established that $c_h = 0$ and $c_s = \frac{1}{\kappa|s_t|}$ define a natural reference frame on the c_s-c_h plane, as they separate areas where $H_c^\pm$ have different signs (see figure 4.2). When $c_h \to 0$ the critical momenta diverge and $H_c^\pm$ have different signs on either side of $c_h = 0$. On the other hand, depending on the sign of s_t, along the line $c_s = \frac{1}{\kappa|s_t|}$ one of $H_c^\pm$ is zero valued. We call $c_s = \frac{1}{\kappa|s_t|}$ the *critical line* and the point $(\frac{1}{\kappa|s_t|}, 0)$ the *critical point*. It is illuminating to visualise the shape of the critical momenta on the c_s-c_h plane as presented in figure 4.3. It features both of the critical momenta using opinion index values $s = 1$ and $s = -1$ for H_c^+ and H_c^- respectively. Due to the divergence at $c_h = 0.0$, cut-off values for the absolute momenta are used to improve visibility. We see that the values of the critical momenta spiral from $-\infty$ to $+\infty$ during a $180°$ turn around the critical point $(\frac{1}{\kappa|s_t|}, 0)$. Additionally, we can observe that a cut-off value defines a region in the vicinity of the critical line, inside which the critical momenta have absolute values below this cut-off.

Let us now consider the position of the critical line $c_s = \frac{1}{\kappa|s_t|}$. It depends hyperbolically on the opinion index $|s_t|$. For polarised noise traders $|s| = 1$, it is at $c_s = \frac{1}{\kappa}$, while for neutral noise traders $s = 0$, it is at $\pm\infty$. We illustrate this very sensitive dependence in figure 4.4, which shows heat-maps of $H_c^\pm$ on the c_s-c_h plane for three different opinion values $s \in \pm\{0.90, 0.95, 1.0\}$ for $H_c^\pm$ respectively. To improve visualisation, we use a cut-off value $|H_c^\pm| < 0.001 \approx 6r_d$, which corresponds to the scale relevant for our market simulations in chapter 6. We can now notice two things: (a) the location of the critical line is very sensitive to the opinion index; (b) the critical momenta have values, which are reachable in our market simulation, only in a narrow double conical region centred at the critical point $(\frac{1}{\kappa|s_t|}, 0)$. Recall that we are considering the critical momenta as the thresholds above or below which one of the switching probabilities $p_t^\pm$ vanishes, which leads to ordered noise traders $|s| = 1$. In this light, we can see that the only relevant position of the critical line corresponds to the polarised noise traders: $c_s = \frac{1}{\kappa}$.

We finish by highlighting the most important results:

1. The criteria for vanishing $p_t^\pm$, and thus ordered noise traders, can be formulated with respect to threshold critical momenta $H_c^\pm$ (see figure 4.1).

2. The shape of $H_c^\pm$ defines a natural reference frame on the c_s-c_h plane, given by: $c_h = 0$ and $c_s = \frac{1}{\kappa}$. These divide the plane into four quarters, where $H_c^\pm$ have different signs (see figure 4.2).

3. The condition $H_c^\pm \leq H_{cutoff}$ defines a double conical shape centred at the *critical point* $(\frac{1}{\kappa}, 0)$ on the c_s-c_h plane.
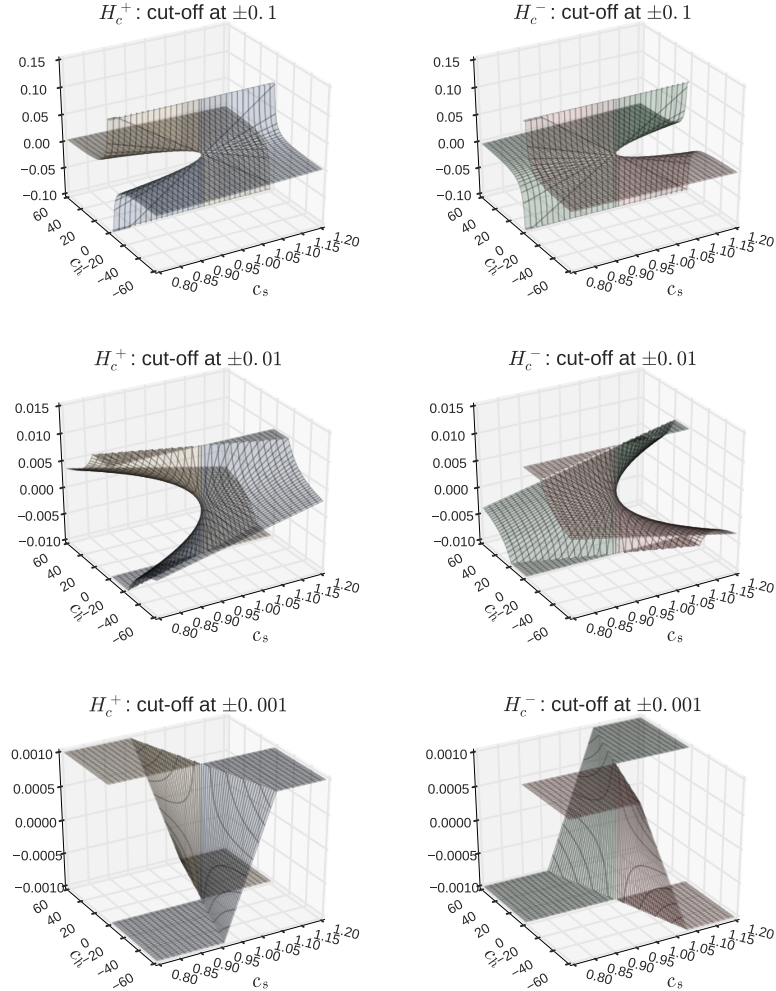
Figure 4.3: Illustration of the spiralling shape of the critical momenta $H_c^\pm$ around critical point $c_s = \frac{1}{\kappa}$ on the noise trader imitation and herding weight coefficients c_s-c_h plane. $H_c^\pm$ are threshold momentum values, below or above which the corresponding switching probability $p_t^\pm$ vanishes, creating a lock-in effect for the respective asset, which leads to polarised noise trader opinion $s = \pm 1$. The critical momenta are defined in equation (4.5). In the above plots we use polarised opinion index values $s = \pm 1$ for $H_c^\pm$ respectively. The critical momentum H_c^+, can be seen in the column on the left hand side column, while the right hand side corresponds to H_c^-. To improve visibility, we use three different cut-off values $|H_c^\pm| \leq H_{cutoff} \in \{0.1, 0.01, 0.001\}$. The cut-off $H_{cutoff} = 0.001$ corresponds to the relevant momentum scale for our market simulations in chapter 6. We can see that for the corresponding polarised opinion values $H_c^\pm$ change sign when crossing the lines $c_h = 0$ and $c_s = \frac{1}{\kappa}$. We use this to define a natural reference frame on the c_s-c_h plane. We see that the values of $H_c^\pm$ spiral from $-\infty$ to $+\infty$ during a 180° turn around the crossing point of the reference frame $(\frac{1}{\kappa}, 0)$. We call this point the *critical point*.
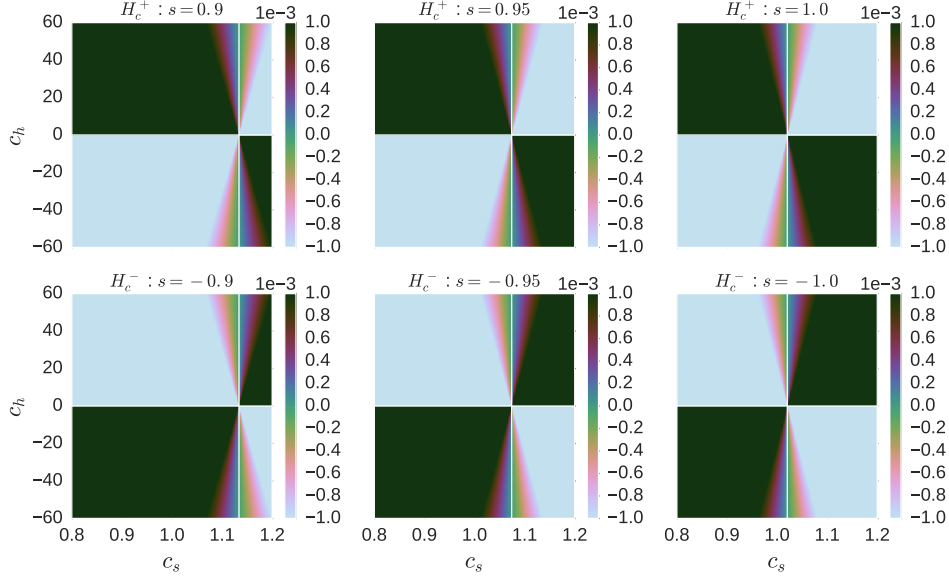
41

Figure 4.4: Illustration of the opinion index dependence of the critical momenta $H_c^{\pm}$ on the noise trader imitation and herding weight coefficients c_s-c_h plane. $H_c^{\pm}$ are threshold momentum values, below or above which the corresponding switching probability $p_t^{\pm}$ vanishes, creating a lock-in effect for the respective asset, which leads to polarised noise trader opinion $s = \pm 1$. The critical momenta are defined in equation (4.5). In the above heat-maps we use four different opinion index values $s \in \pm\{0.90, 0.95, 1.0\}$ for $H_c^{\pm}$ respectively. The critical momentum H_c^+ are in the heat-maps in the upper row and H_c^- in the lower row. To improve visibility we use a cut-off $|H_c^{\pm}| \leq H_{cutoff} = 0.001$, which corresponds to the relevant momentum scale for our market simulations in chapter 6. Therefore, the condition $|H_c^{\pm}| \leq H_{cutoff}$ roughly outlines the region where the critical momenta have values which can be reached in the market simulations presented in chapter 6. This region has a double conical shape centred at the point $(\frac{1}{\kappa|s_t|}, 0)$, which we call the *critical point*. It is also the crossing point of the two perpendicular white lines, which correspond to $c_h = 0$ and $c_s = \frac{1}{\kappa|s_t|}$. We can see that for the opinion index values, used in the above heat-maps, these lines divided the c_s-c_h plane into four quarters based on the signs of $H_c^{\pm}$. Due to this feature, these lines are a natural reference frame on the c_s-c_h plane. Observe, that the c_s coordinate of the critical point has a sensitive hyperbolic dependence on the opinion index $\frac{1}{\kappa|s_t|}$: for $|s| = 1$ the critical point is at $(\frac{1}{\kappa}, 0)$, while for $s = 0$ it is at $(\infty, 0)$. When considering $H_c^{\pm}$ as the threshold values for ordered noise traders $|s| = 1$, the relevant position of the critical point is $(\frac{1}{\kappa}, 0)$.

4.3   Fixed points of the price returns

In section 4.1 we discussed so-called ordered or polarised states, which are limiting regimes, where all noise traders own the same asset type. We argued that the necessary condition for such states are equivalent to conditions for zero valued switching probabilities. In other words, if either p_t^+ or p_t^- vanishes, the noise traders have a lock-in effect for the corresponding asset, which respectively leads to the formation of the positive $s = 1$ or negative $s = -1$ ordered state. We argued that it is convenient to consider the criteria for vanishing $p_t^\pm$ with respect to threshold momentum values $H_c^\pm$. In section 4.2 we analysed these *critical momenta* $H_c^\pm$ in more detail and found that they impose a reference frame on the c_s-c_h plane. In this section, we take it as given that a lock-in effect has occurred and the system is in one of the ordered states. We analyse the corresponding behaviour of the price returns and derive fixed points for it.

Recall our discussion of typical market dynamics in section 3.1. We argued that fundamentalists enforce a connection between the risky asset price and dividends, while the noise traders can induce super-exponential price growth. Indeed, in figure 3.2 we observed such bubble regimes. All of them ended with a plateau-like shape, which was due to noise traders undergoing a lock-in effect. This is, of course, the key feature of the ordered states discussed in sections 4.1 and 4.2. In figure 3.2 we saw that while the system could show high volatility on ordinary times, during these noise trader lock-ins the market dynamics became very calm. We argued that this is because at such times the fundamentalists are the only one actively effecting the market and thus the systems falls to the *fundamental state*, where the average price and dividend growth are similar $R_{avg} \sim R_d$.

In this section we analytically prove the existence of two fixed points of the price growth, which act as rough bounds on the long-term average price growth R_{avg}. Notice, that the limiting noise trader behaviour, *i.e* $x^n = 0$ and $x^n = 1$, correspond to their lowest and highest possible demands for the risky asset. Thus it is reasonable to look for the upper and lower fixed points for the average price growth from these limits. The derivation of the lower fixed point R_{min} (r_{min}) is present in section 4.3.1 and the derivation of the upper fixed point R_{max} (r_{max}) is given in section 4.3.2. Later, in chapter 6 we present numeric results verifying these analytical fixed points.

First, let us reformulate the quadratic price equation (2.25) for the price returns R_t

$$r_t + 1 = R_t = \frac{-b_t^* - \sqrt{b_t^{*2} - 4a_t^* c_t^*}}{2a_t^*}, \tag{4.6}$$

where the terms a_t^*, b_t^* and c_t^* are given by

43

$$a_t^* = \nu_{t-1} x_{t-1}^n \left(x_t^n - 1\right) + x_{t-1}^f \left(x_{min}^f - 1\right), \tag{4.7}$$

$$b_t^* = x_{t-1}^f \frac{1}{\gamma \sigma_{R_{ex}}^2} \frac{d_t R_d}{P_{t-1}}$$
$$+ x_{min}^f \left[x_{t-1}^f \left(\frac{d_t}{P_{t-1}} - R_f\right) + R_f\right] \tag{4.8}$$
$$+ \nu_{t-1} x_t^n \left[x_{t-1}^n \left(\frac{d_t}{P_{t-1}} - R_f\right) + R_f\right],$$

$$c_t^* = \frac{1}{\gamma \sigma_{R_{ex}}^2} \frac{d_t R_d}{P_{t-1}} \left[x_{t-1}^f \left(\frac{d_t}{P_{t-1}} - R_f\right) + R_f\right]. \tag{4.9}$$

4.3.1 Lower fixed point

Let us assume polarised noise traders $x^n = 0$ and insert this into equations (4.7) to (4.9)

$$a_t^* = x_{t-1}^f \left(x_{min}^f - 1\right), \tag{4.10}$$

$$b_t^* = x_{t-1}^f \frac{1}{\gamma \sigma_{R_{ex}}^2} \frac{d_t R_d}{P_{t-1}}$$
$$+ x_{min}^f \left[x_{t-1}^f \left(\frac{d_t}{P_{t-1}} - R_f\right) + R_f\right], \tag{4.11}$$

$$c_t^* = \frac{1}{\gamma \sigma_{R_{ex}}^2} \frac{d_t R_d}{P_{t-1}} \left[x_{t-1}^f \left(\frac{d_t}{P_{t-1}} - R_f\right) + R_f\right]. \tag{4.12}$$

Next, consider the stochastic multiplicative dividend process in equation (2.2). Here we focus on the average behaviour and thus the dividends can be approximated by their average, *i.e* by a deterministic exponential growth with the rate r_d

$$d_t \approx d_0 \left(1 + r_d\right)^t = d_0 R_d^t. \tag{4.13}$$

In the following, we assumed that the average price returns have a lower fixed point $R_{avg} \approx R_{min} = const$, such that the dividend-price ratio can be expressed as

$$\frac{d_t}{P_t} \approx \frac{d_0}{P_0} \left(\frac{R_d}{R_{min}}\right)^t. \tag{4.14}$$

Let us compare the lower fixed point R_{min} with the average dividend growth R_d. There are three possible scenarios: (1) $R_{min} > R_d$; (2) $R_{min} < R_d$; (3) $R_{min} = R_d$. We now treat these cases separately.

Exponentially diminishing dividend-price ratio: $R_{min} > R_d$

First, let us consider the case where $R_{min} > R_d$. This means that on average the price is growing faster than the dividends. Consequently, the dividend-price ratio is exponentially diminishing $\frac{d_t}{P_t} \xrightarrow{t \to \infty} 0$. As a result, the fundamentalist risky fraction converges towards its lower bound $x^f \xrightarrow{t \to \infty} x^f_{min}$. Using these two approximations in equations (4.10) to (4.12), gives

$$a_t^* \approx x^f_{min} \left(x^f_{min} - 1 \right), \tag{4.15}$$

$$b_t^* \approx x^f_{min} \left(1 - x^f_{min} \right) R_f, \tag{4.16}$$

$$c_t^* \approx 0. \tag{4.17}$$

Therefore, if the lower fixed point is larger than the average dividend growth $R_{min} > R_d$, the price returns in equation (4.6) can be expressed as

$$R_{min} \approx -\frac{b_t^*}{a_t^*} = R_f \ \Rightarrow \ R_{min} = R_f. \tag{4.18}$$

We see that, if $R_{min} > R_d$ then the lower fixed point is equal to the risk-free growth $R_{min} = R_f$. Of course, in case $R_d > R_f$, this leads to a contradiction and the case $R_{min} > R_d$ should be discarded.

Exponentially growing dividend-price ratio: $R_{min} < R_d$

Let us turn to the second case, where the lower fixed point is assumed to be smaller than the average dividend growth rate $R_{min} < R_d$. This means that the dividend-price ratio grows exponentially

$$\frac{d_t}{P_t} \approx \frac{d_0}{P_0} \left(\frac{R_d}{R_{min}} \right)^t \xrightarrow{t \to \infty} \infty. \tag{4.19}$$

It should be mentioned, that while noise traders by construction can not have a risky fractions above 1, this is not the case for fundamentalists. The fundamentalist risky fraction, defined by equation (2.13), does not have an upper bound. In other words, fundamentalists can borrow at the risk-free rate r_f and invest that borrowed money into the risky asset. Thus if the dividend-price ratio grows exponentially, then so does the fundamentalist risky fraction. It is clear that the exponentially growing term dominates over the constant x^f_{min} and we can approximate x^f by

$$x_t^f \approx x^f_{min} + \frac{d_0}{P_0} \frac{R_d}{\gamma \sigma^2_{R_{ex}}} \left(\frac{R_d}{R_{min}} \right)^t \approx \frac{d_0}{P_0} \frac{R_d}{\gamma \sigma^2_{R_{ex}}} \left(\frac{R_d}{R_{min}} \right)^t. \tag{4.20}$$

For the following, it is convenient to define

$$C_0 \equiv \frac{d_0}{P_0} \frac{R_d}{\gamma \sigma_{R_{ex}}^2} \quad \text{and} \quad A \equiv \left(\frac{R_d}{R_{min}} \right). \tag{4.21}$$

Now, the terms a_t^*, b_t^* and c_t^* in the quadratic equation (4.6) can be expressed as

$$a_t^* \approx C_0 A^{t-1} \left(x_{min}^f - 1 \right), \tag{4.22}$$

$$
\begin{aligned}
b_t^* &\approx R_d \left(C_0 A^{t-1} \right)^2 \\
&\quad + x_{min}^f \left[C_0 A^{t-1} \left(\gamma \sigma_{R_{ex}}^2 C_0 A^{t-1} - R_f \right) + R_f \right],
\end{aligned} \tag{4.23}
$$

$$c_t^* \approx R_d C_0 A^{t-1} \left[C_0 A^{t-1} \left(\gamma \sigma_{R_{ex}}^2 C_0 A^{t-1} - R_f \right) + R_f \right]. \tag{4.24}$$

Clearly, for large t, the exponentially growing $C_0 A^{t-1}$ dominates the constant R_f and the above expressions can be further simplified into

$$a_t^* \approx C_0 A^{t-1} \left(x_{min}^f - 1 \right), \tag{4.25}$$

$$b_t^* \approx \left(C_0 A^{t-1} \right)^2 \left[R_d + \gamma \sigma_{R_{ex}}^2 x_{min}^f \right], \tag{4.26}$$

$$c_t^* \approx \gamma \sigma_{R_{ex}}^2 R_d \left(C_0 A^{t-1} \right)^3. \tag{4.27}$$

The price returns given by equation (4.6) now read

$$R_{min} = \frac{-b_t^* - \sqrt{b_t^{*2} - 4 a_t^* c_t^*}}{2 a_t^*} \approx C_0 A^{t-1} \zeta, \tag{4.28}$$

where ζ is a constant

$$\zeta \equiv \frac{\left(R_d + \gamma \sigma_{R_{ex}}^2 x_{min}^f \right) + \sqrt{\left(R_d + \gamma \sigma_{R_{ex}}^2 x_{min}^f \right)^2 - 4 \gamma \sigma_{R_{ex}}^2 R_d \left(x_{min}^f - 1 \right)}}{2 \left(1 - x_{min}^f \right)}.$$

Inserting the definitions of C_0 and A from equation (4.21) into equation (4.28) and rearranging terms gives

$$R_{min}^t \approx R_d^t \frac{d_0}{P_0} \frac{\zeta}{\gamma \sigma_{R_{ex}}^2} \Rightarrow$$

$$R_{min} \approx R_d \left(\frac{d_0}{P_0} \frac{\zeta}{\gamma \sigma_{Rex}^2} \right)^{\frac{1}{t}} \xrightarrow{t \to \infty} R_d. \tag{4.29}$$

Thus, even if we assume that at some $\tau < \infty$ the lower fixed point is smaller than the average dividend growth $R_{min,\tau} < R_d$, then as time goes by $t \to \infty$ it approaches $R_{min} \to R_d$. Therefore, we can summarise the results from both assumption $R_{min} > R_d$ and $R_{min} < R_d$, as

$$R_{min} = \begin{cases} R_d, & \text{if } R_d > R_f, \\ R_f, & \text{if } R_d < R_f. \end{cases} \quad \text{and} \quad r_{min} = \begin{cases} r_d, & \text{if } r_d > r_f, \\ r_f, & \text{if } r_d < r_f. \end{cases} \tag{4.30}$$

In chapter 6 we see that the existence of this lower bound is supported by numeric simulations of the artificial market.

4.3.2 Upper fixed point

Now, let us assume the limit of positively ordered noise traders, *i.e* the limit where all noise traders are invested in the risky asset $x^n = 1$. Note, that $x^n = 1$ corresponds to the highest possible demand for the risky asset that noise trader can have, while the limit $x^n = 0$ is the lower possible demand the noise trader can have. Therefore, it is reasonable to expect that if an upper fixed point R_{max} exists, then it is larger than the lower fixed point $R_{max} > R_{min}$. In the following we show that an upper fixed point does indeed exist. We start by inserting the assumption $x^n = 1$ into the terms in equations (4.7) to (4.9), which gives

$$a_t^* = x_{t-1}^f \left(x_{min}^f - 1 \right), \tag{4.31}$$

$$\begin{aligned} b_t^* = x_{t-1}^f \frac{1}{\gamma \sigma_{Rex}^2} \frac{d_t R_d}{P_{t-1}} \\ + x_{min}^f \left[x_{t-1}^f \left(\frac{d_t}{P_{t-1}} - R_f \right) + R_f \right] \\ + \nu_{t-1} \frac{d_t}{P_{t-1}}. \end{aligned} \tag{4.32}$$

$$c_t^* = \frac{1}{\gamma \sigma_{Rex}^2} \frac{d_t R_d}{P_{t-1}} \left[x_{t-1}^f \left(\frac{d_t}{P_{t-1}} - R_f \right) + R_f \right]. \tag{4.33}$$

Recall, that in section 4.3.1 we showed that the lower fixed point equals R_d, if $R_d > R_f$, and R_f otherwise. Thus, we can assume that, if there is an upper fixed point, it is larger than the average dividend growth $R_{max} > R_d$. Of

course, if there is no upper fixed point, the price grows even faster. In the long-run this leads to an exponentially, or faster, diminishing dividend-price ratio $\frac{d_t}{P_t} \xrightarrow{t \to \infty} 0$. Consequently, the fundamentalist risky fraction falls to its minimum value $x^f \xrightarrow{t \to \infty} x^f_{min}$. Besides the dividend-price ratio, consider also the wealth ratio ν_t. From above, we know that $R_{max} > R_f$ and $x^n > x^f$. Note, that if there is no upper bound, then the average price growth is even larger and $R_{avg} > R_f$ still holds. Therefore, noise traders are systematically earning a larger return on their investment than fundamentalists. Accordingly, the wealth ratio grows exponentially, or faster, $\nu_t \xrightarrow{t \to \infty} \infty$. However, it is important to note, that at the moment it is unclear whether the product $\nu_t \frac{d_t}{P_t}$ tends towards zero, infinity or a finite value. Inserting the above assumption into the terms a_t^*, b_t^* and c_t^*, gives

$$a_t^* \approx x^f_{min} \left(x^f_{min} - 1 \right), \tag{4.34}$$

$$b_t^* \approx x^f_{min} \left(1 - x^f_{min} \right) R_f + \nu_{t-1} \frac{d_t}{P_{t-1}}, \tag{4.35}$$

$$c_t^* \approx 0. \tag{4.36}$$

The solution of the quadratic equation for average price returns can now be simplified

$$R_t \approx \frac{-b_t^* - \sqrt{b_t^{*2}}}{2a_t^*} = -\frac{b_t^*}{a_t^*}. \tag{4.37}$$

With a_t^* and b_t^* from equations (4.34) and (4.35), equation (4.37) gives

$$R_t - R_f \approx \frac{\nu_{t-1} \frac{d_t}{P_{t-1}}}{x^f_{min} \left(1 - x^f_{min} \right)}. \tag{4.38}$$

Let us evaluate the relative change of $R_t - R_f$

$$\frac{R_t - R_f}{R_{t-1} - R_f} \approx \frac{\nu_{t-1} \frac{d_t}{P_{t-1}}}{\nu_{t-2} \frac{d_{t-1}}{P_{t-2}}} \approx \frac{\nu_{t-1}}{\nu_{t-2}} \frac{R_d}{R_{t-1}}. \tag{4.39}$$

Consider for a moment the wealth ratio

$$\nu_{t-1} = \nu_{t-2} \frac{x^n_{t-2} \left(R_{t-1} - R_f + \frac{d_{t-1}}{P_{t-2}} \right) + R_f}{x^f_{t-2} \left(R_{t-1} - R_f + \frac{d_{t-1}}{P_{t-2}} \right) + R_f}, \tag{4.40}$$

inserting the same assumptions as before ($x^n = 1.0$, $x^f = x^f_{min}$ and $\frac{d}{P} \to 0$) gives

$$\nu_{t-1} = \nu_{t-2} \frac{R_{t-1} + 1}{x^f_{min}(R_{t-1} - R_f) + R_f}. \tag{4.41}$$

Using the above expression for the wealth ratio together with equation (4.39) gives

$$\frac{R_t - R_f}{R_{t-1} - R_f} \approx \frac{R_d}{x^f_{min}(R_{t-1} - R_f) + R_f}. \tag{4.42}$$

If an upper fixed point R_{max} exists, then then $\frac{R_t - R_f}{R_{t-1} - R_f} = 1$, otherwise $\frac{R_t - R_f}{R_{t-1} - R_f} > 1$. As stated above, it is not clear yet whether there is an upper fixed point, thus consider the inequality

$$\frac{R_t - R_f}{R_{t-1} - R_f} \geq 1 \quad \Rightarrow$$
$$R_d \geq x^f_{min}(R_{t-1} - R_f) + R_f \quad \Rightarrow \tag{4.43}$$
$$\frac{R_d - R_f}{x^f_{min}} \geq R_{t-1} - R_f.$$

We can see that indeed there is an upper fixed point R_{max}, which acts as an upper bound on the long-term average price growth R_{avg}

$$R_{max} \equiv R_f + \frac{R_d - R_f}{x^f_{min}}$$
$$= R_f + \frac{R_d - R_f}{\mathbb{E}_{R_t} - R_f} \gamma \sigma^2_{R_{ex}} \tag{4.44}$$
$$= R_f + \frac{R_d - R_f}{\mathbb{E}_{R_t} - R_f} \frac{\mathbb{E}_{R_t} - R_f + \frac{d_0}{P_0} R_d}{x^f_0}.$$

It is trivial to see that the upper fixed point for the average growth rate r_{avg} is given by

$$r_{max} = R_{max} - 1 = r_f + \frac{R_d - R_f}{\mathbb{E}_{R_t} - R_f} \frac{\mathbb{E}_{R_t} - R_f + \frac{d_0}{P_0} R_d}{x^f_0}. \tag{4.45}$$

The existence of this upper fixed point is supported by numeric results presented in chapter 6.

Chapter 5

Analytical phase diagram

In section 3.2 we introduced an iterative self-referential mean-field Ising based toy model of the noise trader behaviour and profiled its numeric phase diagram on the imitation and trend following weight coefficients c_s-c_h plane. Besides the standard ferromagnetic ordered and paramagnetic disordered regimes, there were two additional ordered phases. One with smooth oscillations and the other with regular jumping behaviour between the two polarised states. From this we concluded that the self-referential nature of the toy model enhances order. This result was foreshadowed by the short fixed point analysis in the end of the toy model definition in section 3.2.2. We showed that compared to the standard mean-field Ising model, the toy model had a lower critical inverse temperature (herding propensity), indicating that its self-referential nature enhances order. In this chapter, we conduct an analogues analysis for the full artificial market. We consider the limiting cases presented in chapter 4 in order to propose an analytical phase diagram for the average market behaviour on the c_s-c_h plane. We refer to this phase diagram as "analytical" in order to differentiate from the numeric phase diagram, which is profiled in chapter 6.

Here, similarly to chapter 4, the key idea is to look at the limiting noise trader behaviour, *i.e* the ordered (polarised) states where all noise traders are invested in the same asset type. These correspond to the risky fraction values $x^n \in \{1, 0\}$ or equivalently to opinion index values $s \in \{1, -1\}$. We call the states $s = \pm 1$ the *positive* and the *negative* ordered states, respectively. In section 4.1 we showed that necessary conditions for such polarised states are equivalent to conditions for the corresponding switching probabilities $p_t^{\pm}$ being zero. When describing the typical model dynamics in the case of Ornstein-Uhlenbeck herding propensity in section 3.1.2, we saw that zero valued switching probabilities create a lock-in effect for the respective asset, risky for $p_t^+ = 0$ and risk-free for $p_t^- = 0$, which leads to the onset of the corresponding ordered state. It is convenient to formulate the criteria for these

lock-ins with respect to threshold momentum values $H_c^{\pm}$ above or below which the corresponding lock-in occurs. Figure 4.1 illustrates that for $c_h > 0$, H_c^+ is the lower threshold above which $p_t^+ = 0$ and H_c^- is the upper threshold below which $p_t^- = 0$. For $c_h < 0$ the inequalities have the opposite direction. Section 4.2 discusses these threshold *critical momenta* $H_c^{\pm}$ in detail and shows that the shape of $H_c^{\pm}$ on the c_s-c_h plane defines a natural reference frame given by the lines $c_h = 0$ and $c_s = \frac{1}{\kappa}$. These lines divided the c_s-c_h plane into four quarters. As illustrated in figure 4.2, depending on the sign of the opinion index s, the critical momenta have different signs on these four quarters.

In sections 5.1 to 5.3 we analyse the possibility and stability of lock-in effects for the risky ($p_t^+ = 0$) and the risk-free ($p_t^- = 0$) assets on the four quarters of c_s-c_h plane. We start with the upper right quarter in section 5.1 and move in a clockwise direction, finishing with the upper left quarter in section 5.4. For all four parts of the plane, the argumentation is rather similar. Figure 4.4 illustrated that the condition $|H_c^{\pm}| < H_{cutoff}$ defines a double conical region centred at the *critical point* $(\frac{1}{\kappa}, 0)$. In the following, conceptually similar conditions are employed to divided each of the quarters into to parts with distinct characteristics. As mentioned above, we are analysing the average model behaviour. Therefore the relevant momentum value is given by the average momentum H_{avg}. In section 4.3 we used the limiting cases of negative and positive ordered noise traders for deriving two positive valued fixed points r_{min} and r_{max} of the price return rate r_t. These fixed points effectively act as rough lower and upper bounds on the average return rate $0 < r_{min} \lesssim r_{avg} \lesssim r_{max}$. As the price momentum H_t is defined as the exponential moving average of the price return rate r_t, these rough bound apply for the average momentum as well: $0 < r_{min} \lesssim H_{avg} \lesssim r_{max}$.

5.1 Upper right quarter $\left(c_s > \frac{1}{\kappa}, c_h > 0.0\right)$

In this section we consider the lock-in effects for the risky ($p_t^+ = 0$) and risk-free ($p_t^- = 0$) assets on the *upper right* quarter of the noise trader imitation and trend following c_s-c_h plane. The plane is divided into four quarters with the natural reference frame imposed by the critical momenta $H_c^{\pm}$ (see section 4.2) and the upper right quarter correspond to: $c_s > c_s^{critical} = \frac{1}{\kappa}$ and $c_h > 0$. Let us recall the necessary conditions for the lock-in effects in the upper right quarter:

1. Lock-in to the risky asset $p_t^+ = 0$ occurs above H_c^+

$$p_t^+ = 0 \text{ if } H \geq H_c^+, \text{ where } H_c^+ = \frac{1}{c_h}\left(\frac{1}{\kappa} - c_s s_t\right),$$

$$\text{such that } \begin{cases} H_c^+ < 0 \text{ if } s > 0, \\ H_c^+ > 0 \text{ if } s < 0. \end{cases} \tag{5.1}$$

2. Lock-in to the risk-free asset $p_t^- = 0$ occurs below H_c^-

$$p_t^- = 0 \text{ if } H \leq H_c^-, \text{ where } H_c^- = -\frac{1}{c_h}\left(\frac{1}{\kappa} + c_s s_t\right),$$

$$\text{such that } \begin{cases} H_c^- < 0 \text{ if } s > 0, \\ H_c^- > 0 \text{ if } s < 0. \end{cases} \tag{5.2}$$

Let us now assume that $0 < s$ and consider whether the lock-in effects can occur. First, take the condition for the lock-in to the risk-free asset: $H \leq H_c^- < 0$. As the long-term average momentum is positive $H_{avg} > 0$, then this condition can never be satisfied stably. Next, consider the condition for the lock-in to the risky asset: $H \geq H_c^+ < 0$. Because $H_{avg} > 0$, this condition is on average always satisfied. Thus we see, if the opinion is positive, then there is always a lock-in for the risky asset and never for the risk-free asset. Consequently, the system falls to the positive ordered state $s = 1$.

We now turn to the case of negative opinion $0 > s$ and consider the possibility of lock-in effects. From equations (5.1) and (5.2) we see that for a negative opinion, both $H_c^\pm > 0$. Consider the stability of the lock-in to the risky asset. If p_t^+ vanishes, the noise trader opinion rapidly rises and becomes positive. At which point, the threshold H_c^+ becomes negative and the condition $H \geq H_c^+$ is always satisfied. The system goes to the ordered phase $s = 1$.

Now, take the condition for the risk-free asset lock-in effect: $H \leq H_c^- > 0$. If the upper threshold is higher then the average momentum $H_c^- > H_{avg}$, then on average this lock-in occurs, while when $H_c^- < H_{avg}$ it does not. It is important to note, that if the lock-in to the risk-free asset occurs, the noise trader opinion plummets and the momentum value decreases. This means, that the lock-in induced noise trader behaviour does not destabilise the lock-in itself. Thus as soon as the condition $H_{avg} < H_c^-$ gets satisfied, the a stable lock-in effect occurs. The condition $H_{avg} = H_c^-$ allows us to separate the upper right quarter into two regions, one in which lock-in to risky asset always occurs and one in which a the lock-in to risky or risk-free asset occurs.

While we do not know the exact value of the average momentum, we do know that it is roughly bound by the fixed points of the price return rate: $r_{min} \lesssim H_{avg} \lesssim r_{max}$. The conditions $H_c^- = r_{min}$ and $H_c^- = r_{max}$ define two lines on the c_s-c_h plane

$$c_h = -\frac{1}{r_{min}}\left(\frac{1}{\kappa} - c_s\right) \text{ and } c_h = -\frac{1}{r_{max}}\left(\frac{1}{\kappa} - c_s\right). \tag{5.3}$$

Somewhere in the area between the lines defined by $H_c^- = r_{min}$ and $H_c^- = r_{max}$ there is a boundary, which divides the upper right quarter into two parts: (1) where on average the lock-in to the risk-free asset $(p_t^- = 0)$ does
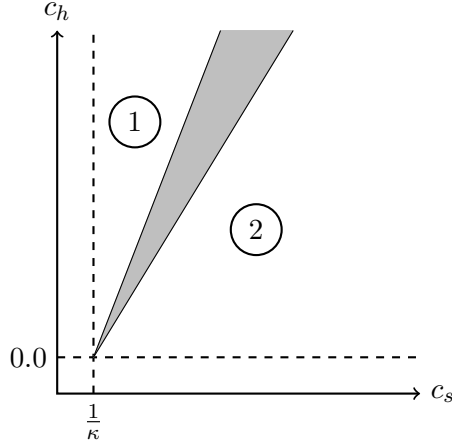
Figure 5.1: Illustrative sketch of the upper right quarter of the analytical phase diagram on the noise trader imitation and trend following weight coefficients c_s-c_h plane. The upper right quarter of the plane corresponds to the regions where $c_h > 0$ and $c_s > \frac{1}{\kappa}$, where κ is the noise trader herding propensity. Here the necessary conditions for the lock-in effects are: $H \geq H_c^+$ for the risky asset ($p_t^+ = 0$) and $H \leq H_c^-$ for the risk-free asset ($p_t^- = 0$). Both of the critical momenta always have the opposite sign than the noise trader opinion index. Considering the conditions for the lock-in effects, the upper right quarter can be divided into two parts: (1) where on average the lock-in to the risk-free asset ($p_t^- = 0$) does not happen, while the lock-in to the risky asset ($p_t^+ = 0$) always does, *i.e* the system is in the positive ordered state $s = 1$; (2) where either $p_t^- = 0$ or $p_t^+ = 0$, depending on which of the lock-ins occurs first, *i.e* the system is either in the positive or the negative ordered state. Which of the polarised regimes gets realised in (2) depends on the initial perturbations of the system. The boundary line between (1) and (2) is expected to be found in the shaded area: it is at or between the lines defined by (a) $H_c^- = r_{min}$ and (b) $H_c^- = r_{max}$. The corresponding line equations are given in equation (5.3). Thus we can expect the slope of the boundary to be in the interval $[\frac{1}{r_{max}}, \frac{1}{r_{max}}]$.

not happen, while the lock-in to the risky asset ($p_t^+ = 0$) always does, *i.e* the system is in the positive ordered state $s = 1$; (2) where either $p_t^- = 0$ or $p_t^+ = 0$, depending on which of the lock-ins occurs first, *i.e* the system is either in the positive or the negative ordered state. The sketch in the figure 5.1 illustrates this division.

5.2   Lower right quarter $\left(c_s > \frac{1}{\kappa}, c_h < 0.0\right)$

In this section we consider the lock-in effects for the risky ($p_t^+ = 0$) and risk-free ($p_t^- = 0$) assets on the *lower right* quarter of the noise trader imitation and trend following c_s-c_h plane. The plane is divided into four quarters with the natural reference frame imposed by the critical momenta $H_c^\pm$ (see section 4.2) and the lower right quarter correspond to: $c_s > c_s^{critical} = \frac{1}{\kappa}$ and $c_h < 0$.

Let us recall the necessary conditions for the lock-in effects in the lower right quarter:

1. Lock-in to the risk-free asset $p_t^+ = 0$ occurs below H_c^+

$$p_t^+ = 0 \ \text{if} \ H \leq H_c^+, \ \text{where} \ H_c^+ = \frac{1}{c_h} \left(\frac{1}{\kappa} - c_s s_t \right),$$

$$\text{such that} \ \begin{cases} H_c^+ > & 0 \ \text{if} \ s > 0, \\ H_c^+ < & 0 \ \text{if} \ s < 0. \end{cases} \tag{5.4}$$

2. Lock-in to the risky asset $p_t^- = 0$ occurs above H_c^-

$$p_t^- = 0 \ \text{if} \ H \geq H_c^-, \ \text{where} \ H_c^- = -\frac{1}{c_h} \left(\frac{1}{\kappa} + c_s s_t \right),$$

$$\text{such that} \ \begin{cases} H_c^- > & 0 \ \text{if} \ s > 0, \\ H_c^- < & 0 \ \text{if} \ s < 0. \end{cases} \tag{5.5}$$

The following analysis is similar to the one for the upper right quarter in section 5.1. Compared to section 5.1, it is more convenient to start with considering the case of negative opinion $s < 0$, in which case both critical momenta are negative $H_c^\pm < 0$ (see equations (5.4) and (5.5)). Thus, as $0 < r_{min} \lesssim H_{avg}$, on average the condition for lock-in to risky asset $H \leq H_c^+ < 0$ is never satisfied, while the condition for lock-in to the risk-free asset $H \geq H_c^- < 0$ always is. Consequently, the system stabilises into the negative ordered phase $s = -1$.

Now, assume positive opinion, in which case both critical momenta are positive $H_c^\pm > 0$ (see equations (5.4) and (5.5)). Consider the stability of the lock-in to the risk-free asset. If the momentum becomes larger than the lower bound H_c^- for vanishing p_t^-, the opinion rapidly lowers until it turns negative. As shown above, in such a case the state $p_t^- = 0$ is stable and the system falls to the negative ordered regime $s = -1$.

Now, take the condition for the risky lock-in: $H \leq H_c^+ > 0$. If the upper threshold for $p_t^+ = 0$ is higher then the average momentum $H_c^+ > H_{avg}$, then on average the lock-in to the risky asset occurs, while if $H_c^+ < H_{avg}$ then it does not. It is important to note, that if the lock-in to the risky asset occurs, the noise trader opinion index start rapidly rising, casing the momentum to also rise. Therefore, the lock-in induced noise trader behaviour destabilises the lock-in if the the momentum rises to values above the threshold value H_c^+. Recall, that the average momentum has a rough upper bound $H_{avg} \lesssim r_{max}$. Therefore, the condition $H_c^+ = r_{max}$ divides the lower right quarter into two regions with a boundary line given as
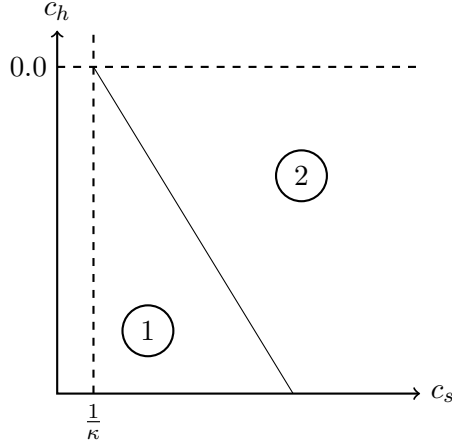
Figure 5.2: Illustrative sketch of the lower right quarter of the analytical phase diagram on the noise trader imitation and trend following weight coefficients c_s-c_h plane. The lower right quarter of the plane corresponds to the regions where $c_h < 0$ and $c_s > \frac{1}{\kappa}$, where κ is the noise trader herding propensity. Here the necessary conditions for the lock-in effects are: $H \leq H_c^+$ for the risky asset ($p_t^+ = 0$) and $H \geq H_c^-$ for the risk-free asset ($p_t^- = 0$). Both of the critical momenta always have the same sign than the noise trader opinion index. Considering the conditions for the lock-in effects, the lower right quarter can be divided into two parts: (1) where on average the lock-in to the risky asset never occurs, but for the risk-free asset it always does, leading the system to the negative ordered phase $s = -1$; (2) where the system is either in the positive or negative ordered phase, depending on which lock-in occurs first. Which of the polarised regimes gets realised in (2) depends on the initial perturbations of the system. The boundary line between (1) and (2) is defined by the condition $H_c^+ = R_{max}$, which gives rise to equation (5.6).

$$c_h = \frac{1}{r_{max}} \left(\frac{1}{\kappa} - c_s \right). \tag{5.6}$$

Figure 5.2 illustrates how the boundary line defined with the condition $H_c^+ = r_{max}$ divides the lower right quarter into two regions: (1) where on average the lock-in to the risky asset never occurs, but for the risk-free asset it always does, leading the system to the negative ordered phase $s = -1$; (2) where the system is either in the positive or negative ordered phase, depending on which lock-in occurs first.

5.3 Lower left quarter $\left(c_s < \frac{1}{\kappa}, c_h < 0.0 \right)$

In this section we consider the lock-in effects for the risky ($p_t^+ = 0$) and risk-free ($p_t^- = 0$) assets on the *lower left* quarter of the noise trader imitation and trend following c_s-c_h plane. The plane is divided into four quarters with the

natural reference frame imposed by the critical momenta $H_c^{\pm}$ (see section 4.2) and the lower left quarter correspond to: $c_s < c_s^{critical} = \frac{1}{\kappa}$ and $c_h < 0$. Let us recall the necessary conditions for the lock-in effects in the lower right quarter:

1. Lock-in to the risk-free asset $p_t^+ = 0$ occurs below H_c^+

$$p_t^+ = 0 \ \text{if} \ H \leq H_c^+, \ \text{where} \ H_c^+ = \frac{1}{c_h}\left(\frac{1}{\kappa} - c_s s_t\right),$$

$$\text{such that} \ \begin{cases} H_c^+ < 0 \ \text{if} \ s > 0, \\ H_c^+ < 0 \ \text{if} \ s < 0. \end{cases} \tag{5.7}$$

2. Lock-in to the risky asset $p_t^- = 0$ occurs above H_c^-

$$p_t^- = 0 \ \text{if} \ H \geq H_c^-, \ \text{where} \ H_c^- = -\frac{1}{c_h}\left(\frac{1}{\kappa} + c_s s_t\right),$$

$$\text{such that} \ \begin{cases} H_c^- > 0 \ \text{if} \ s > 0, \\ H_c^- > 0 \ \text{if} \ s < 0. \end{cases} \tag{5.8}$$

Let us consider the directions of the inequalities stated above. We can see, that on the left hand side of the critical line $c_s^{critical} = \frac{1}{\kappa}$, the signs of $H_c^{\pm}$ are independent of the opinion index. In the lower left quarter $H_c^+ < 0$ and $H_c^- > 0$. In the following we use similar arguments as in the case of upper and lower right quarters in sections 5.1 and 5.2. First, recall that the average momentum is roughly bound by the positive valued fixed points of the price growth rate: $0 < r_{min} \lesssim H_{avg} \lesssim r_{max}$. This allows us to rule out the occurs of a lock-in to the risky asset. Namely, the condition for this is $H \leq H_c^+ < 0$. As the average momentum is positive, then on average this condition is never satisfied.

Now, consider the condition for the lock-in to the risk-free asset: $H \geq H_c^- > 0$. If the critical threshold H_c^- is lower than the average momentum $H_c^- < H_{avg}$, then on average the lock-in to risk-free asset occurs, while if $H_c^- > H_{avg}$ it does not. It is important to note that if the lock-in to the risk-free asset occurs, the noise trader opinion index lowers and correspondingly the momentum decreases as well. Therefore, the lock-in induced noise trader behaviour destabilises the lock-in if the momentum becomes lower than the threshold H_c^-. We know that the average momentum is roughly bound from below $r_{min} \lesssim H_{avg}$. Therefore, the condition $H_c^- = r_{avg}$ divides the lower left quarter into two regions, with a boundary line

$$c_h = -\frac{1}{r_{min}}\left(\frac{1}{\kappa} - c_s\right). \tag{5.9}$$

The division of the lower left quarter is illustrated in figure 5.3. There are two distinct areas: (1) where on average neither of the lock-in effects occurs and
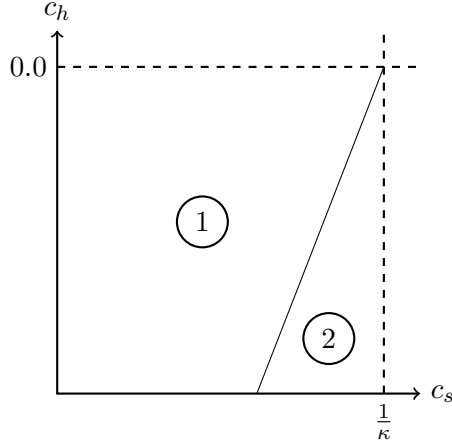
Figure 5.3: Illustrative sketch of the lower left quarter of the analytical phase diagram on the noise trader imitation and trend following weight coefficients c_s-c_h plane. The lower left quarter of the plane corresponds to the regions where $c_h < 0$ and $c_s < \frac{1}{\kappa}$, where κ is the noise trader herding propensity. Here the necessary conditions for the lock-in effects are: $H \leq H_c^+$ for the risky asset ($p_t^+ = 0$) and $H \geq H_c^-$ for the risk-free asset ($p_t^- = 0$). On the left hand side of the plane, the signs of $H_c^\pm$ are independent of the opinion index. In the lower left quarter $H_c^+ < 0$ and $H_c^- > 0$. Considering the conditions for the lock-in effects, the lower left quarter can be divided into two parts: (1) where on average neither of the lock-in effects occurs and the system is in a disordered state $|s| < 0$; (2) where on average the lock-in to the risk-free asset occurs and the system is in the negative ordered state $s = -1$. The boundary between these regions is defined with the condition $H_c^- = r_{min}$, which leads to the line equation (5.9).

the system is in a disordered state $|s| < 0$; (2) where on average the lock-in to the risk-free asset occurs and the system is in the negative ordered state $s = -1$.

5.4   Upper left quarter $\left(c_s < \frac{1}{\kappa}, c_h > 0.0\right)$

In this section we consider the lock-in effects for the risky ($p_t^+ = 0$) and risk-free ($p_t^- = 0$) assets on the *upper left* quarter of the noise trader imitation and trend following c_s-c_h plane. The plane is divided into four quarters with the natural reference frame imposed by the critical momenta $H_c^\pm$ (see section 4.2) and the upper left quarter correspond to: $c_s < c_s^{critical} = \frac{1}{\kappa}$ and $c_h > 0$. Let us recall the necessary conditions for the lock-in effects in the lower right quarter:

1. Lock-in to the risky asset $p_t^+ = 0$ occurs above H_c^+

$$p_t^+ = 0 \text{ if } H \geq H_c^+, \text{ where } H_c^+ = \frac{1}{c_h}\left(\frac{1}{\kappa} - c_s s_t\right),$$

$$\text{such that } \begin{cases} H_c^+ > & 0 \text{ if } s > 0, \\ H_c^+ > & 0 \text{ if } s < 0. \end{cases} \tag{5.10}$$

2. Lock-in to the risk-free asset $p_t^- = 0$ occurs below H_c^-

$$p_t^- = 0 \text{ if } H \leq H_c^-, \text{ where } H_c^- = -\frac{1}{c_h}\left(\frac{1}{\kappa} + c_s s_t\right),$$

$$\text{such that } \begin{cases} H_c^- < & 0 \text{ if } s > 0, \\ H_c^- < & 0 \text{ if } s < 0. \end{cases} \tag{5.11}$$

Considering the conditions in equations (5.10) and (5.11) we can see that in the upper left quarter the signs of the critical momenta are independent of the opinion index: $H_c^+ > 0$ and $H_c^- < 0$. Following similar arguments as for previous regions (see sections 5.1 to 5.3) we can eliminate the possibility for a lock-in to the risk-free assets. First, recall that the average momentum is roughly bound by the positive valued fixed points of the price growth rate: $0 < r_{min} \lesssim H_{avg} \lesssim r_{max}$. Thus, on average the condition $H \leq H_c^- < 0$ is not satisfied.

Now, take the condition for the lock-in to the risky asset: $H \geq H_c^+ > 0$. If the critical threshold is lower then the average momentum $H_c^+ < H_{avg}$ then on average the lock-in occurs, but if $H_c^+ > H_{avg}$ it does not. Note that if the lock-in to the risky asset occurs, the noise trader opinion index rises, which also rises the momentum. Therefore, the lock-in induced noise trader behaviour does not destabilise the lock-in. As soon as the momentum becomes larger than the threshold H_c^+, the lock-in is stable. The condition $H_c^+ = H_{avg}$ can be used for dividing the upper left quarter into two parts. We do not know the exact value of the average momentum, however, we do know that it is roughly bound with the price return rate fixed points r_{min} and r_{max}. The conditions conditions $H_c^+ = r_{min}$ and $H_c^+ = r_{max}$ define two lines on the c_s-c_h plane

$$c_h = \frac{1}{r_{max}}\left(\frac{1}{\kappa} - c_s\right) \text{ and } c_h = \frac{1}{r_{min}}\left(\frac{1}{\kappa} - c_s\right). \tag{5.12}$$

In figure 5.4 we illustrate how this area (shaded in the figure) divides the upper left quarter into two parts: (1) where neither of the lock-in effects ever occur and the system is in the disordered regime $|s| < 0$; (2) where on average the lock-in to the risky asset always occurs and the system is in the positive ordered regime $s = 1$. The boundary between these regions is somewhere in the shaded area defined with conditions $H_c^+ = r_{min}$ and $H_c^+ = r_{max}$.
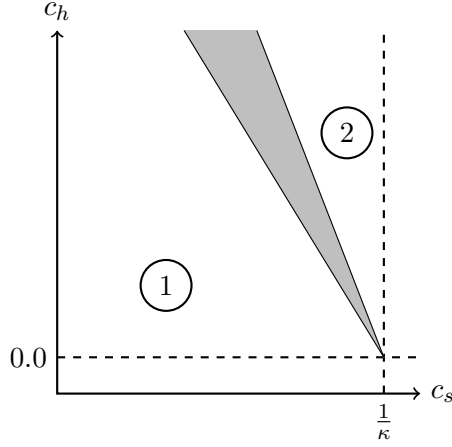
Figure 5.4: Illustrative sketch of the upper left quarter of the analytical phase diagram on the noise trader imitation and trend following weight coefficients c_s-c_h plane. The upper left quarter of the plane corresponds to the regions where $c_h < 0$ and $c_s < \frac{1}{\kappa}$, where κ is the noise trader herding propensity. Here the necessary conditions for the lock-in effects are: $H \geq H_c^+$ for the risky asset ($p_t^+ = 0$) and $H \leq H_c^-$ for the risk-free asset ($p_t^- = 0$). On the left hand side of the plane, the signs of $H_c^{\pm}$ are independent of the opinion index. In the upper left quarter $H_c^+ > 0$ and $H_c^- < 0$. Considering the conditions for the lock-in effects, the lower left quarter can be divided into two parts: ((1) where neither of the lock-in effects ever occur and the system is in the disordered regime $|s| < 0$; (2) where on average the lock-in to the risky asset always occurs and the system is in the positive ordered regime $s = 1$. The boundary between these regions is somewhere in the shaded area defined with the conditions $H_c^+ = r_{min}$ and $H_c^+ = r_{max}$, which lead to the lines defined in equation (5.12).

5.5 The combined phase diagram

In sections 5.1 to 5.4 we have analysed the possibility and stability of lock-in effects for both the risky ($p_t^+ = 0$) and the risk-free ($p_t^- = 0$) asset in the four quarters of the c_s-c_h plane. The plane is divided into four quarters with the natural reference frame imposed by the critical momenta $H_c^{\pm}$ (see section 4.2). For each of the quarters, we have found the existence of two distinct regimes. From the sketches of the four quarters, given in figures 5.1 to 5.4, we can observe that regimes situated next to each other on either sides of the reference lines $c_h = 0$ and $c_s = \frac{1}{\kappa}$ have the same characteristics. This suggest that the results, for the four quarters individually, can be merged into a full phase diagram for the artificial market on the c_s-c_h plane.

Figure 5.5 presents a sketch of this analytical phase diagram. There are four distinct phases centred around the point $(\frac{1}{\kappa}, 0)$: (1a) where noise traders are in the positive ordered phase $s = 1$; (2a) where noise traders are either in the positive $s = 1$ or the negative $s = -1$ ordered state, depending on the initial perturbations of the system; (3a) where noise traders are in the nega-
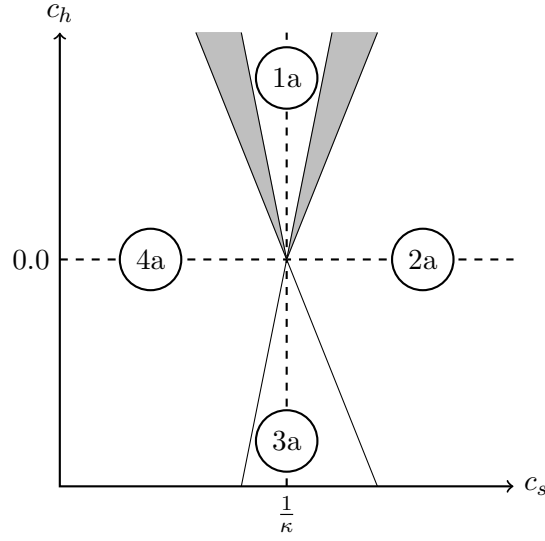
Figure 5.5: Illustrative sketch of the market model analytical phase diagram on the noise trader imitation and trend following weight coefficients c_s-c_h plane. The plane is divided into four quarter by the lines $c_h = 0$ and $c_s = \frac{1}{\kappa}$. The analytical is constructed by considering the possibility and stability of lock-in effect for both asset types in all four quarters of the plane separately. The analysis for each of these quarters is given in sections 5.1 to 5.4. There are four distinct phases centred around the point $(\frac{1}{\kappa}, 0)$: (1a) where noise traders are in the positive ordered phase $s = 1$; (2a) where noise traders are either in the positive $s = 1$ or the negative $s = -1$ ordered state, depending on the initial perturbations of the system; (3a) where noise traders are in the negative ordered phase $s = -1$; (4a) where noise traders are disordered $|s| < 1$. Here s is the noise trader opinion index. The boundaries of the positive ordered phase (1a) can be found in the two triangular shaded areas, which are defined by the conditions $H_c^+ \in [r_{min}, r_{max}]$ and $H_c^- \in [r_{min}, r_{max}]$ for the left and right hand side respectively. The negative ordered phase (3a), however, is outlined from the left by the condition $H_c^- = r_{min}$ and from the right by $H_c^+ = r_{max}$.

tive ordered phase $s = -1$; (4a) where noise traders are disordered $|s| < 1$. The boundaries of the positive ordered phase (1a) can be found in the two triangular shaded areas, which are defined by the conditions $H_c^+ \in [r_{min}, r_{max}]$ and $H_c^- \in [r_{min}, r_{max}]$ for the left and right hand side respectively. The negative ordered phase (3a), however, is outlined from the left by the condition $H_c^- = r_{min}$ and from the right by $H_c^+ = r_{max}$.

Chapter 6

The numerical phase diagram

In chapter 5 we proposed an analytical phase diagram for the artificial market model on the c_s-c_h plane. The key idea for constructing this analytical phase diagram was to consider in which regions are lock-in effects for the risky ($p_t^+ = 0$) and the risk-free ($p_t^- = 0$) assets possible, *i.e* in which regions are noise traders polarised $|s| = 1$. In chapter 4 the limiting cases of ordered noise traders were analysed in detail: necessary criteria for lock-in effects were discussed in sections 4.1 and 4.2 and in section 4.3 we derived two fixed points for the price growth rate r_t. These results were employed in chapter 5 for proposing an analytical phase diagram for the average market behaviour on the c_s-c_h plane. The results from chapter 5 are summarised in the sketch of the analytical phase diagram in figure 5.5, which shows four distinct regions centred around the *critical point* $(\frac{1}{\kappa}, 0)$. In this chapter we construct a numeric phase diagram for the artificial market model. First, in section 6.1 we introduce the phase diagram mapping process and in section 6.2 present the numeric results. We see that the four regimes proposed in the analytical phase diagram are indeed present in the numeric phase diagram and their position and shape corresponds well to the analytic treatment. However, in the numeric phase diagram, we also see a fifth phase, which was not predicted in chapter 5.

6.1 The mapping process

In this section we give an overview of the numeric phase diagram mapping process. Our general work-flow is very similarly to the one used in section 3.2.3 for mapping the phase diagram of the toy model. First, we conduct parameter scans over the c_s-c_h plane. For each pair of coefficient values (c_s, c_h), the market is evolved in a numerical simulation. The time series characterising these simulations are analysed to produce a set of scalar indicators of the market dynamics. The indicators are chosen so that they would enable us to differentiate between different market regimes. We visualise the indicators by

plotting colour coded heat-maps. In the heat-maps, the value of an indicator at a specific point on the plane is given by the colour of that point. We ensure readability, even for greyscale prints, by employing a colour scheme from the cubehelix family introduced by Green (2011) for astrophysical intensity plots.

There is, however, a clear difference between the toy model and the artificial market model. Namely, the toy model is deterministic, while the market model is stochastic. Consequently, the results for the artificial market are averaged over 100 realisations with different random number generator seeds. All other parameters are kept the same. We use the basic parameter set defined in table 3.1. In some cases, we find it necessary to vary a specific parameter for making certain features clearer. In these cases, the changed parameter is always highlighted. All simulations last for $T = 10^5$ time steps.

Let us describe the scalar indicators used for distinguishing the different regimes. Similarly to the toy model phase diagram mapping in section 3.2.3, our choice of indicators has been guided by a variety of exploratory simulations. During these, we observed several distinct features, for example the existence of ordered phases, which had very low volatility, as well as the existence of oscillatory dynamics. The specifics of different regimes are discussed in section 6.2. Below, we explain the set of informative indicators employed in this chapter. All of the listed indicators are averaged over 100 simulations realisations with different random number generator seeds.

1. Prop of $p_t^{\pm} = 0$: The proportion of time steps during which the corresponding switching probability, either p_t^+ or p_t^-, is non-positive.

2. Mean $x_t^{n/f}$: The mean value of the corresponding risky fraction, either x_t^f or x_t^n, average over all $T = 10^5$ time steps.

3. Log of Var $x^{n/f}$: The logarithm of the corresponding risky fraction variance, calculated over all $T = 10^5$ time steps.

4. Final H_t/r_d : The final momentum H_t, calculated as an average over the final 1000 time steps and given in the units of r_d.

5. $\left(H_t^{max} - H_t^{min} \right)/r_d$: The difference of the maximum and minimum momentum, given in the units of r_d.

6. Log of Var H_t/r_d : The logarithm of the momentum H_t variance, calculated over all $T = 10^5$ time steps.

7. Log of final W_t^n/W_t^f : The logarithm of the final wealth ratio $\nu_t = W_t^n/W_t^f$, calculated as an average over the final 1000 time steps.

8. Mean r_t/r_d : The mean value of the price return rate r_t, calculated over all $T = 10^5$ time steps and given in the units of r_d.

9. Log of time scale τ/day : The logarithm of the estimated time scale of the simulation time step given in the units of days.
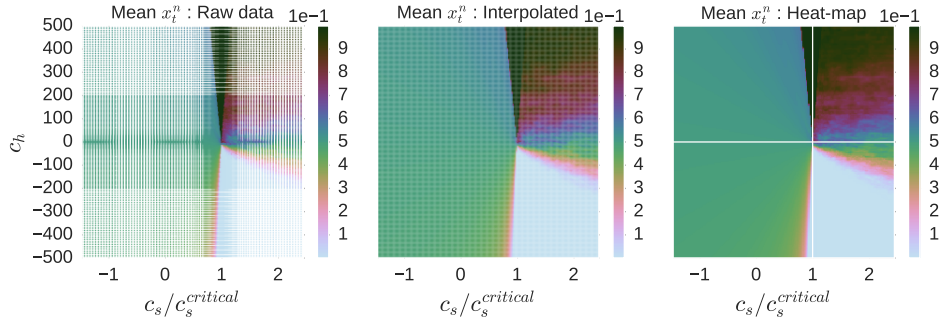
Figure 6.1: Illustration of the non-uniform to uniform grid interpolation during the parameter scan over the imitation and trend following weight coefficients c_s-c_h plane. The illustration uses the data for the mean noise traders risky fraction x^n. In the left most panel, we see the original raw data sampled with the non-uniform grid, in the middle panel we see the corresponding linearly interpolated uniform grid and the right most panel shows the final heat-map. The non-uniform grid is designed so that we sample more densely in the regions near the lines $c_s = c_s^{critical} = \frac{1}{\kappa}$ and $c_h = 0$. The grid covers the region defined by $c_s \in [-1.5, 2.5]$ and $c_h \in [-500, 500]$. When considering these heat-maps, and other in the current chapter, keep in mind that the c_s axis is scaled by its critical value $c_s^{critical} = \frac{1}{\kappa}$. With careful observations, we can already see the relevant phase structure on the non-uniform grid in the left most panel. Thus we can be sure, that the interpolation process just makes it easier to read the plots.

We now explain the parameter scanning over the c_s-c_h plane. Recall that the critical momenta, discussed in section 4.2, defined a natural frame of reference on the c_s-c_h plane with the lines $c_h = 0$ and $c_s = \frac{1}{\kappa}$. Moreover, the crossing point of these lines corresponds to the critical point of the analytical phase diagram $(\frac{1}{\kappa}, 0)$ (see figure 5.5). Motivated by the analytical phase diagram (see chapter 5), we conduct the parameter scan over the c_s-c_h plane using a non-uniform grid, which is denser near the lines $c_h = 0$ and $c_s = \frac{1}{\kappa}$. As the heat-map plotting algorithm requires equally spaced data, we linearly interpolate the raw data onto a uniform grid using methods implemented in the scientific Python package `SciPy` (Jones et al.). This process is illustrated in figure 6.1, where moving from left-to-right we see panels with: (1) raw data on the non-uniform grid; (2) linearly interpolated uniformly spaced data; (3) the final heat-map. The grid covers the region given by $c_s \in [-1.5, 2.5]$ and $c_h \in [-500, 500]$. Notice that, with careful observations we can see the key structure of the heat-map already from the non-uniform raw data, but the linear interpolation allows us to make a better visualisation. The full set of heat-maps of the market model with the basic parameter set (section 3.1.1) can be found in figure 6.2.
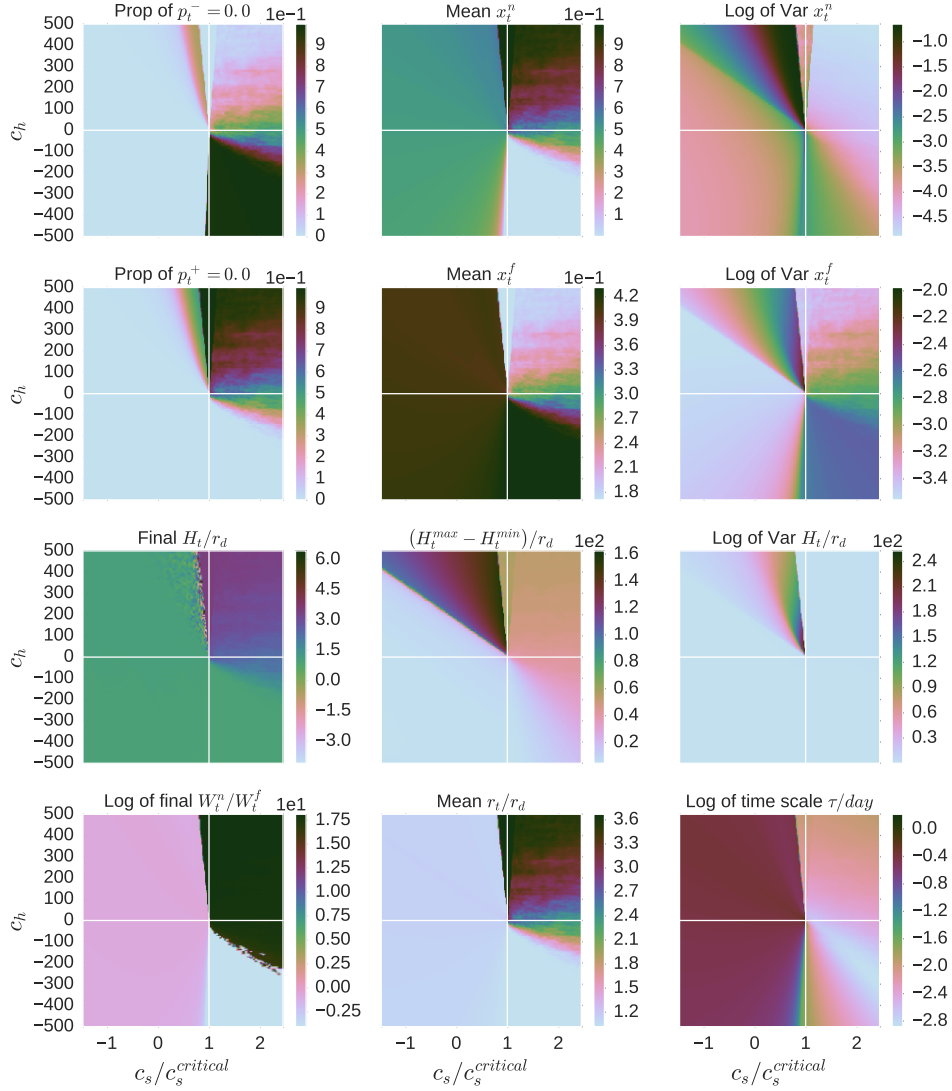
Figure 6.2: The full set of indicator heat-maps used for the numeric market model phase diagram mapping on the noise trader imitation and trend following weight coefficients c_s-c_h plane. All indicators are calculated as averages of 100 simulations with different random number generator seeds. The basic parameter set (table 3.1) is used and all simulations last for $T = 10^5$ time steps. Take care that c_s-axis is scaled with the critical value $c_s^{critical} = \frac{1}{\kappa}$, where κ is the noise trader social herding. The two perpendicular white lines correspond to $c_h = 0$ and $c_s = \frac{1}{\kappa}$, *i.e* they cross at the analytical critical point $(\frac{1}{\kappa}, 0)$, which due to the scaling fall at $(1, 0)$. Notice that there are regions, which are outlines in several heat-maps. For example we can see that the upper right corner is dominated by noise traders ($\nu >> 1$) and has a high noise trader risky fraction, as well as relatively high price return and momentum. Or that the lower right corner is fundamentalist dominated ($\log \nu < 0 \Rightarrow \nu < 1$) and has very low noise trader risky fraction $x^n \approx 0$. Similarly we can notice a triangular region in the upper left quarter, where the trader investment decisions are significantly more volatile then elsewhere. Finally note that right above the critical point there is a narrow triangular region where constantly $p_t^+ = 0$, indicating the positive ordered regime, and below the critical point there is large region where constantly $p_t^- = 0$, indicating the negative ordered regime. A more detailed analysis of the heat-maps is given in section 6.2.

6.2 Results

We presented the methodology used for profiling the numeric phase diagram of the artificial market model in section 6.1. In this section we present results from the numeric mapping process. First, in section 6.2.1, we provide a short general overview of the heat-maps in figure 6.2 and in section 6.2.2 we present the numeric phase diagram. Finally, in section 6.2.3 we conclude with presenting an illustrative sketch of the phase diagram.

6.2.1 General overview of the heat-maps

In this section we shortly describe the full set of indicator heat maps for a market model with the basic parameter set (table 3.1) shown in figure 6.2. Take care that the c_s-axis is in the units of the critical value $c_s^{critical} = \frac{1}{\kappa}$, which for the basic parameter set is $c_s^{critical} = \frac{1}{0.98} \approx 1.02$. In each heat-map we see two white lines, which correspond to the lines $c_h = 0$ and $c_s = c_s^{critical}$. Thus the crossing point $(1, 0)$ of the white lines corresponds to the analytical critical point $(\frac{1}{\kappa}, 0)$. Finally, note that the notation $1e - x$, found on the colour bars of the heat-maps, indicates that the colour bar is in the units of 10^{-x}.

Notice that in figure 6.2 there are regions, which are outlined in several heat-maps. For example we can see that the upper right corner is dominated by noise traders ($\nu \gg 1$) and has a high noise trader risky fraction, as well as relatively high price return and momentum. Or that the lower right corner is fundamentalist dominated ($\nu < 1$) and has very low noise trader risky fraction $x^n \approx 0$. Similarly we can observe a triangular region in the upper left quarter, where the trader investment decisions are significantly more volatile than elsewhere. An other striking feature is that all of the structure seen in figure 6.2 seems to be centred at the crossing point of the lines $c_h = 0$ and $c_s = \frac{1}{\kappa}$. This correspond to the analytical critical point $(\frac{1}{\kappa}, 0)$. A more detailed analysis of the critical point and the phase structure around it is given in section 6.2.2.

Finally, we call attention to the heat-map for the mean price return rate. Note, that r_t is given in the units of the average divided growth rate r_d. Recall the lower and upper fixed points r_{min} and r_{max} of the average price return rate r_{avg} (see equation (4.44)). For the basic parameter set (table 3.1) used in figure 6.2 these are $r_{min} = r_d$ and $r_{max} \approx 3.5 r_d$. We have argued that these fixed points effectively act as bounds on the long-term average price growth. Indeed, we can see that in the fundamentalist dominated lower right corner, where $x^n \approx 0$, the mean price return rate equals the lower fixed point $r_{avg} \approx r_{min} = r_d$. In the upper right corner, where noise traders dominate, we see that r_t becomes progressively larger as the mean noise trader risky fraction becomes larger, culminating at $r_{avg} \approx r_{max}$ in the narrow triangular region above the critical
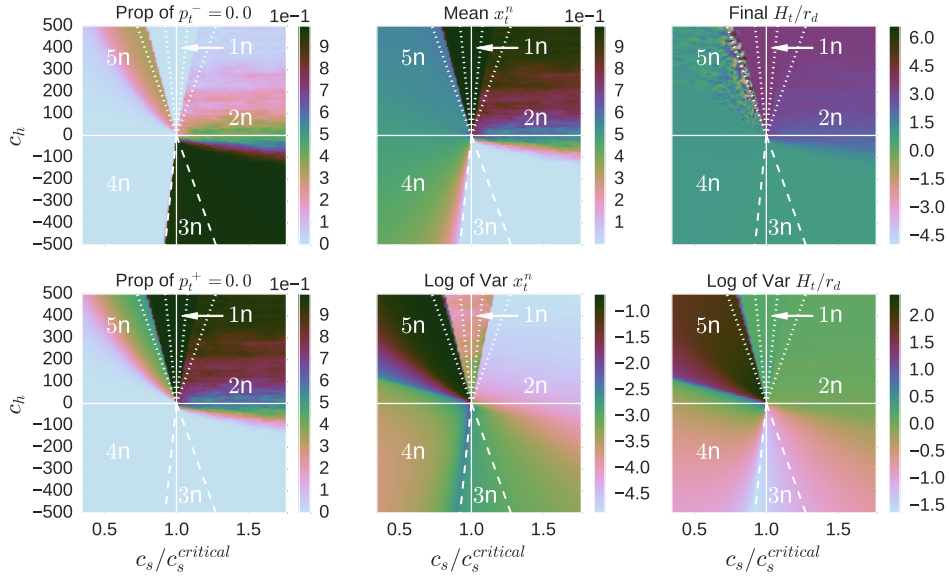
Figure 6.3: A magnification of a selection of heat-maps from figure 6.2, which visualise the phase structure of the artificial market model on noise trader imitation and trend following weight coefficients c_s-c_h plane. The white dashed lines on the lower half of the plane correspond to the analytical boundaries of the negative ordered state (3a) and the dotted white lines on the upper half of the plain define the analytical regions where the boundaries for the positive ordered state (1a) are found (see chapter 5). Recall, that the ordered states corresponded to polarised noise trader opinion $s = 2x^n - 1$. We have observed five different regimes in the numerical phase diagram: (1n) *positive* ordered phase $s = 1$; (2n) *bifurcating* ordered regime, where either $s = 1$ or $s = -1$, depending on the initial perturbation; (3n) *negative* ordered phase $s = -1$; (4n) *disordered* regime $|s| < 1$; (5n) *oscillating* regime, with regular transient lock-in effects. In chapter 5 we proposed an analytical phase diagram for the average market behaviour. It is sketched in figure 5.5. We can observe that the main structure and all four phase of the analytical phase diagram are indeed present in the numerical phase diagram. However, in chapter 5 we were not able to predict the existence of the triangular oscillating regime in the upper left quarter of the plane.

point, where $p_t^+ = 0$ and $x^n = 1$. Throughout the left hand side of the plane, r_t is only slight larger than the lower fixed point.

6.2.2 Regime structure

In this section we discuss the general structure of the numeric phase diagram. Let us turn to figure 6.3, which shows magnified heat-maps for the switching probabilities $p_t^{\pm}$, the mean and variance of the noise trader risky fraction x_t^n, the variance and final value of the momentum H_t. The white dashed lines on the lower half of the plane correspond to the boundaries of the analytical negative ordered state (3a) and the dotted white lines on the upper half of

the plain define the regions where the boundaries of the analytical positive ordered state (1a) are found (see chapter 5). We have highlighted five regions: (1n) *positive* ordered phase $s = 1$; (2n) *bifurcating* ordered regime, where either $s = 1$ or $s = -1$, depending on the initial perturbation; (3n) *negative* ordered phase $s = -1$; (4n) *disordered* regime $|s| < 1$; (5n) *oscillating* regime, with regular transient lock-in effects. The first four were also proposed in the analytical phase diagram sketched in figure 5.5. However, the fifth region (5n) was not. We argue that this is similar to the case of the toy model, where the fixed point analysis was not able to predict the jumping and oscillating phases. In the following we discuss these five regimes in more detail.

First, let us take the left hand side of the c_s-c_h plane. In chapter 3 we already introduced the disordered phase (4n) by describing the time series in figure 3.1, which corresponded to a market with the basic parameter set and $c_s = c_h = 1$. Here we will not re-iterate the detailed description given in section 3.1.2, instead make two general observation about (4n), which can be seen from figure 6.2: (a) the average price return rate is almost the dividend growth rate $r_{avg} \approx r_d$; (b) the wealth ratio is nearly one, or slightly lower, indicating that neither of the traders is strongly dominating. Let us turn to the region (5n). Figure 6.7 gives an example of the typical oscillating behaviour observed in (5n). It features regular switches between the two lock-in effects. From the heat-maps in figures 6.2 and 6.3 we can observe that the properties of region (5n) change smoothly from the border with (1n) to the border with (4n). The corresponding change in the time series is illustrated in figure 6.8, which shows the dynamics of the risky fractions at $c_h = 100$ for different opinion weights $c_s \in \{0.65, 0.7, 0.75, 0.8, 0.85, 0.9, 0.95, 1.0\}$. We see that far from the line $c_s = \frac{1}{\kappa}$, the regular oscillations between $x^n = 0$ and $x^n = 1$ last only for a short time, while closer they last longer. Our simulations show that near the ordered phase (1n), the oscillations last at least until the price becomes too large to be stored as a double precision floating point number and the simulations end due to numeric overflow. Thus, near (1n) the oscillations are effectively permanent.

In the following we discuss the characteristics of the right hand side of the c_s-c_h plane. Let us start with the positive (1n) and negative (3n) ordered states, for which typical time series are presented in figures 6.9 and 6.10, respectively. In case of (1n), in figure 6.9, we see super-exponential price growth until noise traders reach their maximum risky fraction and are locked-in to the positive ordered regime. After this lock-in has occurred, the market becomes calm, essentially deterministic. This behaviour last tills the end of the simulations ($T = 10^5$). For the negative ordered state (3n), in figure 6.10, we see a similar pattern. Although, the relaxation to the negative ordered state $s = -1$ ($x^n = 0$) takes an order of magnitude longer than the relaxation into the positive ordered state. Also, before the lock-in to the negative ordered state occurs, instead of clear super-exponential dynamics, as in figure 6.9, the

time series show behaviour typical of (4n). Nevertheless, once the system reaches the negative ordered phase, fluctuations fade and the market becomes effectively deterministic till the end of the simulation.

Let us consider the region (2n). First, remember the characterisation of the area (2a) for the analytical phase diagram: the system is either in the positive $s = 1$ or the negative $s = -1$ ordered regime, depending on which of the lock-in effects (vanishing switching probability) occurs first. For more details see sections 5.1 and 5.2. Keeping the aforementioned in mind, let us consider region (2n). In figure 6.3 the properties of (2n) seem to be smoothly varying between the two ordered phases (1n) and (3n). However, we call attention to the fact that in chapter 5 we found that depending on the initial perturbations this region should be exhibiting dynamics corresponding either to the positive or negative ordered phase. Our observations from the corresponding time series support this claim. Figure 6.11 shows time series of the price momentum H_t, noise trader switching probabilities $p_t^{\pm}$ and the risky fractions x_t^f and x_t^n in region (2n) for two different random number seeds. For one seed, the dynamics corresponds to the positive ordered phase (figure 6.11a), and for the other, it corresponds to the negative ordered phase (figure 6.11b). We have observed that this is the case throughout the region (2n). Due to this dependence on initial perturbations, we call (2n) the *bifurcating* ordered phase. Now we can interpret the seemingly smooth variation of properties throughout (2n), as a change in the probabilities for the system to stabilise in either $s = 1$ or $s = -1$.

Consider the boundaries between (1n), (2n) and (3n). Recall, that in chapter 5 we proposed straight lines with slopes $\frac{1}{r_{min}}$ and $-\frac{1}{r_{max}}$ as boundaries for the analytical negative ordered phase (3a) on the left and right hand side, respectively. Here r_{min} and r_{max} are the lower and upper fixed points for the average price return rate r_{avg} (see section 4.3). For the analytical positive ordered phase (1a), we proposed that its boundary lines have slopes in the intervals $\pm[\frac{1}{r_{max}}, \frac{1}{r_{min}}]$, where plus and minus correspond to right and left hand side. In figure 6.3 the initial noise trader allocations are $x_0^n = 0.5$. Thus both of the ordered states are symmetric in regards of the initial state of the market. In the light of the bifurcating nature of (2n), it would be natural to consider the boundaries between (1n), (2n) and (3n) from heat-maps where the symmetry between $|s| = \pm$ is broken, *i.e* where $x^n \neq 0.5$. Figure 6.4 shows the mean noise trader risky fraction heat-maps for three different initial noise trader allocations $x_0^n \in \{0.0, 0.5, 1.0\}$. All other parameter correspond to the basic parameter set given in table 3.1. We can observe that adding a bias to the noise trader allocations, *i.e* $x_0^n \neq 0.5$, pushes the bifurcating regime towards the corresponding ordered state. From figure 6.4 we can observe that even when the system is initially in the positive ordered state $x_0^n = 1$, there is a region where it ends up in the negative ordered state $x^n = 0$, and *vice versa*. These correspond to the positive and negative ordered phases (1n) and (3n), respectively. In figure 6.4 the analytical boundaries are drawn with white dot-
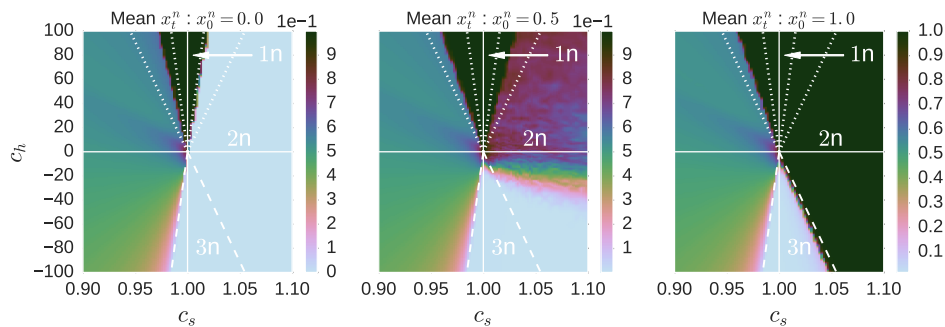
Figure 6.4: Heat-maps for determining the boundary between the positive, negative and bifurcating ordered regimes ((1n), (3n) and (2n)). The heat-maps are given on the noise trader imitation and trend following weight coefficient c_s-c_h plane. In order to effectively observe the boundaries of these phases, it is helpful to break the symmetry between the two ordered states. In the above we show mean noise trader risky fraction heat-maps for three different initial noise trader allocations $x_0^n \in \{0.0, 0.5, 1.0\}$. All other parameter correspond to the basic parameter set given in table 3.1. We can observe that adding a bias to the noise trader allocations, *i.e* $x_0^n \neq 0.5$, pushes the bifurcating regime towards the corresponding ordered state. Recall, that the ordered states corresponded to polarised noise trader opinion $s = 2x^n - 1$. In (1n) and (3n) the noise traders will always fall to the positive and negative ordered state, respectively. In (2a), however, whether the system stabilises at $s = 1$ or $s = -1$ depends on the initial perturbations. This is demonstrated with the time series in figure 6.11, where the system falls into the positive and negative ordered state depending on the random number generator seed. In the above heat-maps we can observe that even when the system is initially in the positive ordered state $x_0^n = 1$, there is a region where it ends up in the negative ordered state $x^n = 0$, and *vice versa*. These correspond to the positive and negative ordered phases (1n) and (3n), respectively. The white dotted and dashed lines in the heat-maps correspond to the analytical boundaries proposed in chapter 5 for (1n) and (3n), respectively. We can observe that the analytical and numerical boundaries are in good accordance.

ted and dashed lines for (1n) and (3n), respectively. We can observe that the analytical boundaries hold for the numeric phase diagram.

Let us now consider the analytical critical point $(\frac{1}{\kappa}, 0)$. For this, turn to figure 6.5, which shows heat-maps for different herding propensity values, keeping all other parameters as in the basic parameter set given in table 3.1. From left to right it shows the mean noise trader risky fraction for $\kappa \in \{1.01, 0.98, 0.95\}$. The corresponding analytical critical point c_s coordinates are $c_s^{1.01} = \frac{1}{1.01} \approx 0.99$, $c_s^{0.98} = \frac{1}{0.98} \approx 1.02$ and $c_s^{0.95} = \frac{1}{0.95} \approx 1.05$. Note, that in order to make the results easier to read in figure 6.5 the c_s-axis is not scaled with the critical coordinate $c_s^{critical}$. We can see that indeed, the c_s coordinate of the critical point is well predicted by $c_s^{critical} = \frac{1}{\kappa}$.
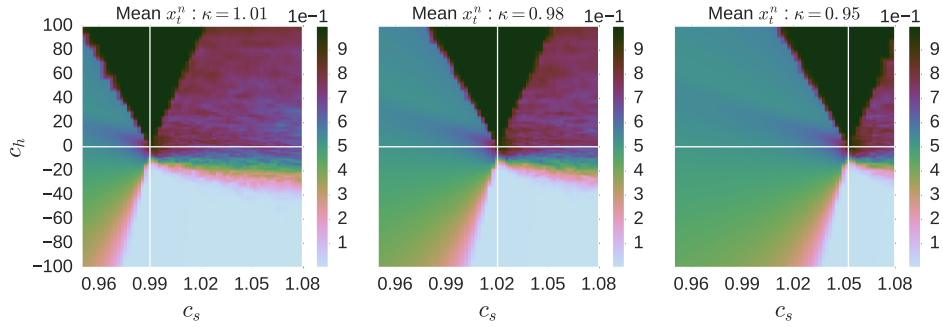
Figure 6.5: Illustration of testing the position of the phase diagram critical point on the noise trader imitation and trend following weight coefficients c_s-c_h plane. In order to test the analytical critical point $(\frac{1}{\kappa}, 0)$ we compare the heat-maps of mean noise trader risky fraction for three different herding propensity values $\kappa \in \{1.01, 0.98, 0.95\}$, which correspond to $c_s^{critical} \in \{0.99, 1.02, 1.05\}$. The rest of the model parameters correspond to the basic parameter set defined in table 3.1. Notice, that here the c_s-axis is not scaled with the critical value. The white lines correspond to $c_h = 0$ and $c_s = \frac{1}{\kappa}$, *i.e* they cross at the analytical critical point $(\frac{1}{\kappa}, 0)$. We can see that the numeric and analytic $c_s^{critical}$ are in good accordance.

Finally, let us test how robust is the phase diagram to added noise. We do this by increasing the standard deviation of the dividend process σ_d. Recall that in the basic parameter set (table 3.1) the standard deviation of the dividend process is $\sigma_d = 0.000016 = 0.1 r_d$. Figure 6.6 shows heat-maps for the mean and variance of the noise trader risky fraction, using $\sigma_d \in \{0.000016, 0.001, 0.01\} \approx \{0.1 r_d, 6 r_d, 60 r_d\}$. All other parameters are given by the basic parameter set (table 3.1). We can observe that the heat-maps for $\sigma_d = 0.1 r_d$ and $\sigma_d \approx 6 r_d$ are almost identical. However, the heat-map for $\sigma_d \approx 60 r_d$ is significantly difference compared to the heat-map for $\sigma_d = 0.1 r_d$. As a 60 fold increase in σ_d does not make a notable difference to the heat-maps, we can conclude that the phase diagram is rather robust to changes in σ_d.
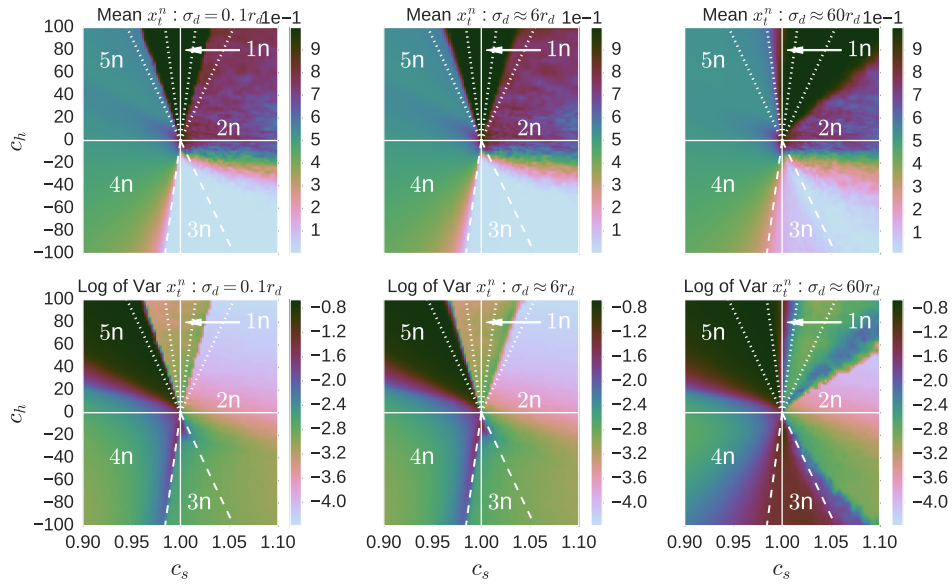
Figure 6.6: Testing the robustness of the phase diagram to change of the standard deviation of the dividend process. Above, we see heat-maps for the mean and variance of the noise trader risky fraction for $\sigma_d \in \{0.000016, 0.001, 0.01\} \approx \{0.1r_d, 6r_d, 60r_d\}$. All other parameters are given by the basic parameter set (table 3.1). In rest of this thesis, we have used $\sigma_d = 0.000016 = 0.1r_d$. We can observe that the heat-maps for $\sigma_d = 0.1r_d$ and $\sigma_d \approx 6r_d$ are almost identical. However, the heat-map for $\sigma_d \approx 60r_d$ is significantly difference compared to the heat-map for $\sigma_d = 0.1r_d$. As a 60 fold increase in σ_d does not make a notable difference to the heat-maps, we can conclude that the phase diagram is rather robust to changes in σ_d.
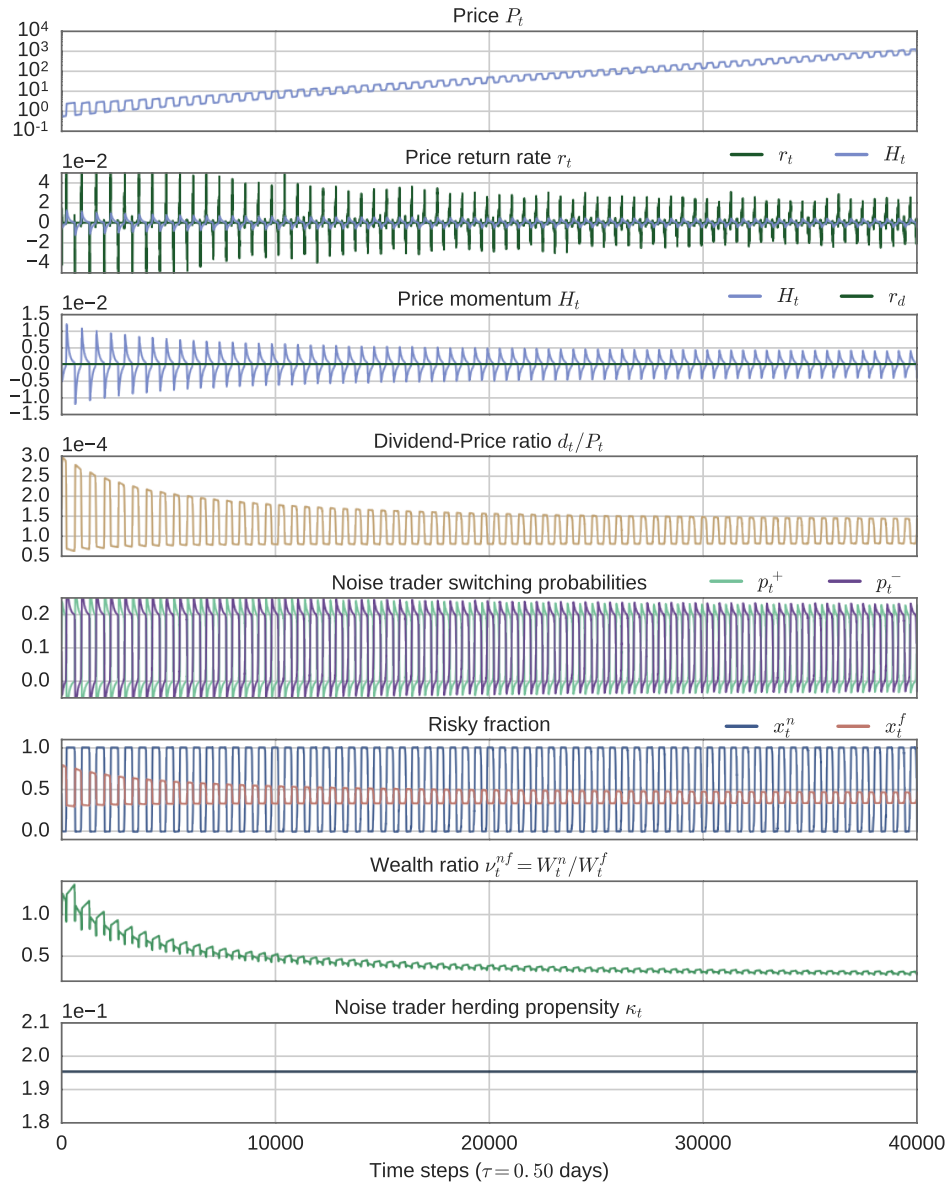
Figure 6.7: Characteristic time series for the oscillating regime (5n), where the system undergoes regular oscillations between the two ordered states $x^n = 1$ and $x^n = 0$. The basic parameter set given in table 3.1 is used. The noise trader imitation and trend following weight coefficients are $c_h = 100$ and $c_s = 0.95$, respectively. Based on equating the daily model- and real-volatility, we estimate that each time step correspond to $\tau \approx 0.50$ days. We can see that the system is regularly switching between two lock-ins. The period of the oscillations (the lock-in time) and the life-time of the oscillations changes throughout the region (5n). Far from the ordered phase (1n), the oscillation life-time (and period) is smaller, than near (1n). We have seen in our simulations, that near the boundary with (1n), the oscillations last at least until the price becomes too large to be stored as a double precision floating point number and the simulation ends due to numeric overflow. The change of oscillations due to change in c_s is illustrated in figure 6.8.
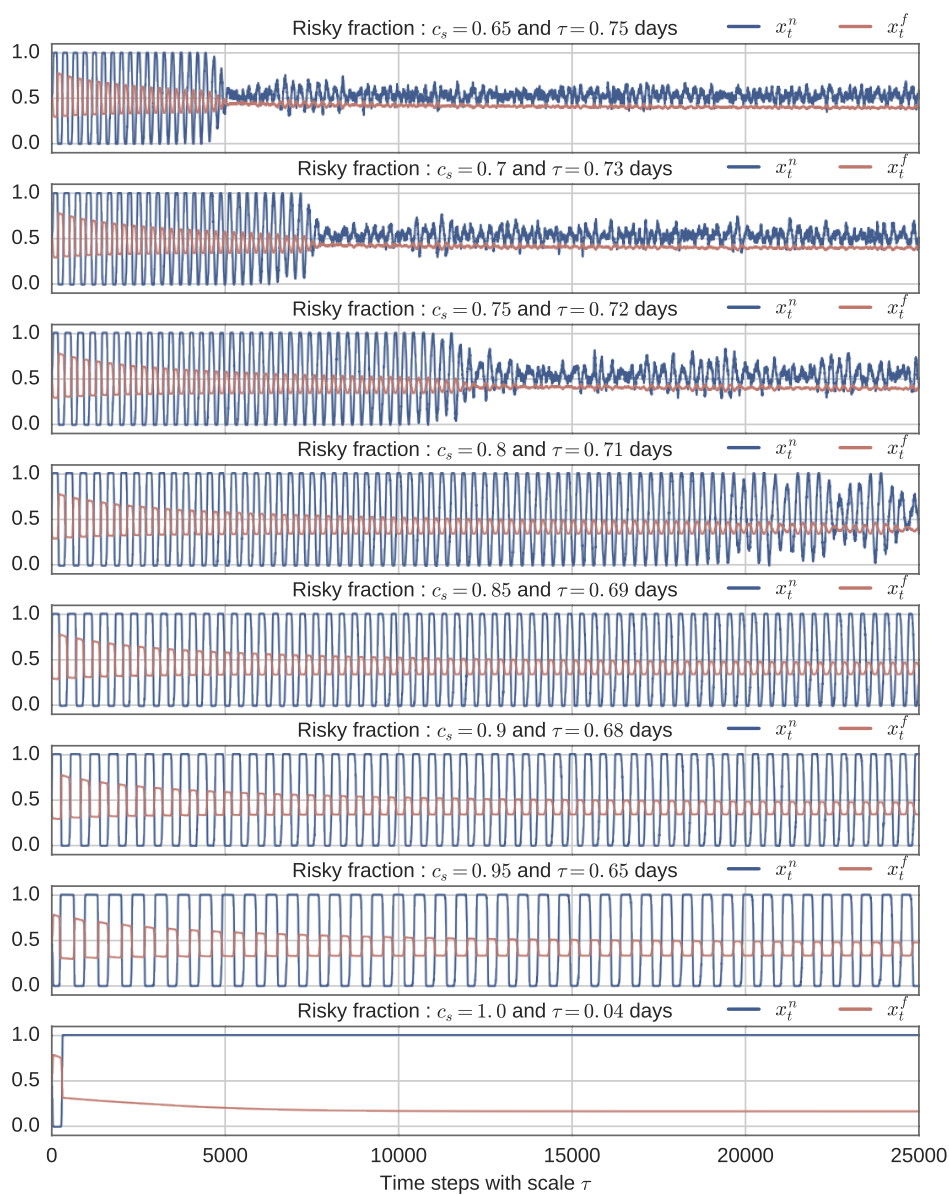
Figure 6.8: Illustration of ~~the~~ the change in the oscillation life time and period throughout the oscillating regime (5n). The basic parameter set given in table 3.1 is used. The noise trader trend following weight coefficient is $c_h = 100$. In above, we see eight panels with showing time series for the risky fraction x_t^f and x_t^n, for different noise trader imitation weight coefficient values $c_s \in \{0.65, 0.7, 0.75, 0.8, 0.85, 0.9, 0.95, 1.0\}$. We can see that the system is regularly switching between two lock-ins. The period of the oscillations (the lock-in time) and the life-time of the oscillations changes throughout the region (5n). Far from the ordered phase (1n) (far from $c_s = \frac{1}{\kappa}$), the oscillation life-time (and period) is smaller, than near (1n). We have seen in our simulations, that near the boundary with (1n), the oscillations last at least until the price becomes too large to be stored as a double precision floating point number and the simulation ends due to numeric overflow. In the last panel we see the system behaviour in the positive ordered regime (1n), but near the border with (5n). We can see that even though the system first has a short lock-in in the risky asset, in the end it becomes permanently locked-in to the risky asset, *i.e* $x^n = 1.0$.
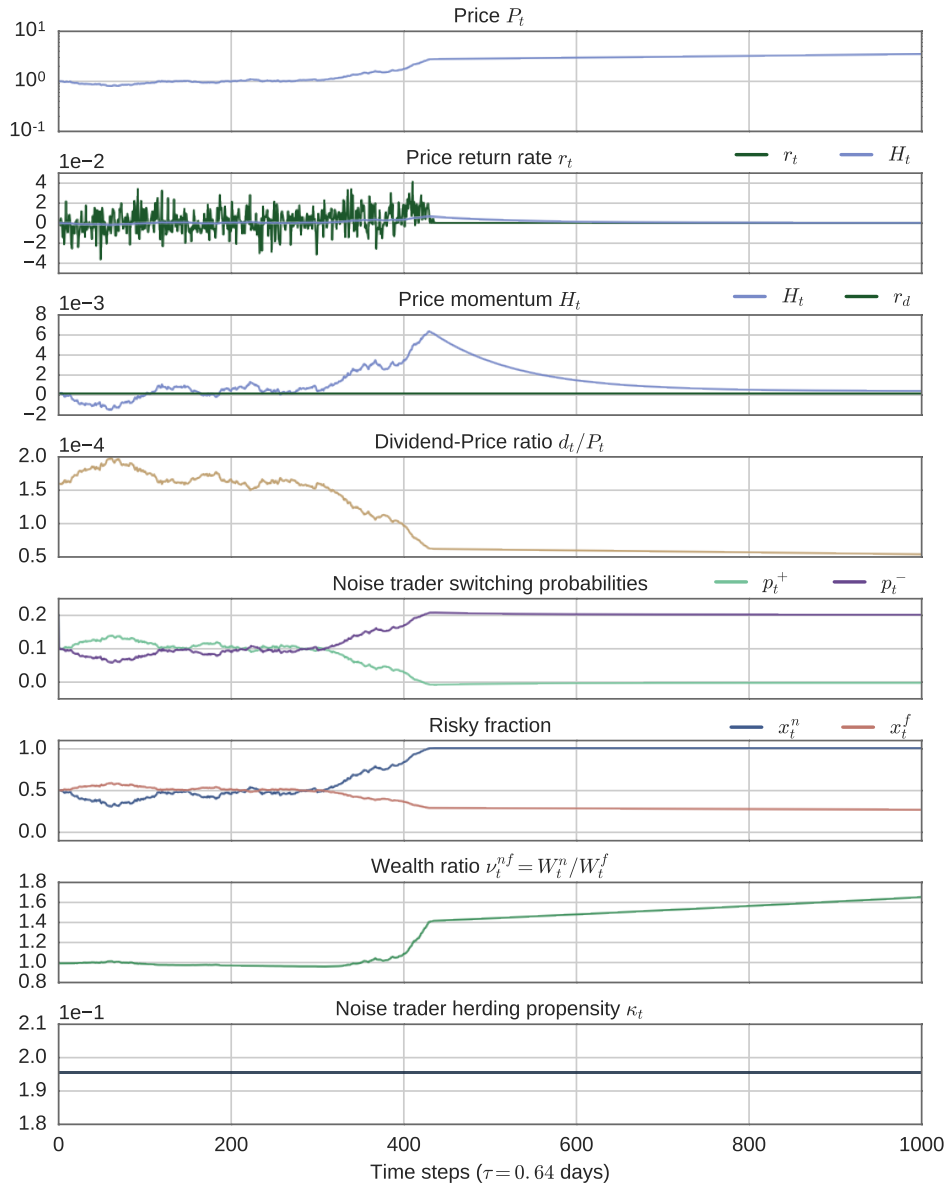
75

Figure 6.9: Characteristic time series for the positive ordered regime (1n), where all noise traders are invested into the risky asset $x^n = 1$ (opinion index: $s = 1$). The basic parameter set given in table 3.1 is used. The noise trader imitation and trend following weight coefficients are $c_s = 1.02$ and $c_h = 10$, respectively. Based on equating the daily model- and real-volatility, we estimate that each time step correspond to $\tau \approx 0.64$ days. We can observe that in the beginning of the simulation, the price grows super-exponentially, until noise traders reach their maximum risky fraction, at which point the market dynamics effectively become deterministic. Our observations show that this deterministic behaviour continues till the asset price becomes too large to be represented as a double precision floating point number and the simulations end due to numeric overflow. Thus, we can conclude that the lock-in effect is effectively permanent.
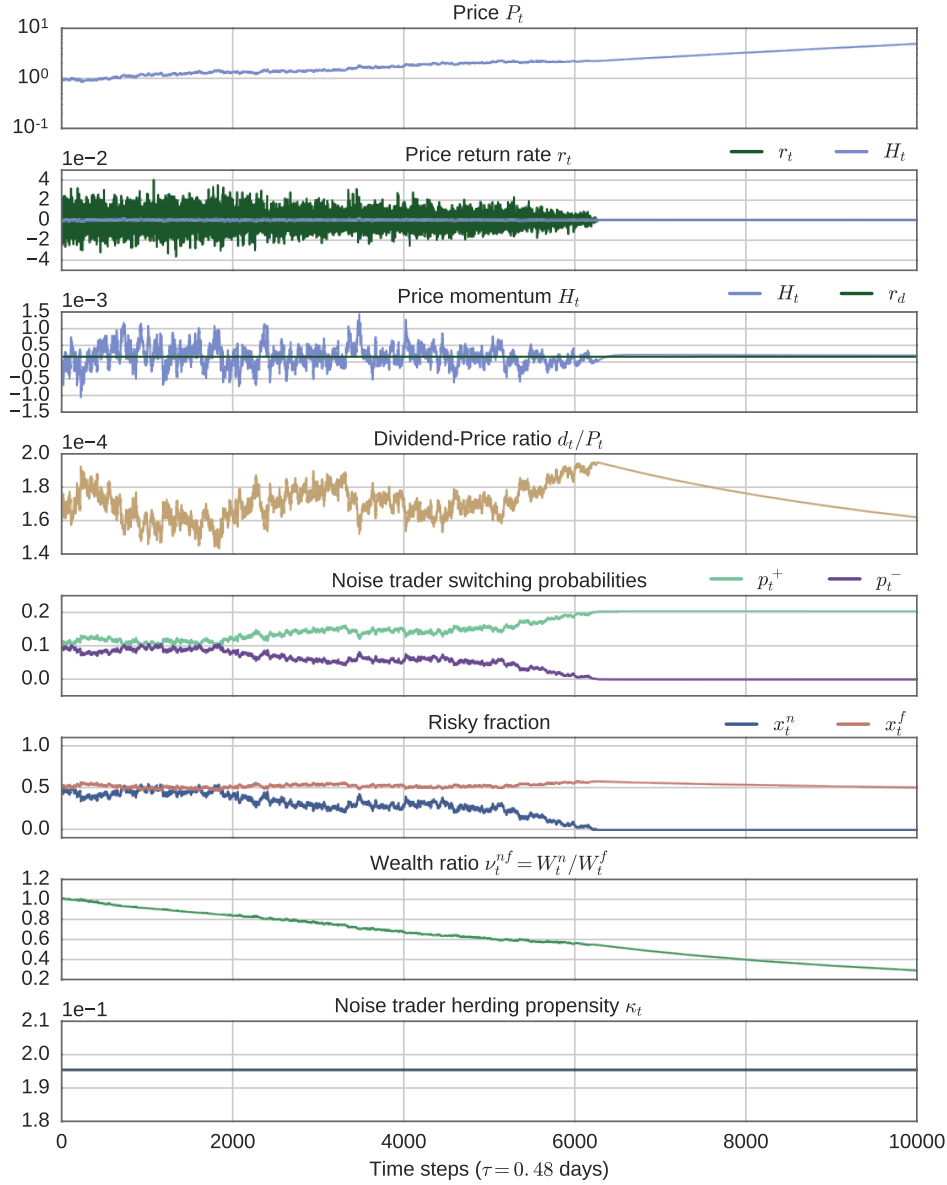
Figure 6.10: Characteristic time series for the negative ordered regime (3n), where all noise traders are invested into the risk-free asset $x^n = 0$ (opinion index: $s = -1$). The basic parameter set given in table 3.1 is used. The noise trader imitation and trend following weight coefficients are $c_s = 1.02$ and $c_h = -30$, respectively. Based on equating the daily model- and real-volatility, we estimate that each time step correspond to $\tau \approx 0.48$ days. We can observe that in the beginning of the simulation, the market dynamics is similar to that of the disordered regime (4n), for which characteristic time series can be seen in figure 3.1. When the noise trader risky fraction becomes $x^n = 0$, there is a lock-in effect and the market dynamics effectively become deterministic. Our observations show that this deterministic behaviour continues till the asset price becomes too large to be represented as a double precision floating point number and the simulations end due to numeric overflow. Thus, we can conclude that the lock-in effect is effectively permanent.

77
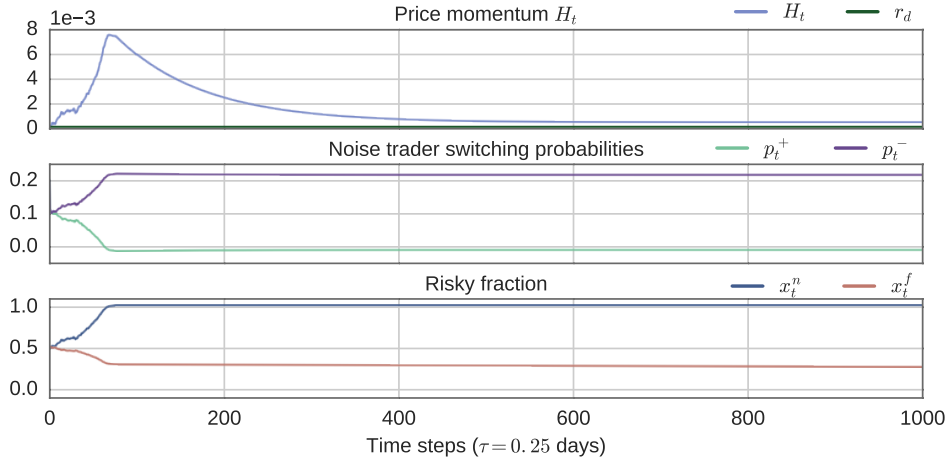
(a) Bifurcating phase (2n) at $c_s = 1.15$ and $c_h = 5$ with seed 10408
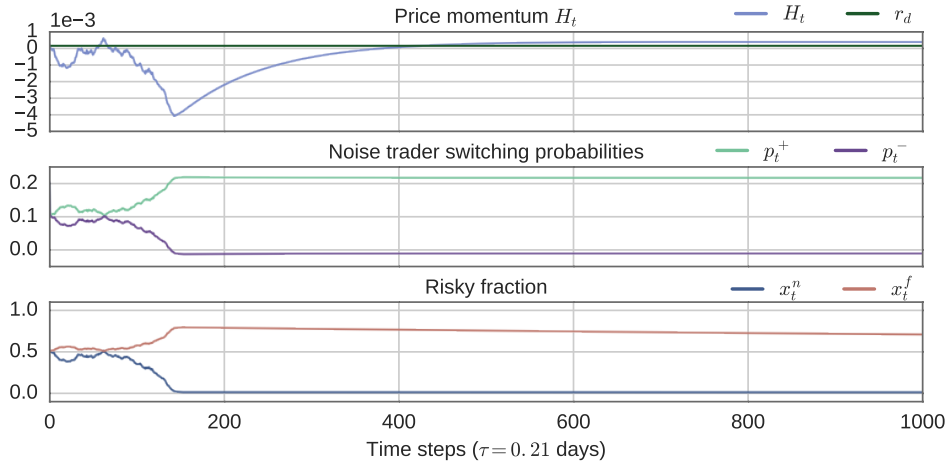
(b) Bifurcating phase (2n) at $c_s = 1.15$ and $c_h = 5$ with seed 1518

Figure 6.11: Illustration of the bifurcating nature of the regime (2n). The basic parameter set given in table 3.1 is used. The noise trader imitation and trend following weight coefficients are $c_s = 1.15$ and $c_h = 5$, respectively. Panel (a) shows the time series for the random number generator seed 10408 and panel (b) for 1518. Based on equating the daily model- and real-volatility, we estimate that each time step correspond to $\tau_a \approx 0.25$ and $\tau_b \approx 0.25$ days for panel (a) and (b) respectively. Observe, that the market dynamics in panels (a) and (b) are significantly different. In panel (a), the noise traders order into the positive ordered phase $x^n = 1$, while in panel (b) they stabilise in the negative ordered phase (b). The corresponding characteristic time series for the positive and negative ordered state can be seen in figures 6.9 and 6.10, respectively. We re-iterate that the only difference between the two simulations is in the seed of the random number generator. Thus, we can conclude that in (2n) the system is highly susceptible to initial perturbations. Due to this, we name this regime the *bifurcating ordered* phase.

6.2.3 Phase diagram summary

In section 6.1 we described the mapping procedure of the numeric phase diagram and in section 6.2.2 we present a detailed overview of the regime structure of the phase diagram. Here we summaries these results with the sketch in figure 6.12, which shows five regimes centred at the critical point $(\frac{1}{\kappa}, 0)$: (1n) *positive* ordered phase $s = 1$; (2n) *bifurcating* ordered regime, where either $s = 1$ or $s = -1$, depending on the initial perturbation; (3n) *negative* ordered phase $s = -1$; (4n) *disordered* regime $|s| < 1$; (5n) *oscillating* regime, with regular transient lock-in effects. The regimes (1n)–(4n) correspond well with the four phases found for the analytical phase diagram in chapter 5. The analytical phase diagram is sketched in figure 5.5. Comparing the two sketches, we can see that they are the same, except for (5n) in the numeric case.

The numeric phase diagram in figure 6.12 has been constructed using a constant noise trader herding propensity κ. However, if the herding propensity is time-depended, then this can be though of as moving on the phase diagram in figure 6.12. For example, assume that the noise trader imitation and trend following weight coefficients are kept fixed at some values c_s^* and c_h^*. If the herding propensity κ is time dependent, then this means that the system is moving along a line defined by c_s^* and c_h^* in the c_s-c_h plane. While moving along this line, the system can cross between different phases. Thus, the above phase diagram can be applied for analysing the time-depended regime structure of the market model. Although, this is beyond the scope of this thesis.
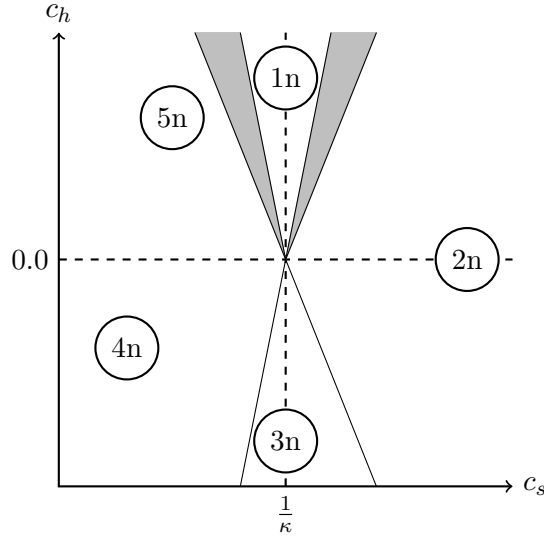
Figure 6.12: Illustrative sketch of the numerical phase diagram of the artificial market model on the noise trader imitation and trend following weight coefficients c_s-c_h plane. The numeric phase diagram has five separable regions which are centred at the *critical point* $(\frac{1}{\kappa}, 0)$, where κ is the noise trader herding propensity. These five regimes are: (1n) *positive* ordered phase $s = 1$; (2n) *bifurcating* ordered regime, where either $s = 1$ or $s = -1$, depending on the initial perturbation; (3n) *negative* ordered phase $s = -1$; (4n) *disordered* regime $|s| < 1$; (5n) *oscillating* regime, with regular transient lock-in effects. Here s is the noise trader opinion index. The analytical boundaries of the positive ordered phase (1n) can be found in the two triangular shaded areas; the slopes of these boundary lines are in the intervals $\pm[\frac{1}{r_{max}}, \frac{1}{r_{min}}]$, where minus and plus correspond to left and right hand side, respectively. The boundaries for the negative ordered phase (3a), have slopes $\frac{1}{r_{min}}$ and $-\frac{1}{r_{max}}$ on the left and right hand side, respectively. The regimes (1n)–(4n) correspond well with the four phases found for the analytical phase diagram in chapter 5. The analytical phase diagram is sketched in figure 5.5. Comparing the two sketches, we can see that they are the same, except for (5n) in the numeric case.

Chapter 7

Conclusion and discussion

The goal of this thesis was to study the different market regimes in the artificial market model introduced by Kaizoji et al. (2015) and extended by Kohrt (2016). In its essence, the model is an equilibrium model of fundamentalist and noise traders. It has two assets, a constant interest rate risk-free asset and a dividend paying risky asset, whose price is determined by the market clearing condition. The fundamentalists base their investment decisions on maximising their constant risk aversion expected utility, which leads them to the value investor strategy: buy-low-and-sell-high. The noise traders, however, guide their decisions by the opinion of other noise traders and the market trend. The strength of the noise trader response to these signals is given by their *herding propensity*. Kaizoji et al. (2015) showed that with a time depended herding propensity, following an Ornstein-Uhlenbeck process, the market model exhibits transient faster-than-exponential bubble growth.

In this thesis, we have explored the effects of the noise trader imitation and trend following in greater detail. In Kaizoji et al. (2015) and Kohrt (2016) the noise trader decision process relied equally on social factors and the market trend. We extended the model by adding weight coefficients to these signals, so that their relative importance can be controlled. This allowed us to view the market regimes, *e.g* transient super-exponential bobble growth, from a different perspective. Keeping the herding propensity a constant and varying the imitation and trend following weight coefficients, we have mapped a phase diagram of the market model on the plane defined by these weight coefficients. The case of a time-dependent herding propensity, *e.g* in Kaizoji et al. (2015), can now be though of as moving on this phase diagram, thus providing a way to consider the regime switching during the market simulation.

In section 3.2 we introduced a mean-field Ising based toy model for elaborating on the effects of the noise trader self-referential behaviour. The toy model consisted of two coupled iterative equations. One for the magnetisation, which we used to model the noise trader opinion, and one for the external field, which

we used to model the price momentum. Compared to the full market model, the toy model substitutes the stochastic noise trader decision process with a threshold like behaviour given by the hyperbolic tangent function and approximates the relation between the noise trader opinion and the price growth rate with an one-to-one correspondence. We mapped a phase diagram of this toy model on the imitation and trend following weight coefficients plane. Besides the standard ferromagnetic ordered and paramagnetic disordered phases, we observed two additional ordered regimes. One exhibited regular jumps between the two polarised states, while the other showed smoothly oscillating dynamics.

In chapter 4 we considered the limiting cases of noise trader behaviour. We derived two fixed points for the price growth in section 4.3. One for both *ordered* noise trader state, *i.e* regimes where all noise traders are invested into the same asset. These fixed points effectively act as upper and lower bound for the long-term average price growth, which is proven numerically in chapter 6. In section 4.1, we showed that the necessary condition for the onset of these polarised noise trader regimes, is to have a lock-in effect for one of the assets, which can be achieved by a zero valued probability for noise traders to sell that asset. It is convenient to define threshold momentum values above or below which the noise trader switching probabilities vanish, inducing an ordered state. In section 4.2, we showed that these threshold *critical momenta* introduce a natural frame of reference on the noise trader imitation and trend following plane. In chapter 5 the centre of this reference frame is shown to correspond to the critical point of the market model phase diagram.

The results from chapter 4 were used in chapter 5 to propose an analytical phase diagram for the market model on the noise trader imitation and trend following weight coefficients plane. We found four different regimes centred at the critical point $(\frac{1}{\kappa}, 0)$, where κ is the constant noise trader herding propensity. Figure 5.5 illustrates these four regimes: (1) *positive* ordered phase, where all noise traders are invested in the risky asset; (2) *bifurcating* ordered state, where depending on the initial perturbations all noise traders are either invested in the risky or the risk-free asset; (3) *negative* ordered phase, where all noise traders are invested in the risk-free asset; (4) *disordered* regime, where around half of the noise traders is invested in the risky asset and the rest in the risk-free asset. In chapter 6 we mapped a numeric phase diagram, which is sketched in figure 6.12. We found that the analytical predicted the general structure of the phase diagram well. However, for the numeric phase diagram we also found a fifth phase: (5) *oscillating* phase, where the noise traders regularly shift between lock-in effects for the risky and the risk-free asset.

Farmer and Foley (2009) have argued that incorporating agent-based models into the policy making process would greatly benefit the society. With this in

mind, the current thesis has elaborated on the regime structure of the market model introduced by Kaizoji et al. (2015) and Kohrt (2016). This model has been shown to exhibit emergent transient super-exponential bubble growth, making it a potential testing environment for financial bubble detection mechanism. Our work has empowered future use of this model by mapping a phase diagram of different market regimes in this model. Such a phase diagram can for example be used for designing numeric "experiments" in the model or guiding calibration to the real-world markets. Regarding the phase diagram itself, the exact mechanism behind the oscillating phase is still unknown. This is a question for future work. We have also introduced a simple mean-field Ising based toy model of the noise trader behaviour. We find that further investigation of this toy model could prove enlightening.

Bibliography

Kenneth Joseph Arrow. *Aspects of the theory of risk-bearing*. Yrjö Jahnssonin Säätiö, 1965.

Kenneth Joseph Arrow. Essays in the theory of risk-bearing. Technical report, 1970.

W Brian Arthur. Complexity and the Economy. *Science (80-.).*, 284:107–109, 1999. doi: 10.1126/science.284.5411.107.

Marianne Baxter and Urban J. Jermann. The International Diversification Puzzel Is Worse Than You Think. *Natl. Bur. Econ. Res.*, (w5019), 1997.

Eric Bonabeau. Agent-based modeling: Methods and techniques for simulating human systems. *Proc. Natl. Acad. Sci.*, 99:7280–7287, 2002. doi: 10.1073/pnas.082080899. URL `http://www.pnas.org/content/99/suppl{_}3/7280.abstract`.

Stephen G. Brush. History of the Lenz-Ising Model. *Rev. Mod. Phys.*, 39(4): 883–893, 1967.

Claudio Castellano, Santo Fortunato, and Vittorio Loreto. Statistical physics of social dynamics. *Rev. Mod. Phys.*, 81(2):591–646, may 2009. doi: 10.1103/RevModPhys.81.591. URL `http://link.aps.org/doi/10.1103/RevModPhys.81.591`.

Anirban Chakraborti, Ioane Muni Toke, Marco Patriarca, and Frédéric Abergel. Econophysics review: II. Agent-based models. *Quant. Financ.*, 11(7):1013–1041, 2011. doi: 10.1080/14697688.2010.539249. URL `http://dx.doi.org/10.1080/14697688.2010.539249`.

Werner F. M. De Bondt and Richard Thaler. Does the Stock Market Overreact? *J. Finance*, 40(3), 1985.

Werner F. M. De Bondt and Richard Thaler. Further Evidence on Investor Overreaction and Stock Market Seasonality. *J. Finance*, 42(3), 1987.

J Doyne Farmer and Duncan Foley. The economy needs agent-based modelling. *Nature*, 460(7256):685–686, 2009.

Serge Galam, Yuval Gefen, and Yonathan Shapir. Sociophysics: A new approach of sociological collective behaviour. I. mean-behaviour description of a strike. *J. Math. Sociol.*, 9(1):1–13, 1982.

D A Green. A colour scheme for the display of astronomical intensity images. *Bull. Astr. Soc. India*, 39:289–295, 2011.

Anders Johansen and Didier Sornette. Critical Crashes. *eprint arXiv:cond-mat/9901035*, page 7, 1999. ISSN 0129-1831. doi: 10.1142/S0129183199000553. URL `http://arxiv.org/abs/cond-mat/9901035`.

Anders Johansen, Olivier Ledoit, and Didier Sornette. Crashes as critical points. *Int. J. Theor. Appl. Financ.*, 3(02):219–255, 2000. ISSN 0219-0249. doi: 10.1142/S0219024900000115. URL `http://www.worldscientific.com/doi/abs/10.1142/S0219024900000115`.

Eric Jones, Travis Oliphant, Pearu Peterson, and Others. {SciPy}: Open source scientific tools for {Python}. URL `http://www.scipy.org/`.

Taisei Kaizoji, Matthias Leiss, Alexander Saichev, and Didier Sornette. Superexponential endogenous bubbles in an equilibrium model of fundamentalist and chartist traders. *J. Econ. Behav. Organ.*, 112(2015):289–310, 2015. ISSN 01672681. doi: 10.1016/j.jebo.2015.02.001. URL `http://dx.doi.org/10.1016/j.jebo.2015.02.001`.

Morgan Kelly. All their eggs in one basket : Portfolio diversification of US households. *J. Econ. Behav. Organ.*, 27:87–96, 1995.

Ralf Kohrt. *The market impact of exploiting financial bubbles*. Master's thesis, ETHZ, 2016.

Thomas Lux and Michele Marchesi. Scaling and criticality in a stochastic multi-agent model of a financial market. *Nature*, 397(February):498–500, 1999. ISSN 00280836. doi: 10.1038/17290. URL `http://finance.martinsewell.com/stylized-facts/scaling/LuxMarchesi1999.pdf`.

Denis Phan, Mirta B Gordon, and Jean-Pierre Nadal. *Social Interactions in Economic Theory: An Insight from Statistical Mechanics*, pages 335–358. Springer Berlin Heidelberg, Berlin, Heidelberg, 2004. ISBN 978-3-540-24708-1. doi: 10.1007/978-3-540-24708-1_20. URL `http://dx.doi.org/10.1007/978-3-540-24708-1{_}20`.

John W Pratt. Risk Aversion in the Small and in the Large. *Econometrica*, 32(1/2):122–136, 1964. ISSN 00129682, 14680262. URL `http://www.jstor.org/stable/1913738`.

E Samanidou, E Zschischang, D Stauffer, and T Lux. Agent-based models of financial markets. *Reports Prog. Phys.*, 70(3):409, 2007. URL `http://stacks.iop.org/0034-4885/70/i=3/a=R03`.

Thomas C Schelling. Dynamic models of segregation†. *J. Math. Sociol.*, 1(2): 143–186, 1971.

Didier Sornette. *Why stock markets crash: critical events in complex financial systems.* Princeton University Press, 2009.

Didier Sornette. Physics and Financial Economics (1776-2014): Puzzles, Ising and Agent-Based models. *Swiss Financ. Inst. Res. Pap. Ser.*, No. 14-25, 2014.

Didier Sornette and Anders Johansen. Large financial crashes. *Physica A*, 245(october 1929):14, 1997. ISSN 03784371. doi: 10.1016/S0378-4371(97) 00318-X. URL `http://arxiv.org/abs/cond-mat/9704127`.

Dietrich Stauffer. A Biased Review of Sociophysics. *J. Stat. Phys*, 151:9–20, 2013. doi: 10.1007/s10955-012-0604-9.

Léon Walras. *Eléments d'Economie Politique Pure.* L. Corbaz, Lausanne, 1874.

Wolfgang Weidlich. The statistical description of polarization phenomena in society. *Br. J. Math. Stat. Psychol.*, 24(2):251–266, 1971.

Ivo Welch. Herding among security analysts. *J. financ. econ.*, 58(November 1999), 2000.

![ETH logo]

Eidgenössische Technische Hochschule Zürich
Swiss Federal Institute of Technology Zurich

Declaration of originality

The signed declaration of originality is a component of every semester paper, Bachelor's thesis, Master's thesis and any other degree paper undertaken during the course of studies, including the respective electronic versions.

Lecturers may also require a declaration of originality for other written papers compiled for their courses.

_____

I hereby confirm that I am the sole author of the written work here enclosed and that I have compiled it in my own words. Parts excepted are corrections of form and content by the supervisor.

Title of work (in block letters):

MULTIPLE MARKET REGIMES IN AN EQUILIBRIUM MODEL OF FUNDAMENTALIST AND NOISE TRADERS

Authored by (in block letters):
For papers written by groups the names of all authors are required.

Name(s):	**First name(s):**
OLLIKAINEN	MADIS

With my signature I confirm that
- I have committed none of the forms of plagiarism described in the 'Citation etiquette' information sheet.
- I have documented all methods, data and processes truthfully.
- I have not manipulated any data.
- I have mentioned all persons who were significant facilitators of the work.

I am aware that the work may be screened electronically for plagiarism.

Place, date	**Signature(s)**
Zürich, 26.09.2016	

For papers written by groups the names of all authors are required. Their signatures collectively guarantee the entire content of the written paper.